

# Development of a FEM waveguide code, incorporating Fast Frequency Techniques, for numerical synthesis

Samuel R. Clarke



Thesis presented in partial fulfilment of the requirements for the degree of Master of Science in Engineering at the University of Stellenbosch.

Supervisor:

Prof. David B. Davidson

December 2002

## Declaration

"I, the undersigned, hereby declare that the work contained in this thesis is, unless stated otherwise, my own original work and that I have not previously in its entirety or in part submitted it at any university for a degree."

∩

# Summary

A computational tool for numerical synthesis via optimization is developed. Only two port waveguide devices are considered. The Finite Element Method (FEM) is used for the electromagnetic analysis. Specifically, the frequency domain electric field FEM is used with vector curl-conforming constant tangential / linear normal brick-shaped elements. Special boundary conditions are used at the ports. These boundary conditions only consider dominant mode propagation. The issues surrounding the implementation of this formulation are discussed. The results generated using this code compare favorably to examples from independent sources. A parametric mesher that is used in conjunction with the FEM is developed. This is done to eliminate the need for human intervention during each iteration of the synthesis procedure. Fast Frequency (FF) techniques are presented to reduce the computational requirements of the synthesis. FF techniques reduce the cost of calculating many frequency samples in a specified band and do not reduce the computational requirements of computing a FEM solution at a single frequency. The FF techniques presented are: Asymptotic Waveform Evaluation (AWE), Model Based Asymptotic Waveform Evaluation (MB-AWE) and Model Based Parameter Estimation (MBPE). The results obtained using these techniques are compared and the most suitable technique for the synthesizer is selected. MBPE is selected as the most suitable technique for this application. An adaptive sampling algorithm for Model Based Parameter Estimation is presented. The algorithm relies on the difference between multiple models generated from the same samples to determine the sample locations. The use of this algorithm enables a model of a narrow band filter at X-band to be determined using only fourteen FEM solutions. The difference between the model- and the FEM solutions is less than -100dB across the band. A sample synthesis using generalized simulated annealing is presented. A single pole filter in X-band waveguide is successfully synthesized to illustrate the usefulness of the code. The use of FF techniques results in a computational cost saving of a factor of forty times.



# Opsomming

'n Rekenaar werktuig vir numeriese sintese deur middel van optimering word ontwikkel. Slegs twee-poort golfleierkomponente word beskou.

Die Eindige Element-metode (EEM) word vir die elektromagnetiese analise gebruik. Meer spesifiek, die frekwensiegebied, elektriese-veld EE-formuleering word gebruik, met curl-ondersteunende, konstant-tagensiaal/lineêr-normaal, baksteen-vormige vektorelemente. Spesiale grensvoorwaardes word by die poorte gebruik. Hierdie grensvoorwaardes neem slegs voortplanting van die dominante modus in ag. Die kwessies rondom die implementering van hierdie EEM word bespreek. Resultate wat met hierdie kode verkry word, vergelyk goed met dié vanuit onafhanklike bronne. 'n Parametriese diskretisasie prosedure in ontwikkel, vir gebruik saam met die genoemde EEM, met die doel om menslike interaksie uit die weg te ruim, tydens die sintese proses.

Vinnige Frekwensie (VF) tegnieke word beskryf, met die doel om die berekeningskoste van die sintese te verminder. VF tegnieke verminder die berekeningskoste verbonde aan 'n reeks EEM oplossings binne 'n gegewe frekwensieband, maar verminder nie die koste verbonde aan 'n enkel-frekwensie EEM oplossing nie. Die VF tegnieke wat beskryf word, is die volgende: Asimptotiese Golfvorm Evaluasie (AGE), Model Gebaseerder Asimptotiese Golfvormevaluasie (MGAGE) en Model-Gebaseerde Parameterekstraksie (MGPE). Die resultate wat met hierdie metodes verkry word, word vergelyk om sodoende die mees toepaslike VF tegniek te kies. MGPE word gekies as die mees toepaslike tegniek.

'n Aanpasbase monsteringsalgoritme vir MGPE word beskryf. Die algoritme berus op die verskil tussen twee modelle wat vanaf dieselfde stel punte geskep word, om monstrefrekwensiewaardes te bepaal. Die gebruik van hierdie algoritme lei tot 'n model van 'n nou-, X-band filter, vanuit slegs veertien EEM oplossings. Die verskil tussen hierdie model en enige EEM oplossings binne die band, is kleiner as -100dB. 'n Voorbeeld sintese, wat gebruik maak van veralgemeende, gesimuleerde versmelting, word beskryf. 'n Enkel-pool filter by X-band word suksesvol gesintetiseer om die bruikbaarheid van die kode te illustreer. 'n Faktor veertig vermindering in berekeningskoste word behaal deur gebruik te maak van VF tegnieke.



# Acknowledgements

Many people have contributed enormously to my studies and development. I especially thank the following:

- Firstly, my promoter Prof. D.B. Davidson, not for only the constructive guidance in my research, but also for always being available and free with advice; contributing to my professional development. Thanks Prof. D. for the nurturing my interest in CEM and for assisting in obtaining part time employment, that has resulted in much needed additional financial support and invaluable experience.
- Matthys Botha, who endured a year of sharing an office with me, and who was always willing to enter into a discussion or explanation. Your advice was always readily available and always reliable.
- The staff at EM Software and Systems for teaching me, during vacation work, how to use CEM tools effectively. I would like to make a special mention of Mr. D. Le Roux, Dr. U. Jakobus, Dr. J.J. Van Tonder and Dr. A.G. Smith. The experience that I obtained during my vacation work has helped me mature in the use and understanding of CEM techniques.
- The National Research Foundation, for providing financial support during the course of my studies.
- All the staff and students in the EEM group at Stellenbosch University, for all the questions and explanations, and for creating an environment where research is encouraged. Special mention of Prof. J.H. Cloete, Prof. K.D. Palmer, Dr. C. van Niekerk and Prof. H.C. Reader must be made for their input and guidance.
- My parents and family, for your constant encouragement, putting up with my ups and downs with regards to my work, proofreading this dissertation, support, prayer and love.
- Ruth-Frances, for being loving and understanding and never getting angry with me for spending nights and weekends in my office. Thank-you for pretending to understand when I tried to explain my latest frustration.
- My friends for always being willing to have a cup of coffee.
- Marimar Ropero, for giving me permission to reprint my favorite dilbert cartoon.
- Prof. D. Knuth and Dr. L. Lamport, for L<sup>A</sup>T<sub>E</sub>X, which was used to typeset this document.

- And finally, our Creator, for giving us this fascinating world to study.

# Abbreviations

EM	- Electromagnetic
FEM	- Finite Element Method
MoM	- Method of Moments
ABC	- Absorbing Boundary Condition
FE/BI	- Finite Element / Boundary Integral
$k_0$	- Free space wavenumber
$k_{x10}$	- $TE_{10}$ wavenumber in a waveguide
FF	- Fast Frequency
MOR	- Model Order Reduction
AWE	- Asymptotic Waveform Evaluation
MB-AWE	- Model Based Asymptotic Waveform Evaluation
MBPE	- Model Based Parameter Estimation
PVL	- Padé via Lanczos
AFS	- Adaptive Frequency Sampling
CFH	- Complex Frequency Hopping



# Contents

<b>Summary</b>	<b>i</b>
<b>Opsomming</b>	<b>iii</b>
<b>Acknowledgements</b>	<b>iv</b>
<b>Abbreviations</b>	<b>vi</b>
<b>Notation</b>	<b>vii</b>
<b>1 Introduction</b>	<b>2</b>
<b>2 Implementation of the FEM</b>	<b>4</b>
2.1 Overview of the Finite Element Method Formulation . . . . .	4
2.1.1 The Outline of a general FEM Algorithm . . . . .	4
2.1.2 What do the degrees of freedom represent? . . . . .	5
2.1.3 Port discontinuities and boundary conditions of the third kind . . . . .	5
2.1.4 The functional . . . . .	6
2.1.5 Rendering the functional stationary . . . . .	6
2.2 Implementation Issues . . . . .	7
2.2.1 Element shape . . . . .	7
2.2.2 The fields within the element . . . . .	7
2.2.3 Discretization of the functional . . . . .	9
2.2.4 Evaluation of the elemental matrices . . . . .	10
2.2.5 Choosing data structures . . . . .	11
2.2.6 Mesher . . . . .	11
2.2.7 Assembling the system matrix . . . . .	13

## CONTENTS

viii

2.2.8	Matrix storage . . . . .	14
2.2.9	Matrix solution . . . . .	15
2.2.10	Calculating observables . . . . .	15
2.3	Validation . . . . .	16
2.3.1	Two-pole filter . . . . .	16
2.3.2	Dielectric loaded waveguide . . . . .	17
2.4	Conclusion . . . . .	17
<b>3</b>	<b>Fast Frequency Techniques</b>	<b>20</b>
3.1	A note on fitting models used . . . . .	21
3.2	Asymptotic Waveform Evaluation . . . . .	22
3.2.1	AWE formulation . . . . .	22
3.2.2	AWE implementation issues . . . . .	25
3.2.3	AWE results . . . . .	26
3.3	Model Based Asymptotic Waveform Evaluation . . . . .	35
3.3.1	MB-AWE formulation . . . . .	35
3.3.2	MB-AWE implementation issues . . . . .	36
3.3.3	MB-AWE results . . . . .	36
3.3.4	Investigation into undesired performance of MB-AWE . . . . .	42
3.4	Model Based Parameter Estimation . . . . .	44
3.4.1	MBPE formulation . . . . .	44
3.4.2	MBPE implementation issues . . . . .	48
3.4.3	MBPE results . . . . .	48
3.5	Discussion and Comparison of Fast Frequency Techniques . . . . .	58
3.5.1	A note on computational costs . . . . .	58
3.5.2	A note: pre- and post- processing costs . . . . .	60
3.5.3	Pre-conditioners and iterative solvers . . . . .	61
3.5.4	The computational cost of a FEM frequency solution . . . . .	61
3.5.5	The computational cost of an AWE solution . . . . .	61
3.5.6	The computational cost of a MB-AWE solution . . . . .	62
3.5.7	The computational cost of a MBPE solution . . . . .	62
3.5.8	Comparison between the Fast Frequency Techniques . . . . .	62

*CONTENTS*

ix

3.6	Conclusion . . . . .	64
<b>4</b>	<b>Adaptive Sampling for Fast Frequency Techniques</b>	<b>65</b>
4.1	Adaptive method formulations . . . . .	65
4.2	Complex Frequency Hopping . . . . .	66
4.3	Adaptive Frequency Sampling . . . . .	67
4.4	Results on a test function . . . . .	68
4.5	Adaptive Results of FE Systems . . . . .	68
4.5.1	Single inductive septum . . . . .	69
4.5.2	Single pole filter . . . . .	69
4.5.3	Two pole filter . . . . .	69
4.6	Conclusion . . . . .	74
<b>5</b>	<b>A Sample Optimization Routine</b>	<b>75</b>
5.1	The proposed synthesis specifications . . . . .	75
5.2	Random Number Generator . . . . .	76
5.2.1	Generalized Simulated Annealing . . . . .	76
5.3	The objective function . . . . .	77
5.4	The physical structure limitations for the synthesis algorithm . . . . .	78
5.5	Choice of the optimizer parameters . . . . .	78
5.6	Results . . . . .	79
5.7	Conclusion . . . . .	81
<b>6</b>	<b>General Conclusions</b>	<b>82</b>
<b>A</b>	<b>Derivation of Taylor series for linear equation</b>	<b>84</b>



# List of Figures

2.1	The brick element as proposed in [2]. . . . .	8
2.2	The dimensions of the two-pole filter. . . . .	17
2.3	The reflection coefficient of the two-pole filter. . . . .	18
2.4	The dimensions of the dielectric loaded waveguide. . . . .	19
2.5	The reflection coefficient results for the dielectric loaded waveguide. . . . .	19
3.1	$k_{x10}$ vs. $k_0$ . . . . .	23
3.2	Error in linear approximation of $k_{x10}$ . . . . .	24
3.3	The sum of the squares of the magnitudes of the reflection and transmission coefficients for a single inductive septum: comparison of FEM and AWE results. . . . .	28
3.4	Reflection coefficient of the single inductive septum: comparison of FEM and AWE results. . . . .	29
3.5	Transmission coefficient of the single inductive septum: comparison of FEM and AWE results. . . . .	29
3.6	The dimensions of the single pole filter. . . . .	30
3.7	The sum of the squares of the magnitudes of the reflection and transmission coefficients for the single pole filters: comparison of FEM and AWE results. . . . .	31
3.8	Reflection coefficient of the single pole filter: comparison of FEM and AWE results. . . . .	31
3.9	Transmission coefficient of the single pole filter: comparison of FEM and AWE results. . . . .	32
3.10	The sum of the squares of the magnitudes of the reflection and transmission coefficients for the two pole filter: comparison of FEM and AWE results. . . . .	33
3.11	Reflection coefficient of the two pole filter: comparison of FEM and AWE results. . . . .	34
3.12	Transmission coefficient of the two pole filter: comparison of FEM and AWE results. . . . .	34
3.13	The sum of the squares of the magnitudes of the reflection and transmission coefficients for a single inductive septum: comparison of FEM and MB-AWE results. . . . .	36

## LIST OF FIGURES

xi

3.14	Reflection coefficient of the single inductive septum: comparison of FEM and MB-AWE results. . . . .	37
3.15	Transmission coefficient of the single inductive septum: comparison of FEM and MB-AWE results. . . . .	37
3.16	The sum of the squares of the magnitudes of the reflection and transmission coefficients for the single pole filter: comparison of FEM and MB-AWE results. . . . .	38
3.17	Reflection coefficient of the single pole filter: comparison of FEM and MB-AWE results. . . . .	39
3.18	Transmission coefficient of the single pole filter: comparison of FEM and MB-AWE results. . . . .	39
3.19	The sum of the squares of the magnitudes of the reflection and transmission coefficients for the two pole filter: comparison of FEM and MB-AWE results. . . . .	40
3.20	Reflection coefficient of the two pole filter: comparison of FEM and MB-AWE results. . . . .	41
3.21	Transmission coefficient of the two pole filter: comparison of FEM and MB-AWE results. . . . .	41
3.22	The sum of the squares of the magnitudes of the reflection and transmission coefficients for the single pole filter, comparison between different order MB-AWE models. . . . .	43
3.23	The sum of the squares of the magnitudes of the reflection and transmission coefficients of the single inductive septum: comparison of FEM and MBPE (Parameter Sampling) results. . . . .	49
3.24	Reflection coefficient of the single inductive septum: comparison of FEM and MBPE (Parameter Sampling) results. . . . .	50
3.25	Transmission coefficient of the single inductive septum: comparison of FEM and MBPE (Parameter Sampling) results. . . . .	50
3.26	Reflection coefficient of the single inductive septum: comparison of FEM and MBPE (Derivative Sampling) results. . . . .	51
3.27	The sum of the squares of the magnitudes of the reflection and transmission coefficients for the single pole filters: comparison of FEM and MBPE (Parameter Sampling) results. . . . .	52
3.28	Reflection coefficient of the single pole filter: comparison of FEM and MBPE (Parameter Sampling) results. . . . .	53
3.29	Transmission coefficient of the single pole filter: comparison of FEM and MBPE (Parameter Sampling) results. . . . .	53
3.30	Reflection coefficient of the single pole filter: comparison of FEM and MBPE (Derivative Sampling) results. . . . .	54



## LIST OF FIGURES

xii

3.31	The sum of the squares of the magnitudes of the reflection and transmission coefficients for the two pole filter: comparison of FEM and MBPE (Parameter Sampling) results. . . . .	55
3.32	Reflection coefficient of the two pole filter: comparison of FEM and MBPE (Parameter Sampling) results. . . . .	56
3.33	Transmission coefficient of the two pole filter: comparison of FEM and MBPE (Parameter Sampling) results. . . . .	56
3.34	Reflection coefficient of the two pole filter: comparison of FEM and MBPE (Derivative Sampling) results. . . . .	57
3.35	Reflection coefficient of the two pole filter: comparison of FEM and MBPE (Derivative Sampling) results. . . . .	57
4.1	The sum of the squares of the magnitudes of the reflection and transmission coefficients for the two pole filter: MBPE (Adaptive Sampling) results and support points. . . . .	70
4.2	Reflection coefficient of the two pole filter: MBPE (Adaptive Sampling) results and support points. . . . .	70
4.3	Transmission coefficient of the two pole filter: MBPE (Adaptive Sampling) results and support points. . . . .	71
4.4	Error in reflection coefficient of the two pole filter between MBPE (Adaptive Sampling) and FE solution. . . . .	72
4.5	Error in transmission coefficient of the two pole filter between MBPE (Adaptive Sampling) and FE solution. . . . .	72
4.6	Error in reflection coefficient of the two pole filter between Linear interpolation (Adaptive Samples) and FE solution. . . . .	73
4.7	Error in transmission coefficient of the two pole filter between Linear interpolation (Adaptive Samples) and FE solution. . . . .	73
5.1	Dilbert on Random numbers. Reprinted with permission . . . . .	76
5.2	Random number distribution for the random number generator proposed by Park . . . . .	77
5.3	Objective function score versus iteration number for the simulated annealing synthesis. . . . .	79
5.4	Magnitude of the reflection coefficient of the synthesized filter. . . . .	80



# List of Tables

2.1	The proposed data structures . . . . .	12
2.2	Currently implemented 'building block' parameters for the mesher. . . . .	14
3.1	Definition of the variables to assist computational cost discussion. . . . .	59
3.2	The computational cost of a selection of Mathematical operators . . . . .	60

# Chapter 1

## Introduction

The continuing increase in computational power available to electromagnetic device design engineers, has seen the widespread use of numerical techniques to solve electromagnetic problems. Numerical techniques enable rapid and cost-effective testing of devices prior to prototyping. The use of numerical techniques in electromagnetic device synthesis has been proposed. Johnson and Samii [1] is a recent example of a publication on numerical synthesis. In order for device synthesis by numerical optimization to be investigated, a solver code must be available. The optimization process will typically vary a few physical parameters of a device, and then use an EM solver to establish the influence of the physical parameter on the design specifications. This means that the input to the EM solver should be in the form of physical parameters and the output should contain EM observables that are typically used for design specification. The purpose of this project is to provide an EM solver that meets the requirements of a numerical optimization process, both with regards to accuracy and speed.

The only class of EM device that is considered in this study is waveguide devices. These devices perform an important role in many EM applications.

The first stage in obtaining a numerical EM solution of a device, is to discretize the geometric structure of the device. The discretized form of the geometry is called a 'mesh'. The input to the discretization process (also called a mesher) should be in the form of physical parameters. The output from the mesher is a mesh that is suited to the EM solver.

One of the available numerical electromagnetic solution techniques is the finite element method (FEM). The FEM usually calculates the field, in the frequency domain, for a specified mesh. The FEM formulation is presented for waveguide structures. The formulation is presented before the mesher, as the output of the mesher is dependant on several decisions made while implementing the FEM. The observables of interest (usually S-parameters for waveguide devices) also need to be calculated from the field distribution obtained using the FEM.

The FEM formulation is a frequency domain solver, meaning that the method solves for the fields at one frequency at a time. Waveguide devices are usually characterized by a response in a frequency window or band. This means that the FEM needs to be used repeatedly at many frequencies, to obtain a specified sample density in the frequency band of interest. Fast frequency (FF) techniques are presented as a method to reduce the number of frequency samples that need to be solved using the FEM, while still obtaining accurate results at the desired density.

FF techniques depend on a few FEM solutions that are used to obtain parameters required

by the FF technique. The location, in frequency, of the samples can affect the accuracy of the model. Adaptive sampling techniques are used to minimize the number of FEM solutions required by choosing the sample locations that contribute the most to the model. The adaptive techniques available in the literature are examined and one is implemented.

The effectiveness of the algorithm in electromagnetic device synthesis via numerical optimization is investigated by implementing a generalized simulated annealing optimizer and using it to synthesize a filter in X-band waveguide.

Chapter 2 deals with the theory and implementation of the FEM. Validation results for the FEM algorithm are also given in Chapter 2. Chapter 3 shows the theory, implementation and results of three FF techniques. Chapter 4 show the development of an adaptive technique for MBPE. The algorithm as a whole is validated in Chapter 5, where synthesis via numerical optimization is shown.



# Chapter 2

## Implementation of the FEM

### 2.1 Overview of the Finite Element Method Formulation

The first step in performing numerical synthesis is to have access to an EM solver. This chapter shows the formulation and implementation of an **E**-field FEM algorithm. This algorithm is specifically written to solve waveguide problems, at one frequency point, that have no more than two ports and no boundaries other than metallic walls (Dirichlet) or boundaries of the third kind [2]. These limitations are imposed and not inherent. The boundary condition used on the ports is for the dominant  $TE_{10}$  mode only. This can be extended to handle more modes quite easily. Other methods of mesh termination (such as Absorbing Boundary Conditions (ABC) or the finite element-boundary integral method (FE/BI) ) can be included as well [2]. These extensions have not been included in this study, as they are not needed to obtain solutions for the devices under consideration.

A coordinate system for the problem geometry needs to be chosen. The examples in [2] are solved with the propagation direction along the  $z$ -axis. As the formulation presented is independent of this direction, the waveguide is orientated with the direction of propagation along the positive  $x$ -axis. The wide side of the waveguide is in the  $y$  direction and the narrow side in the  $z$  direction. The input port is located at  $x = 0$  and the output port at  $x = x_{len}$  where  $x_{len}$  is the total length of the waveguide. Note that the waveguide should extend at least  $\frac{\lambda_g}{2}$  to either side of any obstruction inside of the waveguide, as non-propagating higher order modes in the vicinity of the obstruction need to attenuate before reaching the port.

#### 2.1.1 The Outline of a general FEM Algorithm

The finite element formulation relies on calculating an energy-related functional in the problem domain. A solution of the system is found when this functional is minimized [3].

The functional can only be evaluated once the field in the problem space is known. The problem space is therefore subdivided into small elements with an assumed field distribution. The functional is now evaluated in each element (see section 2.2.4). The field inside the volume elements is described by a set of basis functions with known form and unknown coefficients (see section 2.2.2). This field description is also valid on the surface of the element. The system



matrix is assembled by adding all the elemental contributions to the functional. The elements are connected by setting the fields on the coincident surfaces of adjoining elements equal. The process is explained in more detail in section 2.2.7. Boundary conditions such as Dirichlet, Neumann or boundaries of the third kind are implemented by adding additional constraints to unknowns within the system matrix.

If this system matrix is made stationary with respect to the unknown coefficients, the system response is found as the values of the unknowns [3].

The desired observables ( $S$ -parameters for instance) can then be calculated using these stationary values.

### 2.1.2 What do the degrees of freedom represent?

The degrees of freedom must describe the field in the problem space. Any set of values that can describe the field entirely can therefore be used. The set of values used to describe the field must therefore be chosen. This decision has a very significant impact on the ease of implementation of the code.

The first decision required is whether to use nodal or vector elements. The use of nodal based elements has several drawbacks. The first is that fictitious resonant cavity modes, called spurious modes, can be excited in the mesh. Spurious modes can couple to waveguide modes and render the solution invalid. These modes occur because the field is forced to be fully continuous, instead of only having tangential continuity [4]. The second problem when using nodal elements is that enforcing boundary conditions becomes more tedious, as the unknown is associated with the entire field at a point and not just one component of the field.

The advantages of vector elements are discussed by Webb in [4]. Vector elements have the tangential field as unknown along each edge of the element. Boundary conditions are conveniently implemented using these elements as normal field discontinuity is allowed. The only propagating mode under consideration is the dominant  $TE_{10}$  mode. The  $\mathbf{E}$ -field at any cross sectional plane through the waveguide is purely tangential (there is no  $\mathbf{E}$ -field in the direction of propagation), and therefore the most logical unknown is the tangential  $E$ -field. Exactly how the field is defined within the element is described in section 2.2.2.

Vector elements of higher orders can be implemented to improve accuracy for a specified number of degrees of freedom [5, 6]. The evaluation of the element integrals (see section 2.2.4 for these integrals) has not been tabulated for higher order brick elements. The choice of element shape is discussed with this in mind in section 2.2.1.

The decision is therefore made to use the lowest order vector elements, with the tangential  $E$ -field as unknown along each edge of the element.

### 2.1.3 Port discontinuities and boundary conditions of the third kind

The port formulation presented here only models the  $TE_{10}$  mode propagating infinitely. Additional modes can easily be included by including additional terms for those fields. Jin shows that the ports can be modelled using what he terms boundary conditions of the third kind [2]. This is shown by firstly expressing the field at port 1 as a superposition of an incident  $TE_{10}$



wave and reflected  $TE_{10}$  wave.

$$\begin{aligned}\mathbf{E}(x, y, z) &= \mathbf{E}^{inc}(x, y, z) + \mathbf{E}^{ref}(x, y, z) \\ &= E_0 e_{10}(y, z) e^{-jk_{x10}x} + RE_0 e_{10}(y, z) e^{jk_{x10}x}\end{aligned}\quad (2.1)$$

where  $E_0$  is the magnitude of the incident wave,  $R$  is the reflection coefficient and  $\mathbf{e}_{10}$  and  $k_{x10}$  are given by:

$$\mathbf{e}_{10}(y, z) = \hat{y} \sin\left(\frac{\pi y}{a}\right) \quad (2.2)$$

$$k_{x10} = \sqrt{k_0^2 - \left(\frac{\pi}{a}\right)^2} \quad (2.3)$$

Jin [2] then shows that the field at this port can be written as

$$\hat{n} \times (\nabla \times \mathbf{E}) + \gamma \hat{n} \times (\hat{n} \times \mathbf{E}) = \mathbf{U}^{inc} \quad (2.4)$$

where,  $\gamma = jk_{x10}$  and  $\mathbf{U}^{inc} = -2jk_{x10}\mathbf{E}^{inc}$ . A similar expression for the field at port 2 is also derived by Jin in [2]. Careful study of this form of the fields reveals that this expression is identical to that of fields at a boundary of the third kind [2]. This implies that the ports can be modelled using boundary conditions of the third kind.

### 2.1.4 The functional

The derivation of the energy-related functional that is used is found in [2]. The variational functional, including the terms to incorporate the port discontinuities, is given by:

$$\begin{aligned}F(\mathbf{E}) &= \frac{1}{2} \iiint_V \left[ \frac{1}{\mu_r} (\nabla \times \mathbf{E}) \cdot (\nabla \times \mathbf{E}) - k_0^2 \epsilon_r \mathbf{E} \cdot \mathbf{E} \right] dV \\ &\quad + \int \int_{S_1} \left[ \frac{\gamma}{2} (\hat{n} \times \mathbf{E}) \cdot (\hat{n} \times \mathbf{E}) + \mathbf{E} \cdot \mathbf{U}^{inc} \right] dS \\ &\quad + \int \int_{S_2} \left[ \frac{\gamma}{2} (\hat{n} \times \mathbf{E}) \cdot (\hat{n} \times \mathbf{E}) \right] dS\end{aligned}\quad (2.5)$$

In this equation  $S_1$  is the cross sectional surface that defines the first port and  $S_2$  is that of for the second port.  $V$  is the entire three dimensional problem space.  $\gamma$  and  $\mathbf{U}^{inc}$  are defined in section 2.1.3. (Note that evaluation of this functional requires continuous integration of the unknown field values over the entire problem space. In order to evaluate the integral over the entire problem space, the problem space must first be discretized.)

### 2.1.5 Rendering the functional stationary

The derivative of the functional is taken with respect to each of the global degrees of freedom and set to zero. The elemental coefficients (and their derivatives) that lie on homogenous Dirichlet boundaries are zero (see section 2.1.2). This means that all degrees of freedom that contribute to the derivative do not lie on the Dirichlet boundaries of the mesh. This technique



is shown by Silvester Ferrari in [3] for nodal elements.

The solver makes use of this fact by excluding the contributions from edges that lie on a Dirichlet boundary when assembling the system matrix. Thus contributions to the system matrix that do not contribute to the derivative of the system matrix are excluded. This is a standard approach in FEM; explicit implementation of a derivative algorithm is therefore avoided.

## 2.2 Implementation Issues

This section details the process that needs to transform the continuous formulation already presented into a discretized form that can be solved on a computer.

### 2.2.1 Element shape

Any three dimensional volume can be used to discretize the problem space. Tetrahedrons are commonly used because of their ability to model interfaces that are not parallel to Cartesian planes.

When choosing the element shape, one consideration is that tabulated results are available for higher order tetrahedral elements. Higher order elements of other shapes would need to be researched first. Element shape is discussed more comprehensively in [7].

The algorithm described here is implemented with a parametric meshing algorithm, and the use of tetrahedrons complicates the meshing process. Rectangular or 'brick' elements were ultimately chosen, as the mesher would be able to generate meshes very quickly and be comparatively easy to implement.

There are three significant drawbacks to using brick elements. They are:

- Structures within the waveguide that do not have edges parallel to the cartesian planes will not be accurately modelled. Many waveguide structures do have edges in the cartesian directions or can be adequately modelled using geometric approximations for structures that do not conform to this specification. A structure such as a round dielectric post with a high dielectric constant will not be well modelled using these elements.
- Higher order elements will not be considered as the implementation of these elements is beyond the scope of this project.
- The mesh will have to be very regular. This is a significant drawback as the mesh will need to be fine in regions of the structure where it is unnecessary, thus wasting degrees of freedom and computational resources.

These drawbacks are acceptable as they do not compromise the accuracy of the technique and their implementation will not redirect research effort.

### 2.2.2 The fields within the element

The element used is presented by Jin in [2] and is shown in figure 2.1. The field inside the

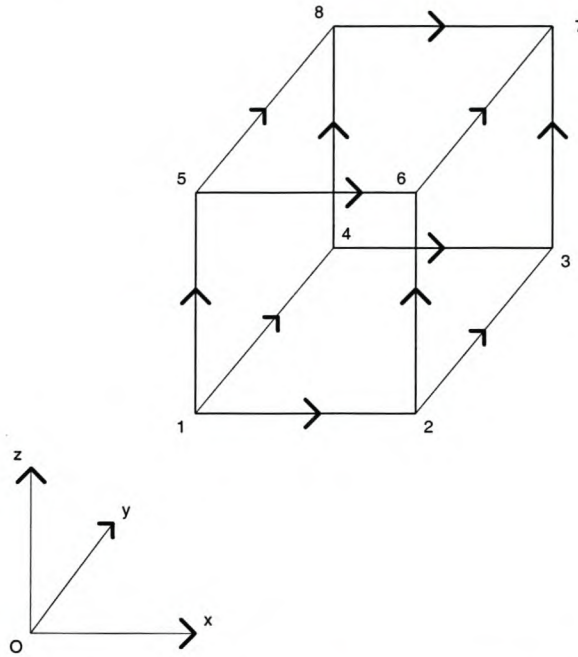


Figure 2.1: The brick element as proposed in [2].

element is given by the sum of 12 basis functions. There are 12 degrees of freedom associated with each element, 4 in each (local) Cartesian direction. Along each edge, the contribution of all of the other basis functions in the same cartesian direction is zero, and the electric field in the specified direction is given by the value of the unknown associated with that edge. Equation 2.6 can be used to calculate the field anywhere in the element or on the surface of the element.

$$\mathbf{E}^e = \sum_{i=1}^{12} \mathbf{N}_i^e E_i^e \quad (2.6)$$

where  $\mathbf{N}_i^e$  are the basis functions and  $E_i^e$  are the unknowns (degrees of freedom) associated with the element. The basis functions are listed in [2], with the subscript  $c$  interpreted as the center of the element in a certain direction and  $l$  the element length in the direction denoted by the subscript, as:

$$\begin{aligned} N_1^e = N_{x1}^e &= \frac{1}{l_y^e l_z^e} \left( y_c^e + \frac{l_y^e}{2} - y \right) \left( z_c^e + \frac{l_z^e}{2} - z \right) \\ N_2^e = N_{x2}^e &= \frac{1}{l_y^e l_z^e} \left( y - y_c^e + \frac{l_y^e}{2} \right) \left( z_c^e + \frac{l_z^e}{2} - z \right) \\ N_3^e = N_{x3}^e &= \frac{1}{l_y^e l_z^e} \left( y_c^e + \frac{l_y^e}{2} - y \right) \left( z - z_c^e + \frac{l_z^e}{2} \right) \\ N_4^e = N_{x4}^e &= \frac{1}{l_y^e l_z^e} \left( y - y_c^e + \frac{l_y^e}{2} \right) \left( z - z_c^e + \frac{l_z^e}{2} \right) \\ N_5^e = N_{y1}^e &= \frac{1}{l_x^e l_z^e} \left( z_c^e + \frac{l_z^e}{2} - z \right) \left( x_c^e + \frac{l_x^e}{2} - x \right) \end{aligned}$$



$$\begin{aligned}
N_6^e &= N_{y2}^e = \frac{1}{l_x^e l_z^e} \left( z - z_c^e + \frac{l_z^e}{2} \right) \left( x_c^e + \frac{l_x^e}{2} - x \right) \\
N_7^e &= N_{y3}^e = \frac{1}{l_x^e l_z^e} \left( z_c^e + \frac{l_z^e}{2} - z \right) \left( x - x_c^e + \frac{l_x^e}{2} \right) \\
N_8^e &= N_{y4}^e = \frac{1}{l_x^e l_z^e} \left( z - z_c^e + \frac{l_z^e}{2} \right) \left( x - x_c^e + \frac{l_x^e}{2} \right) \\
N_9^e &= N_{z1}^e = \frac{1}{l_x^e l_y^e} \left( x_c^e + \frac{l_x^e}{2} - x \right) \left( y_c^e + \frac{l_y^e}{2} - y \right) \\
N_{10}^e &= N_{z2}^e = \frac{1}{l_x^e l_y^e} \left( x - x_c^e + \frac{l_x^e}{2} \right) \left( y_c^e + \frac{l_y^e}{2} - y \right) \\
N_{11}^e &= N_{z3}^e = \frac{1}{l_x^e l_y^e} \left( x_c^e + \frac{l_x^e}{2} - x \right) \left( y - y_c^e + \frac{l_y^e}{2} \right) \\
N_{12}^e &= N_{z4}^e = \frac{1}{l_x^e l_y^e} \left( x - x_c^e + \frac{l_x^e}{2} \right) \left( y - y_c^e + \frac{l_y^e}{2} \right)
\end{aligned} \tag{2.7}$$

These elements are called Constant Tangential/Linear Normal (CT/LN), since the field approximation of the tangential component is constant along each edge and the normal component of the field approximation varies linearly along the edge.

### 2.2.3 Discretization of the functional

The functional is continuous as shown in equation 2.5. In order to evaluate it, it must be discretized. The discretization technique is standard, and can be found in [2]. The electric field at any point in or on the element is given by equation 2.6. The electric field inside the element is seen to be continuous, as a function of the unknowns. The functional can therefore be evaluated analytically (as a function of the unknowns) inside each element. The entire functional can now be approximated by the sum of these contributions. The discretized functional is shown in equation 2.8.

$$\begin{aligned}
F &= \frac{1}{2} \sum_{e=1}^M (\{E^e\}^T [S^e] \{E^e\} - k_0^2 \{E\}^T [T^e] \{E\}) \\
&\quad + \frac{1}{2} \sum_{s=1}^{M_s} \{E^s\}^T [B^s] \{E^s\} - \sum_{s=1}^{M_{s1}} \{E^s\}^T \{b^s\}
\end{aligned} \tag{2.8}$$

where,

$$\begin{aligned}
[S^e] &= \frac{1}{\mu_r} \int \int \int_{V^e} \{\nabla \times \mathbf{N}^e\} \cdot \{\nabla \times \mathbf{N}^e\}^T dV \\
[T^e] &= \epsilon_r \int \int \int_{V^e} \{\mathbf{N}^e\} \cdot \{\mathbf{N}^e\}^T dV \\
[B^s] &= \gamma \int \int_{S_s} \{\hat{n} \times \mathbf{N}^s\} \cdot \{\hat{n} \times \mathbf{N}^s\} dS \\
\{b^s\} &= \int \int_{S_s} \{\hat{n} \times \mathbf{N}^s\} \cdot \{U^{inc} \times \hat{n}\} dS
\end{aligned} \tag{2.9}$$



Note that  $\gamma$  and  $U^{inc}$  have been defined in section 2.1.3.

This function is valid for inhomogeneous media as well as homogenous media. The average element properties must be taken into account at the time of the elemental function evaluation as shown in equation 2.9.

## 2.2.4 Evaluation of the elemental matrices

Section 2.2.3 showed how the problem space can be discretized into elements where the form of the field inside them is known. The results of the analytical evaluation of the integrals for  $[S^e]$  and  $[T^e]$  are given in [2] and presented in this section. The results for  $[B^s]$  and  $\{b^s\}$  are not given and need to be calculated.

The integration can be done analytically, although it is suggested that numerical quadrature be used. Quadrature is already implemented in MATLAB and is almost as efficient as analytic integration. Numerical integration only needs to be done in one cartesian direction for rectangular CT/LN elements, as the variation in the other cartesian direction is constant. The surface integration therefore reduces to a linear integration. The MATLAB built-in quadrature routine is used for the work here.  $\{b\}$  must be determined in the same fashion, however there is a *sine* function inside the integration and the use of analytical integration, while possible, is time consuming and error-prone if done by hand.

The integrals for  $[S^e]$  and  $[T^e]$  are evaluated by substituting equation 2.7 into equation 2.9 and integrating. Since all the basis functions are polynomials, this integration involves differentiation and integration of polynomials only.

$$[S^e] = \begin{bmatrix} S_{xx}^e & S_{xy}^e & S_{xz}^e \\ [S_{xy}^e]^T & S_{yy}^e & S_{yz}^e \\ [S_{xz}^e]^T & [S_{yz}^e]^T & S_{zz}^e \end{bmatrix}$$

where,

$$S_{xx}^e = \frac{l_x^e l_z^e}{6l_y^e} [K_1] + \frac{l_x^e l_y^e}{6l_z^e} [K_2]$$

$$S_{yy}^e = \frac{l_x^e l_y^e}{6l_z^e} [K_1] + \frac{l_y^e l_z^e}{6l_x^e} [K_2]$$

$$S_{zz}^e = \frac{l_y^e l_z^e}{6l_x^e} [K_1] + \frac{l_x^e l_z^e}{6l_y^e} [K_2]$$

$$S_{xy}^e = -\frac{l_z^e}{6} [K_3]$$

$$S_{xz}^e = -\frac{l_y^e}{6} [K_3]^T$$

$$S_{zy}^e = -\frac{l_x^e}{6} [K_3]$$

with,

$$\begin{aligned}
[K_1] &= \begin{bmatrix} 2 & -2 & 1 & -1 \\ -2 & 2 & -1 & 1 \\ 1 & -1 & 2 & -2 \\ -1 & 1 & -2 & 2 \end{bmatrix} \\
[K_2] &= \begin{bmatrix} 2 & 1 & -2 & -1 \\ 1 & 2 & -1 & -2 \\ -2 & -1 & 2 & 1 \\ -1 & -2 & 1 & 2 \end{bmatrix} \\
[K_3] &= \begin{bmatrix} 2 & 1 & -2 & -1 \\ -2 & -1 & 2 & 1 \\ 1 & 2 & -1 & -2 \\ -1 & -2 & 1 & 2 \end{bmatrix}
\end{aligned} \tag{2.10}$$

similarly,

$$[T^e] = \begin{bmatrix} T_{xx}^e & 0 & 0 \\ 0 & T_{yy}^e & 0 \\ 0 & 0 & T_{zz}^e \end{bmatrix}$$

where,

$$[T_{pp}^e] = \frac{l_x^e l_y^e l_z^e}{36} \begin{bmatrix} 4 & 2 & 2 & 1 \\ 2 & 4 & 1 & 2 \\ 2 & 1 & 4 & 2 \\ 1 & 2 & 2 & 4 \end{bmatrix}$$

with,

$$p = x, y, z \tag{2.11}$$

### 2.2.5 Choosing data structures

Choosing effective data structures is important if an efficient program is to be written. The data structures used to prepare this paper are proposed by Davidson in [7]. Not all of the structures proposed in [7] are required as those structures include the capability of further upgrading to higher polynomial order elements. The proposed structures are listed in table 2.1.

### 2.2.6 Mesher

The problem space is discretized using a mesher developed by the author, to allow the input to the program to be parameters of a waveguide structure. This is especially attractive for optimization purposes. Another advantage is that the mesher can generate the geometric information as required by the FE Method. For instance, all the node numbering, edge numbering, element edge ordering etc. is done by the mesher, thus the mesh does not need to be searched for this information.

The mesher is implemented to automatically numbers elements by their global edges and nodes. If an edge is on a PEC boundary (Dirichlet, in this case), the degree of freedom associated with



Table 2.1: The proposed data structures

Structure name	Size	Description
[vertices]	$(N_{nodes}, 3)$	Stores $(x,y,z)$ coordinates of each node in the mesh.
[nodes]	$(N_{elements}, 8)$	Stores the node numbers of the nodes associated with each element. A node number corresponds to a line number in the [vertices] matrix.
[edge_nodes]	$(N_{edges}, 2)$	Stores the numbers of the two nodes that define an edge.
[dof]	$(N_{edges}, 1)$	Stores the global degree of freedom corresponding to each edge.
[materials]	$(N_{elements}, 2)$	Stores the material parameters of the elements. The first column is $\epsilon_r$ and the second is $\mu_r$ .
[el_edges]	$(N_{elements}, 12)$	Stores the global edges numbers associated with each element. This structure is not given in [7], as it can be derived from [nodes] and [edge_nodes]. It is used here as the availability of this matrix simplifies many operations in the code and trades off using fewer loops at the cost of additional memory. This is necessary as the code is implemented in MATLAB and MATLAB is designed to handle matrices and not loops.
[S], [T], [B] and {b}	various	Associated with terms in the discretized functional.

that edge is not assigned. If the edge is not on a PEC boundary, the mesher automatically allocates a global degree of freedom to it.

As a rectangular mesh is limited on how irregular it can be, most of the meshing can be vectorized, thus speeding up the meshing process. Implementing the mesher is not intrinsically complicated and is not discussed further. A brief description of the input required by the mesher is given.

### Information required by mesher

The waveguide is divided into different regions in the direction of propagation ( $x$  direction). Each region can contain a different ‘building block’ for a structure. These ‘building blocks’ can be septums, posts etc. New building blocks can be defined, but must be written into the code. Six parameters are passed to the mesher. They are:



1.  $y\_length$  - The width of the waveguide in the  $y$  direction.
2.  $z\_length$  - The height of the waveguide in the  $z$  direction.
3.  $\{region\_length\}$  - A vector containing the length (in the  $x$  direction) of each region.
4.  $\{max\_edge\_length\}$  - A vector containing the maximum edge length to be used during the discretization of each region (An edge length refers to the length of the edge of an element). Note that the mesh must be regular in the  $yz$  cross sectional plane, and edge length can only be varied between regions in the direction of propagation ( $x$ ). The smallest maximum edge length is used to discretize the  $yz$  cross section.
5.  $\{region\_type\}$  - This vector contains a number identifying it as containing a specific building block. For instance, region type 4 is an air filled waveguide with an inductive pin in it.
6.  $[param]$  - The parameters required by each building block (dimensions etc.) fill a row in this matrix. The number of rows is therefore the number of building blocks.

The region types and parameters that are currently implemented are shown in table 2.2. This algorithm is limited to handling structures that can be defined by the building blocks shown in table 2.2. The FEM formulation is not limited to the same degree. Any building block can be added to the list to extend the capabilities of the algorithm, provided that the FEM formulation as presented includes terms in the functional for these structures. For instance, the addition of an extra building block that defines a radiating structure cannot be added (without extending the FEM formulation), but one that provides a description for the inclusion of dielectric posts can be.

### 2.2.7 Assembling the system matrix

The contributions of each element need to be added together (see section 2.2.3) to form the system matrix. The system matrix in this section refers to the elements remaining after homogenous Dirichlet boundary conditions have been enforced, as in section 2.1.5.

For explanation purposes, a connection scheme is often described that uses a large connection matrix to connect a large matrix of elemental contributions to the system matrix by means of matrix multiplication. In practical codes, more memory efficient techniques are used. One such scheme is presented by Silvester and Ferrari in [3]. This method enlarges the system matrix as new elements are evaluated. A modified version of this technique is used in this algorithm and described for the  $[S]$  matrix only. The scheme is identical for the other matrices.

Initially a zero matrix is made for  $[S]$  with dimensions  $(N_{dof}, N_{dof})$ . This means that all the edges that do not contribute to the derivative of the functional (i.e. unknowns on the PEC boundaries) are not stored. The elemental contribution to the matrix is then calculated as described in section 2.2.4. The resultant elemental contribution is connected to the global degrees of freedom by means of a simple matrix multiplication as outlined in [3].

This method relies on the number of degrees of freedom being known and global numbering assigned prior to execution. This information is available from the mesher. If this information is not available, the full method described in [3] must be implemented.



Table 2.2: Currently implemented 'building block' parameters for the mesher.

Region type	Description	P1	P2	P3	P4	P5
4	An inductive pin in the waveguide, extending from the bottom ( $z = 0$ ) to the top ( $z = z\_length$ ) of the waveguide.	dimension in the $y$ direction	dimension in the $x$ direction	position in the waveguide in the $y$ direction	position in the waveguide in the $x$ direction (measured from the start of the region)	not used
5	An inductive septum in the waveguide, extending from the bottom ( $z = 0$ ) to the top ( $z = z\_length$ ) of the waveguide. The septum is infinitely thin in the $y$ direction.	not used	dimension in the $x$ direction	position in the waveguide in the $y$ direction	position in the waveguide in the $x$ direction (measured from the start of the region)	not used
6	A dielectric block with the bottom coincident with the waveguide bottom ( $z = 0$ ). The block extends to the edges of the region in the $x$ direction.	dimension in the $y$ direction	dimension in the $z$ direction	position in the waveguide in the $y$ direction	dielectric property $\epsilon_r$	dielectric property $\mu_r$

### 2.2.8 Matrix storage

The matrices used by the FE method are inherently sparse. The use of a sparse storage scheme significantly reduces the amount of memory required to store the matrices. MATLAB has sparse functionality built in, with most operators being overloaded to handle these matrices. Many different sparse storage schemes are available, with libraries of operators for various programming languages.

MATLAB stores all variables in double precision, thus increasing memory requirements. New variables can be defined in single precision, but then overloaded operators for these variables



will have to either be obtained or written. This drawback limits the size of problem that can be solved.

### 2.2.9 Matrix solution

The discretized functional is given in equation 2.8. This equation can also be written with  $\{E\}$  being the vector of global unknown degrees of freedom, after the summation shown in equation 2.8, in a shorthand form as,

$$F = ([S] - k_0^2[T] + [B])\{E\} - \{b\} \quad (2.12)$$

The partial derivative of this functional with respect to each global degree of freedom (Ritz procedure), is set to 0. The result can be written as

$$([S] - k_0^2[T] + [B])\{E\} = \{b\} \quad (2.13)$$

If this matrix equation is solved for  $\{E\}$ , the solution of the system is found.

Traditionally, linear equations were solved using full matrix inversion. The first and most significant drawback of this method is that the inverse of a sparse matrix is potentially densely populated. Thus the memory requirements are dominated by the space required to store the inverse and not the system matrix. Another disadvantage is that matrix inversion is an  $\mathcal{O}(N^3)$  computation. For an extensive discussion on computation times, see section 3.5.

Iterative solvers have been developed to reduce the computational drawbacks of using matrix inversion. Iterative solvers generally require less memory than full inversion, as the sparse nature of the matrices is preserved. The length of time required varies from solution to solution, as the solvers terminate on a solution tolerance condition. The speed at which the solution is approached depends on the convergence of the system. A comparison between different iterative solvers can be found in [8]. MATLAB already incorporates most of these solvers. The Bi-conjugate gradient solver is preferred, as it uses limited storage [8]. Pre-conditioning the system matrix can improve the efficiency of the iterative solver by improving the convergence rate of the iterative method [8]. These pre-conditioners were briefly investigated but not used, as severely slowly converging solutions were not encountered.

The entire process has to be repeated at each frequency of interest. Note that the  $[S]$  and  $[T]$  matrices are independent of frequency and do not need to be re-calculated.  $[B]$  and  $\{b\}$  are dependent on frequency and need to be re-calculated. The integration of  $[B]$  and  $\{b\}$  is not necessary at each frequency as the frequency dependant term is a coefficient to the integration.

### 2.2.10 Calculating observables

Once system matrix has been solved and a vector  $\{E\}$  has been obtained, the system observables can be calculated as follows. The  $\{E\}$  vector contains the coefficients of the basis functions for the element (see section 2.2.2). For waveguide problems, the required output is usually in the form of two-port scattering parameters. Since the system is lossless and only reciprocal media are used, the parameters are symmetrical and thus only a reflection ( $R$ ) and transmission ( $T$ ) coefficient are required to be calculated.



Since the dominant waveguide mode is orthogonal to all other modes, and the magnitude and form of the dominant mode is known, the scalar product between the field at the port and the form of the dominant mode can be integrated over the surface of the port [2]. This removes the influence of higher order modes on the calculation of  $R$  and  $T$ . The result can then be normalized by the magnitude of the impressed mode and the area of the port. The dominant (impressed) mode is given by  $E_0 \mathbf{e}_{10}(y, z)$ . The continuous form of these equations is:

$$R = S_{11} = \frac{2}{y_l z_l E_0} \int \int_{S_1} \mathbf{E}(0, y, z) \cdot \mathbf{e}_{10}(y, z) dS - 1$$

and

$$T = S_{12} = \frac{2}{y_l z_l E_0} \int \int_{S_2} \mathbf{E}(x_{length}, y, z) \cdot \mathbf{e}_{10}(y, z) dS \quad (2.14)$$

Note that these equations have been modified to set the phase at the first port at zero, unlike the equations presented in [2]. These equations now need to be discretized in the same way as presented in section 2.2.3. The integral is evaluated using numerical quadrature instead of the analytic solution.

## 2.3 Validation

The FEM formulation has been shown in section 2.1 and the issues surrounding the implementation of the FEM discussed in section 2.2. This implementation needs to be validated against previously published results. Two waveguide problems are presented as validation, the first is a two-pole filter and the second is a dielectric loaded waveguide. The comparison of the FEM results and those obtained by other methods agree well.

### 2.3.1 Two-pole filter

The two-pole narrow-band wave guide, as designed by Meyer in [9], is used as the first validation example. Using this filter, the code is validated against measurements and an independent FEM solver. The independent solver used for validation is FEMFEKO, another code under development at the University of Stellenbosch.

The filter is a narrow bandpass filter at 10.45 GHz in standard X-band waveguide. The filter has three inductive septums in it. The inductive septa are 0.2mm thick in the wide plane of the waveguide and extend from the top to the bottom of the waveguide. They are positioned along the centreline of the waveguide in the wide plane. Figure 2.2 shows the dimensions of the filter in a cross section through the narrow side of the waveguide. The septa are modelled as being infinitely thin in the FEM model. The measured data is obtained from [9]. The FEMFEKO result is obtained with 4 968 tetrahedral Quadratic Tangential/Quadratic Normal (QT/QN) elements, resulting in 41 526 degrees of freedom.

The result obtained using this implementation has 13 990 degrees of freedom. The larger the number of degrees of freedom, the more accurate the solution that is obtained. The graph shown in figure 2.3 clearly shows that this implementation works, with a slight shift in center

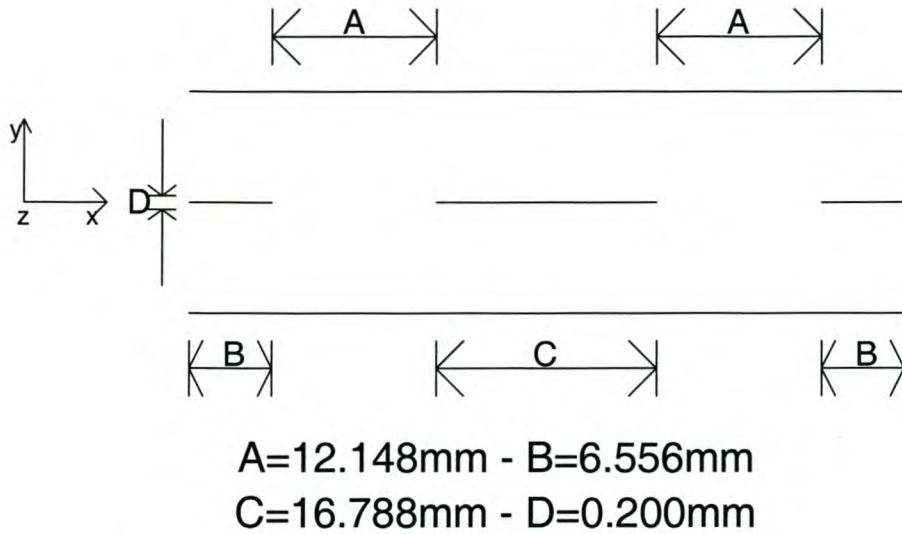


Figure 2.2: The dimensions of the two-pole filter.

frequency. This shift could be reduced by increasing the discretization. A frequency shift is a typical error in FE algorithms, as a result of dispersion. The manufacturing tolerance of the filter is not specified, and the accuracy of the measurement cannot be determined.

### 2.3.2 Dielectric loaded waveguide

Ise et al. [10] implemented a FEM solver using brick edge based elements. One of the example solutions is of a dielectric load,  $\epsilon_r = 6$ , positioned on the lower face of a waveguide. The waveguide has an aspect ratio of 2:1. The geometry is shown in figure 2.4. The waveguide height is  $b$ , the width is  $2b$  and the length is  $2.4b$ . The load is symmetrically located in the wide- $(\hat{y})$  and long  $(\hat{x})$ - planes of the waveguide. The block is  $0.888b$  wide,  $0.8b$  long and  $0.399b$  high. This problem is also solved using FEMFEKO [6], with results comparable to those of Ise et al.

The problem is meshed with 5 850 elements, resulting in 16 812 degrees of freedom. The solution is obtained at 21 frequency points. The results are plotted against normalized wavenumber,  $k_0b$ . The solution shown in figure 2.5 is obtained.

## 2.4 Conclusion

This Chapter has shown the theory and implementation of a FEM algorithm. The algorithm was validated against measurements and results from independent algorithms. A comparison between these results showed that accurate results are obtained. A slight (approximately 0.5%) frequency shift is noticed. This is a typical result of a FEM algorithm, and can be improved by either a finer mesh and/or higher order elements.



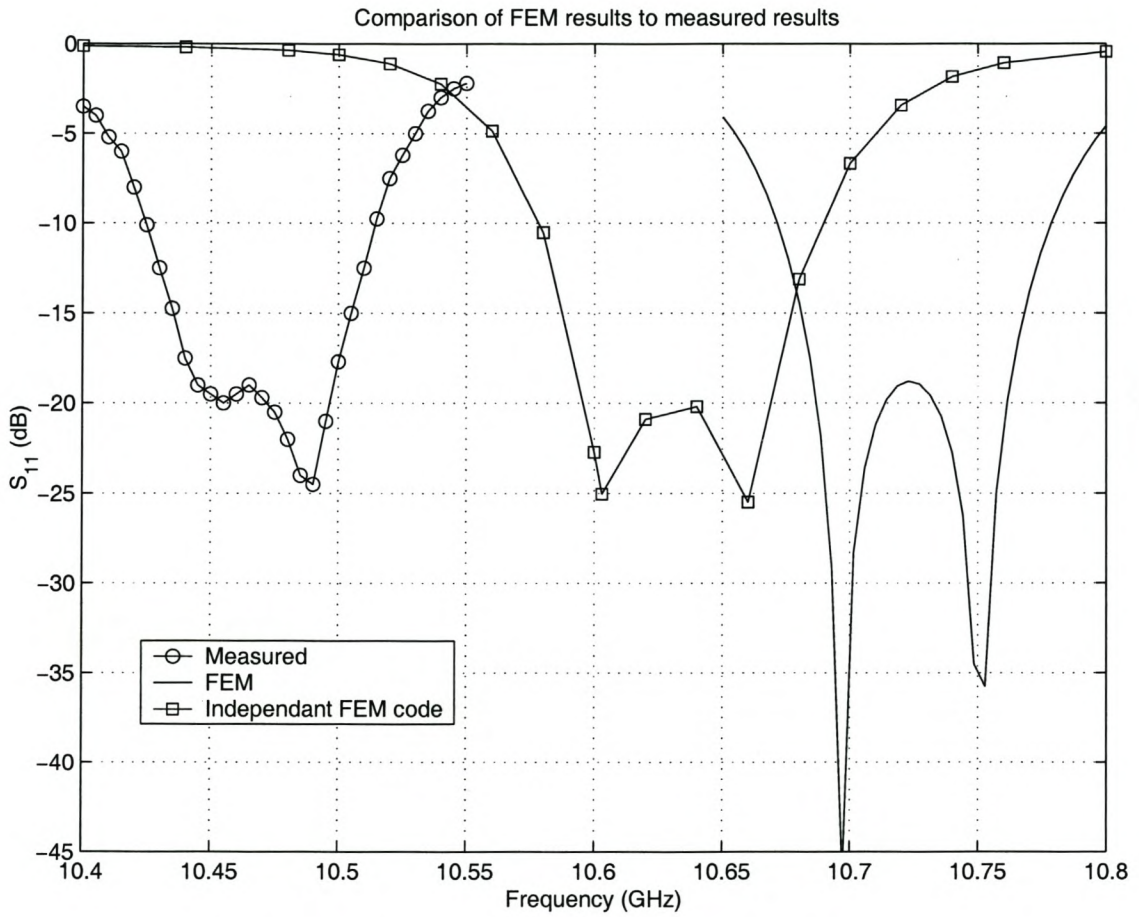


Figure 2.3: The reflection coefficient of the two-pole filter.

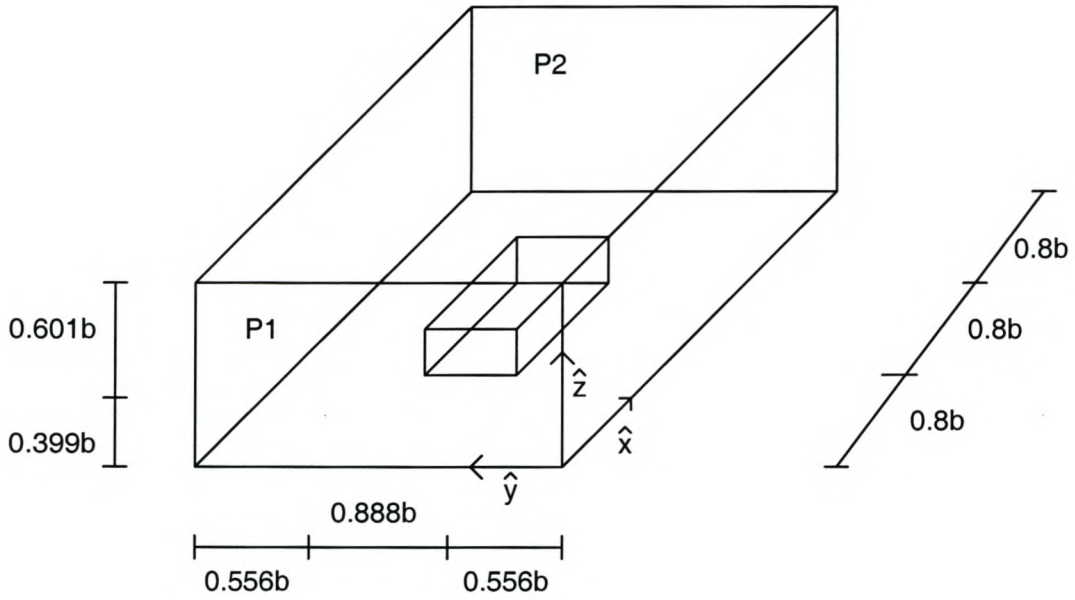


Figure 2.4: The dimensions of the dielectric loaded waveguide.

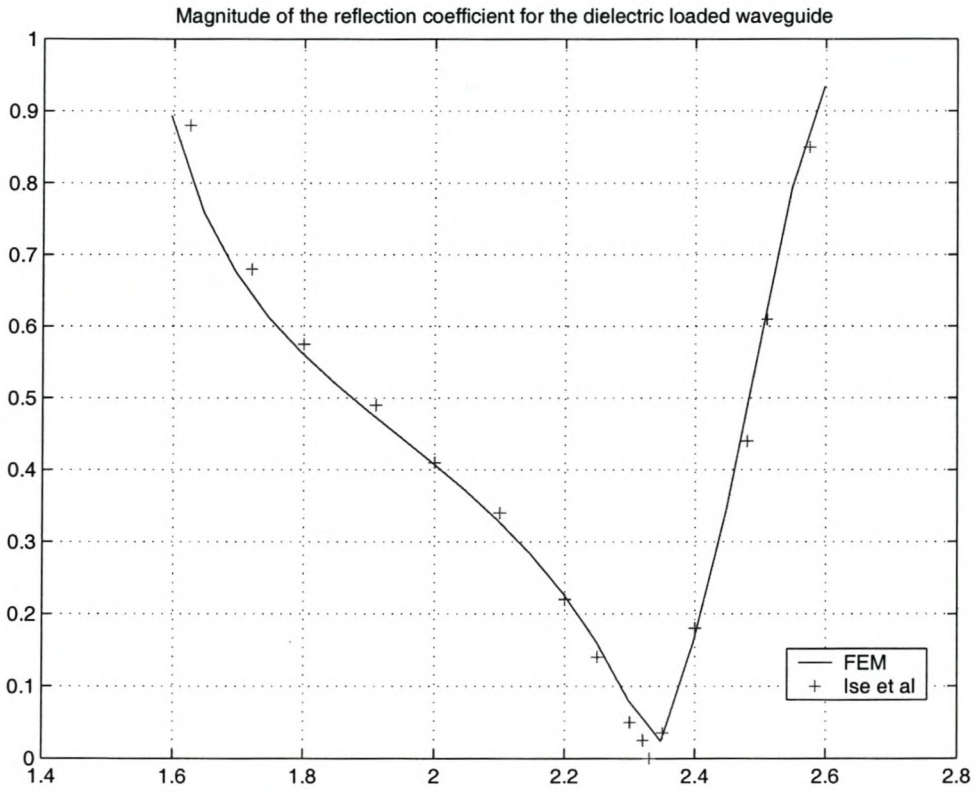


Figure 2.5: The reflection coefficient results for the dielectric loaded waveguide.



## Chapter 3

# Fast Frequency Techniques

The FE method presented thus far is solved at specific frequencies. It is often desirable to have a response as a function of frequency. The full FE method needs to be solved at each discrete frequency of interest. Each solution of the FE method is potentially an  $\mathcal{O}(N^3)$  operation (see section 3.5). Fast Frequency (FF) Techniques are used in an attempt to reduce the computational cost of these solutions. These techniques generally attempt to generate reduced order models. This is known as model order reduction (MOR). These models can then be solved inexpensively at multiple frequencies.

The published MOR techniques can be grouped together into two main categories; those that generate a model of the FE unknowns and those that generate a model of the observables. The naming convention of MOR techniques is not clear, as there are many hybrids of the same techniques. Where possible, the names used most frequently in literature are used in this document.

Three MOR techniques are presented in this chapter. Asymptotic waveform evaluation (AWE) reduces the order of the model by taking a Taylor expansion of the set of linear equations that are used to obtain the FEM solution (equation 2.13). The Taylor expansion provides an accurate solution of the linear equations in a region around the expansion point. This technique is discussed in more detail in section 3.2.

Model based asymptotic waveform evaluation (MB-AWE) is then presented. This technique is an extension of the AWE technique. The Taylor coefficients obtained using AWE are mapped onto a fitting model in an attempt to enlarge the region of accuracy of the model. MB-AWE is presented in section 3.3

Finally, model based parameter estimation (MBPE) is presented. This technique differs significantly from the previous two. The observables (typically S-parameters) are sampled and interpolated using a model fitting function. The model parameters can either be calculated using samples of the parameter, or derivatives of the same. The formulation used and the results obtained using these techniques are presented in section 3.4.

### 3.1 A note on fitting models used

All the model based techniques rely on a mathematical model of the function. This model can be derived physically or otherwise. This inclusion of physical information into the solution results in an accurate reduced order model. Miller [11] presents models for several typical EM problems. It is suggested that a series of complex poles and zeros is used to model field variables in EM problems, as a function of frequency, because such series are often found in the solutions of the differential equations found in EM problem descriptions.

The use of rational functions of polynomial numerators and denominators is also called a Padé approximation.

The success of any model based technique is heavily dependant on the model chosen. All the work presented here uses the model suggested by the relevant literature, and no new models are developed.



## 3.2 Asymptotic Waveform Evaluation

Asymptotic Waveform Evaluation (AWE) has been presented as a MOR technique [12, 13, 14, 15, 16, 17, 18, 19, 20, 21, 22, 23, 24] for EM analysis.

AWE uses spectral solutions of a linear system to approximate the system transfer function [12]. AWE is presented here for FEM analysis of waveguide structures. Note that this technique produces a reduced order model for the degrees of freedom and not for the system observables.

### 3.2.1 AWE formulation

The first step in AWE is to write the linear equation as a polynomial function of frequency. Each term in the equation is then written as a Taylor series about a specified frequency point. The Taylor series coefficients are then equated using moment matching. The Taylor coefficients for the series corresponding to the unknown vector can be solved for. The process is shown in both [13] and [12] and only a summary is presented here.

The application of the FEM, as formulated in chapter 2, results in set of linear equations (equation 2.13)

$$([S] + [B] - k_0^2[T])\{E\} = \{b\}$$

Neither the  $[S]$  nor the  $[T]$  matrices are functions of frequency.  $[B]$  and  $\{b\}$  need to be written with the frequency dependance clearly shown. From the integrals presented in equation 2.9 it should be clear that  $[B]$  and  $\{b\}$  can be rewritten as:

$$\begin{aligned} [B] &= k_{x10} \left( j \int \int_{S^s} \{\hat{n} \times \mathbf{N}^s\} \cdot \{\hat{n} \times \mathbf{N}^s\} dS \right) \\ &= k_{x10} [B'] \end{aligned}$$

and

$$\begin{aligned} \{b\} &= k_{x10} \left( \int \int_{S^s} \{\hat{n} \times \mathbf{N}^s\} \cdot \{(-2j\mathbf{E}^{inc} \times \hat{n})\} dS \right) \\ &= k_{x10} \{b'\} \end{aligned} \tag{3.1}$$

where  $k_{x10}$  is the waveguide wavenumber given by [25]

$$k_{x10} = \sqrt{k_0^2 - \left( \frac{\pi}{y_{length}} \right)^2} \tag{3.2}$$

Equation 2.13 can now be rewritten as:

$$([S] + k_{x10}[B'] - k_0^2[T])\{E\} = k_{x10}\{b'\} \tag{3.3}$$

When calculating the Taylor series coefficients of equation 3.3, the derivatives of equation 3.2 need to be taken. The calculation of these derivatives is lengthy and error prone. A linear approximation of  $k_{x10} / k_0$  relationship was thus investigated. If AWE is used as a MOR technique for method of moments (MoM) or finite element-boundary integral (FE-BI) solutions, all matrices are functions of the free space wavenumber. The derivatives of equation

3.2 need not be taken in these cases. The approach presented here was not found in the available literature. Equation 3.2 is written as:

$$k_{x10} \approx (mk_0 + c) \quad (3.4)$$

Both the linear and the approximate relationship between  $k_{x10}$  and  $k_0$  is plotted in figure 3.1. The difference between the approximations is shown in figure 3.2. The linear approximation resulted in a maximum error of 7% over a 40% bandwidth. The Taylor series is known to only provide a convergent series for a finite radius around the expansion point. It is expected that the Taylor series will show a divergence before the error in the approximation becomes significant. If wide-band accuracy is available from a single expansion point, further orders can be added to the polynomial approximation, or even analytical derivatives used. This will only be possible for frequencies far from system poles.

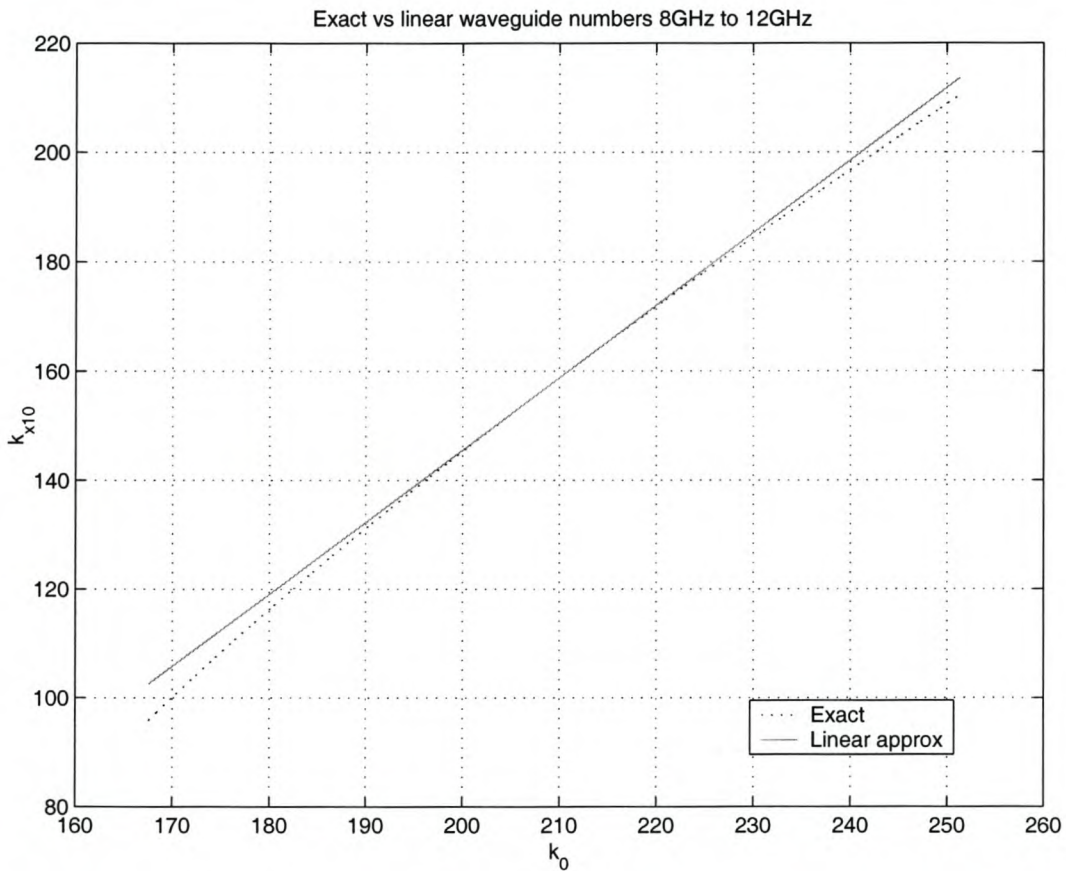
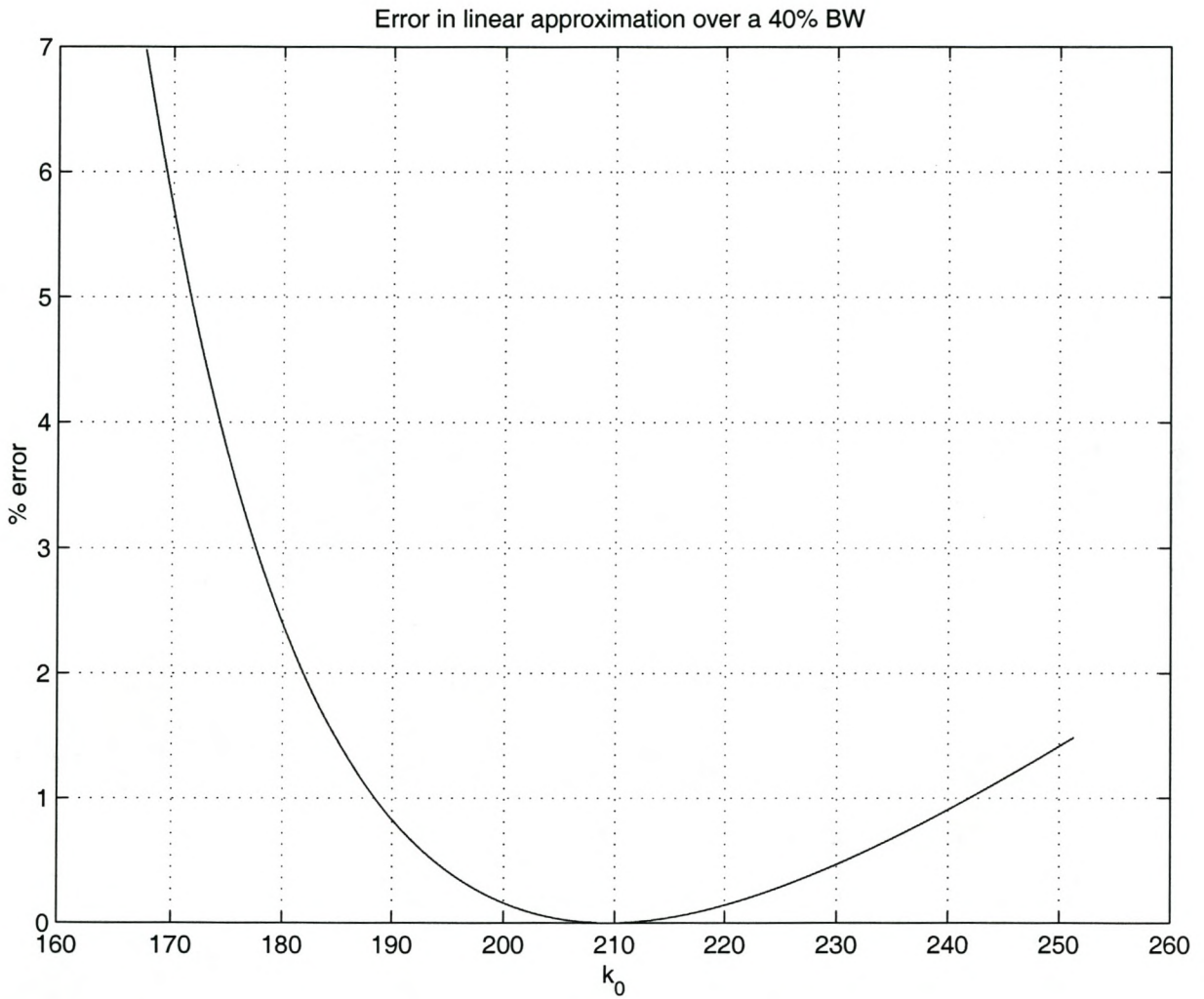


Figure 3.1:  $k_{x10}$  vs.  $k_0$



Figure 3.2: Error in linear approximation of  $k_{x10}$

Using this relationship between  $k_{x10}$  and  $k_0$ , equation 3.3 can be rewritten in the following form:

$$\begin{aligned} ([S] + (mk_0 + c)[B'] - k_0^2[T])\{E\} &= (mk_0 + c)\{b'\} \\ \text{or,} \\ ([A_0] + k[A_1] + k^2[A_2])\{E\} &= (mk + c)\{f\} \end{aligned} \quad (3.5)$$

where,

$$\begin{aligned} [A_0] &= [S] + c[B'] \\ [A_1] &= m[B'] \\ [A_2] &= -[T] \\ \{f\} &= \{b'\} \end{aligned}$$

Equation 3.5 is now in a form similar to the form given in [12]. The only difference is the constant factor in the excitation vector. This difference should only affect the constant term, as the first derivative of the constant factor is zero. The calculation of the first two terms is shown in Appendix A and proves just that. The resulting Taylor coefficients for the unknown vector  $\{E\}$ , around expansion point  $k_{cent}$ , are given by:

$$\begin{aligned} \{E_0\} &= [\bar{A}_{cent}]^{-1}(mk_{cent} + c)f \\ \{E_1\} &= [\bar{A}_{cent}]^{-1}(mf - [A_1]\{E_0\} - 2k_{cent}[A_2]\{E_0\}) \\ \{E_2\} &= -[\bar{A}_{cent}]^{-1}([A_1]\{E_1\} + [A_2](\{E_0\} + 2k_{cent}\{E_1\})) \\ &\vdots \\ \{E_n\} &= -[\bar{A}_{cent}]^{-1}([A_1]\{E_{n-1}\} + [A_2](\{E_{n-2}\} + 2k_{cent}\{E_{n-1}\})) \end{aligned}$$

where,

$$[\bar{A}_{cent}] = ([A_0] + k_{cent}[A_1] + k_{cent}^2[A_2]) \quad (3.6)$$

The solution vector can now be computed at frequencies other than  $k_{cent}$  by substituting the Taylor coefficients into the Taylor series, obtaining:

$$\begin{aligned} \{E\} &= \{E_0\} + (k - k_{cent})\{E_1\} + (k - k_{cent})^2\{E_2\} + \dots \\ &\quad + (k - k_{cent})^n\{E_n\} + O\{(k - k_{cent})^{n+1}\} \end{aligned} \quad (3.7)$$

## 3.2.2 AWE implementation issues

Before the formulation presented in Section 3.2.1 is implemented into the code, several issues need to be addressed. These issues and their implications are discussed in this section.

### 3.2.2.1 Approximate linear mapping of the free space wavenumber to the waveguide wave number

As shown in section 3.2.1, the formulation as presented, requires the waveguide wavenumber to be written as a linear function of the free space wavenumber. This linearization can be



implemented in a variety of manners.

The first possibility is to calculate the linear coefficients for the entire bandwidth once and use them in all solutions regardless of frequency. In this calculation there is an inherent error based on the location of the frequency window of interest and has thus not been utilized.

A second possibility is to calculate the exact wave numbers at the extremities of the frequency window of interest and to calculate the linear coefficients from the line connecting these two points. This idea is discarded as there is no error at the extremities of the frequency window and the largest error in the center of the window.

The third, and ultimately chosen, method would be to calculate the linear coefficients at the same frequency as the expansion point of the Taylor series. This means that there is no error in either approximation at this frequency and the error contribution from both approximations increases as further frequency points are evaluated. This is the most meaningful method, as the least error from the linearization is in the convergence radius of the Taylor series.

### 3.2.2.2 Matrix inversion

Equation 3.6 shows that full matrix inversion must be used to calculate the Taylor coefficients. This is computationally expensive ( $\mathcal{O}(N^3)$ , see section 3.5) and memory inefficient.

It is however noticed that by pre-multiplying both sides of equation 3.6 by  $[\bar{A}_{cent}]$ , the Taylor moments can be solved for iteratively. This is once again potentially an  $\mathcal{O}(N^3)$  computation. However, the memory expense is saved, as the full inverse is never calculated. The disadvantage of this method is that the iterative solution needs to be repeated for each moment of the Taylor series (each  $\{E_n\}$  in equation 3.6). If the inverse had been calculated, each additional moment requires only a matrix multiplication. The iterative solution is used for the results presented here.

### 3.2.2.3 Order of the Taylor series expansion

Initially, as the order of the Taylor series expansion is increased, the convergence region of the approximation increases. After a certain number of terms in the series this no longer happens. Zhang et al. [13] suggest testing the linear dependance of the moments and to stop adding moments when the moments become linearly dependant. Alternatively, the number of moments can be chosen arbitrarily for an investigation of this nature. All the results presented here used seven moments. Bracken et al. [24] suggest using 10 to 20 moments. However, the formulation presented in [24] uses the full inverse, and the calculation of additional moments is not computationally expensive.

## 3.2.3 AWE results

Results for the AWE implementation are shown below. Three structures were used to test the algorithm. The first is a single inductive septum in a piece of X-band waveguide and the second is a single pole filter, also in X-band waveguide. The last is the two-pole filter already presented

in section 2.3.1.

Solution run-times are not given, as they are highly dependant on the system used to run them and on what background tasks that system has running. The evaluation of the computational complexity of the FF techniques is shown in section 3.5.

The characteristic convergence radius of the Taylor series is apparent in all the results. For the single inductive septum, relatively wide band results are obtained using the same number of moments as the two filters. The reason for this is that the system poles are closer to the expansion points for the filter structures.

### 3.2.3.1 Single Inductive septum

The geometry is very simple. An inductive septum in the center of a 58.7 mm long piece of X-band waveguide. The septum is 9.7 mm long and extends from the bottom of the waveguide to the top of the waveguide.

This problem is meshed into 672 elements, corresponding to 1 560 degrees of freedom. The FEM is used to solve the system at 41 frequency points between 8 and 9 GHz. The AWE technique is used to obtain the system solution at 81 frequency points in the same frequency window. The Taylor series is calculated with seven coefficients about 8.5 GHz. This means that seven sets of linear equations need to be solved.

In terms of execution time, AWE is far superior to solving the system at discrete frequency points. From figure 3.3 it is clear that one expansion point (seven linear equation solutions) is almost sufficient for the entire band. The convergence radius of the Taylor series can clearly be seen by looking at the sum of the magnitudes of the reflection and transmission coefficients. For lossless structures,  $|S_{11}|^2 + |S_{12}|^2 = 1$ . When this identity does not hold, the solution has non-physical behavior and is therefore invalid. Unfortunately, the converse is not true i.e. if the identity holds, it does not mean that the solution is guaranteed to be accurate.



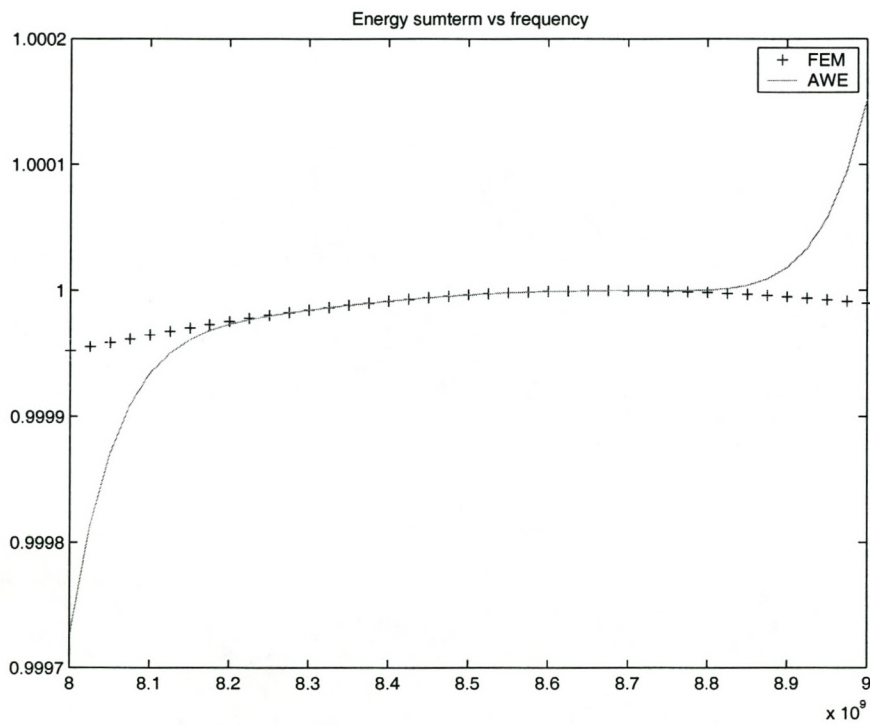


Figure 3.3: The sum of the squares of the magnitudes of the reflection and transmission coefficients for a single inductive septum: comparison of FEM and AWE results.

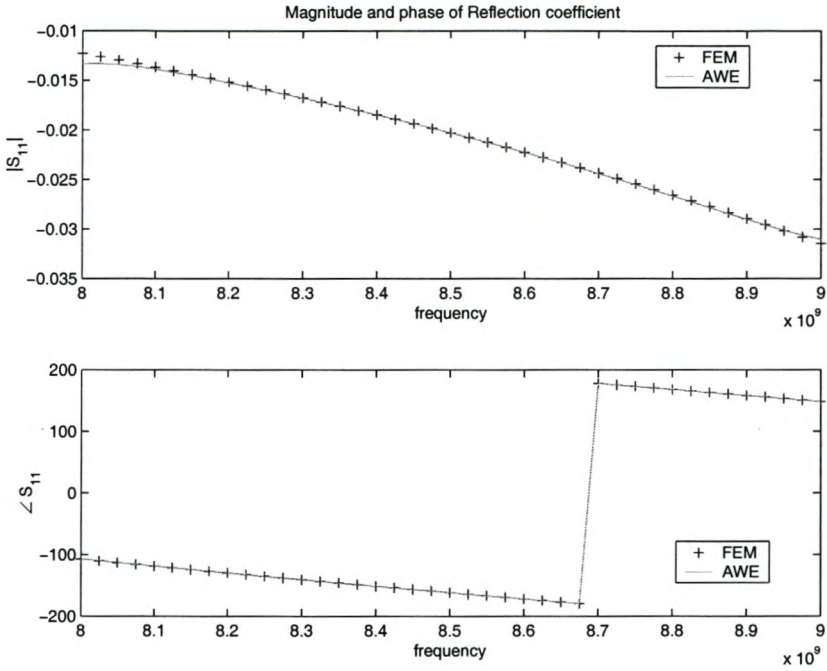


Figure 3.4: Reflection coefficient of the single inductive septum: comparison of FEM and AWE results.

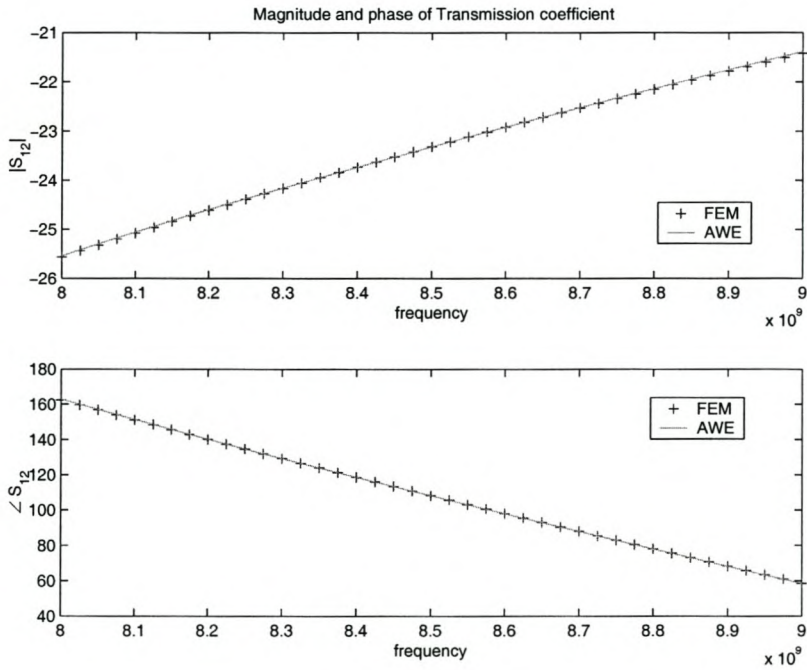


Figure 3.5: Transmission coefficient of the single inductive septum: comparison of FEM and AWE results.



### 3.2.3.2 Single pole filter

The dimensions of the filter are shown in figure 3.6. This problem space is meshed into 1 800

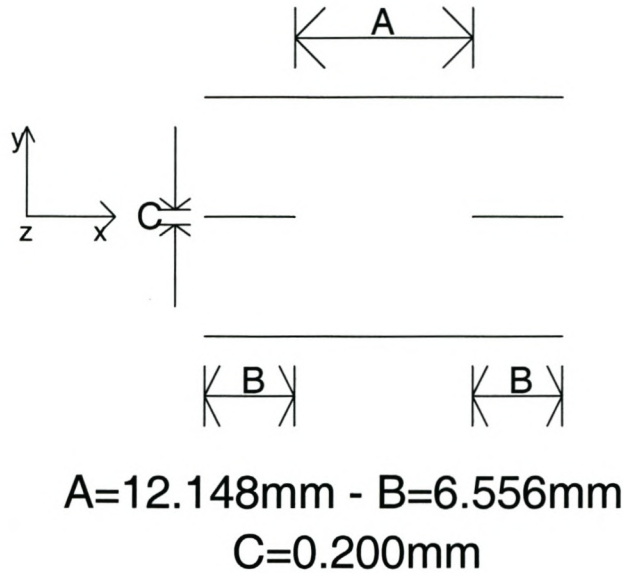


Figure 3.6: The dimensions of the single pole filter.

elements, corresponding to 4 449 degrees of freedom. The FEM is used to solve the system at 31 frequency points between 10.75 and 10.85 GHz. The AWE technique is used to obtain the system solution at 51 frequency points in the same frequency window. The Taylor series is calculated about 10.78 GHz.

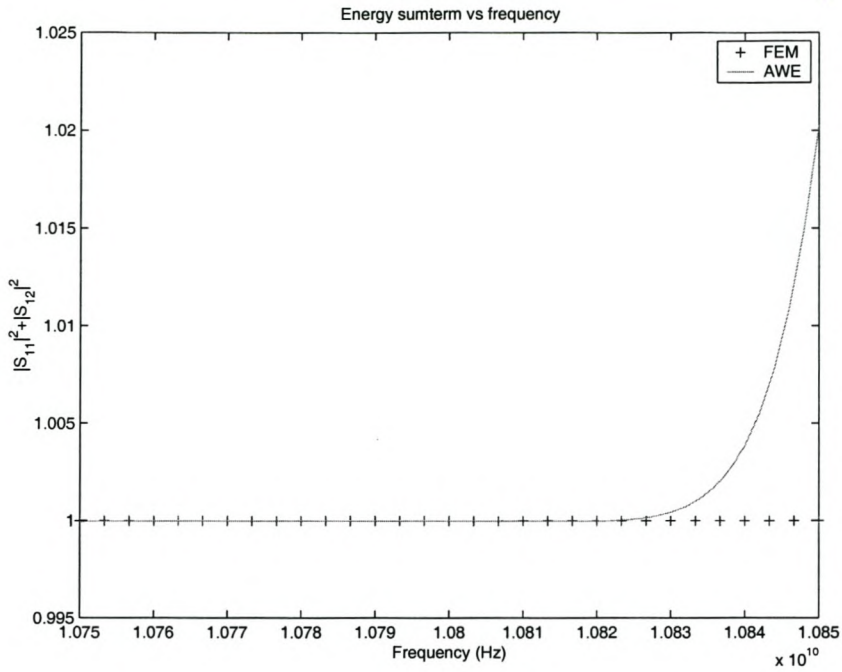


Figure 3.7: The sum of the squares of the magnitudes of the reflection and transmission coefficients for the single pole filters: comparison of FEM and AWE results.

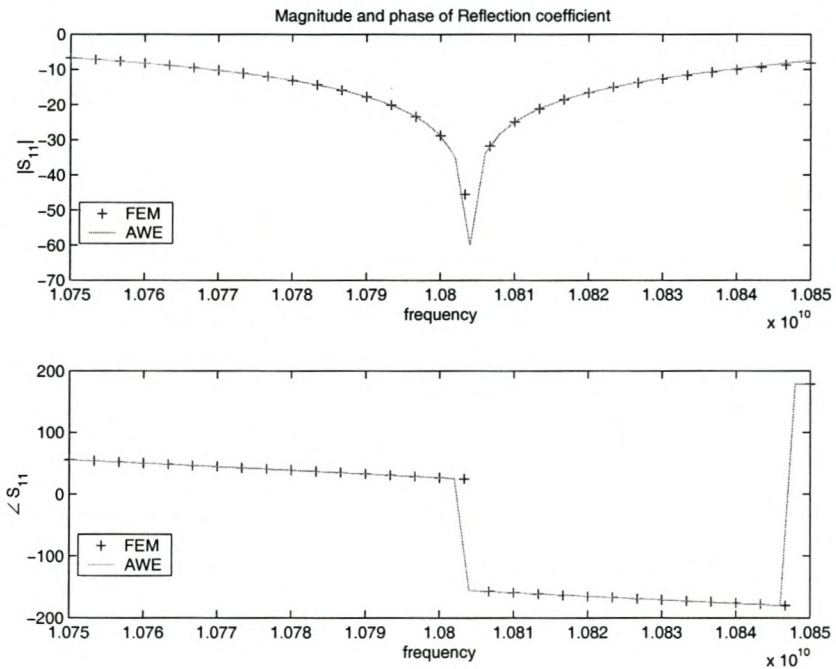


Figure 3.8: Reflection coefficient of the single pole filter: comparison of FEM and AWE results.



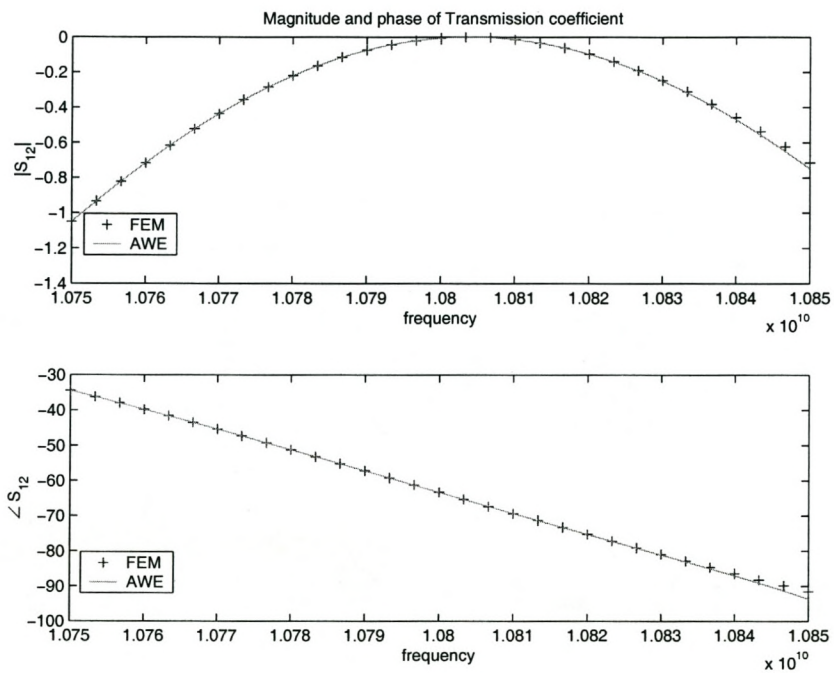


Figure 3.9: Transmission coefficient of the single pole filter: comparison of FEM and AWE results.

### 3.2.3.3 Two pole filter

The geometric description of the filter has been provided in section 2.3.1.

This problem space is meshed into 3 000 elements, corresponding to 7 312 degrees of freedom. The FEM is used to solve the system at 31 frequency points between 10.65 GHz and 10.95 GHz. The AWE technique is used to obtain the system solution at 61 frequency points in the same frequency window. The Taylor series is calculated about 10.8 GHz.

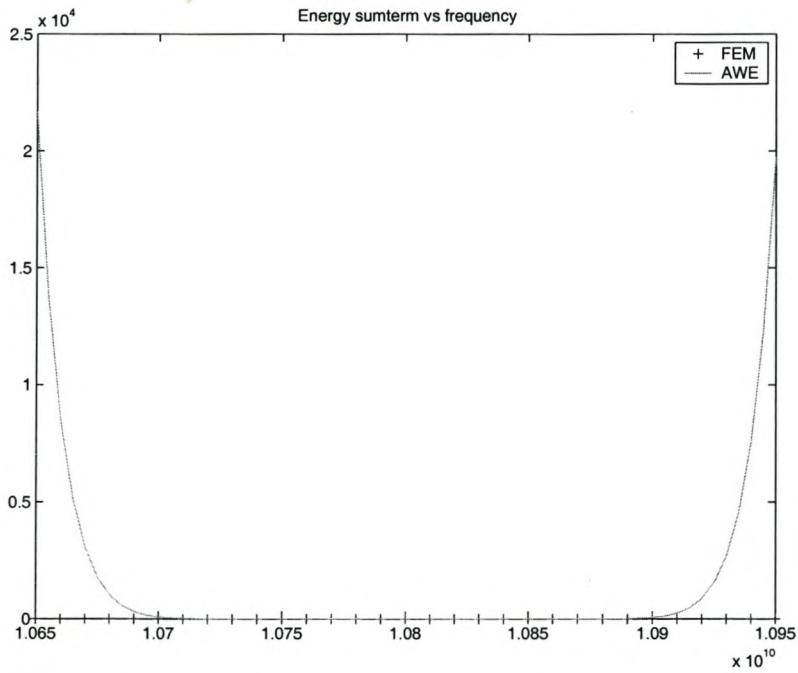


Figure 3.10: The sum of the squares of the magnitudes of the reflection and transmission coefficients for the two pole filter: comparison of FEM and AWE results.



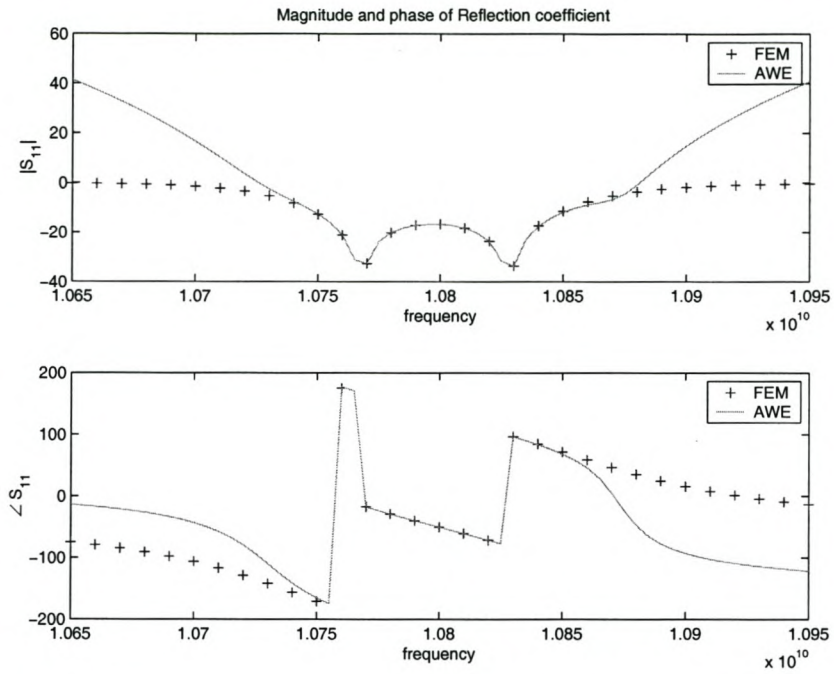


Figure 3.11: Reflection coefficient of the two pole filter: comparison of FEM and AWE results.

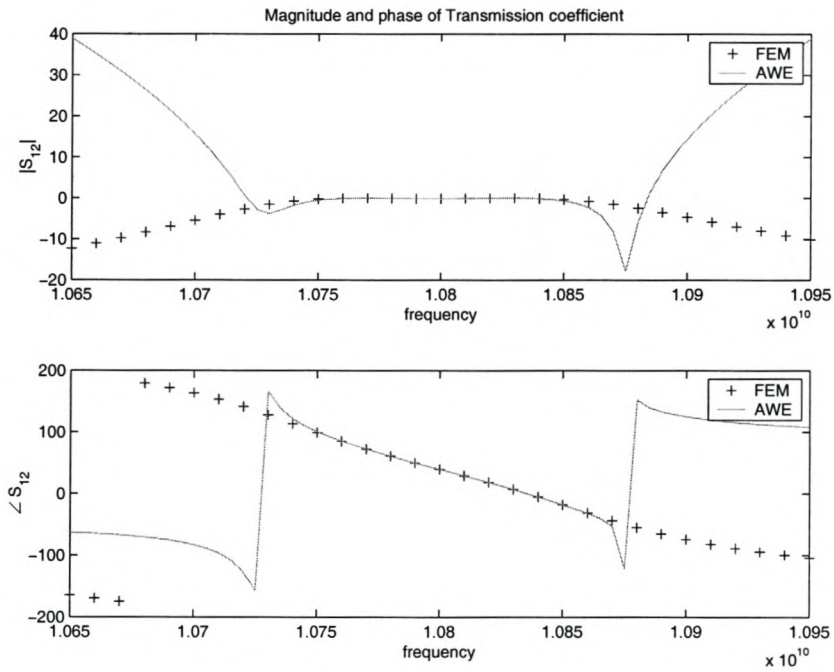


Figure 3.12: Transmission coefficient of the two pole filter: comparison of FEM and AWE results.

### 3.3 Model Based Asymptotic Waveform Evaluation

MB-AWE improves on AWE by taking the spectral solutions and mapping them onto a fitting model. A Padé model is proposed by [12, 13, 14, 15, 18, 19, 20, 21, 22, 23, 24, 26]. Note that, as with AWE, the technique obtains a reduced order model for the degrees of freedom and not the observables.

#### 3.3.1 MB-AWE formulation

The central idea behind this method is that a polynomial fitting function, with its coefficients calculated in the convergent region of the AWE solution (at the expansion point), will be a better model outside of this convergent region of the Taylor series. The choice of fitting function is therefore not arbitrary and should be chosen to model the expected behavior of the degrees of freedom. All the papers referenced above suggest that the applicable model is a Padé model. No references were found that suggest any other model. The Padé model is implemented here. Note that the Padé model is equivalent to the Taylor series if the order of the denominator is chosen as 1.

The formulation presented here follows the presentation in [14] quite closely. The AWE formulation from section 3.2 results in a solution vector of the form (see equation 3.7):

$$\{E(k)\} = \sum_{n=0}^Q \{E_n\} (k - k_{cent})^n \quad (3.8)$$

A Padé fitting model is given by:

$$\{E(k)\} = \frac{\sum_{i=0}^L a_i (k - k_{cent})^i}{1 + \sum_{j=0}^M b_j (k - k_{cent})^j} \quad (3.9)$$

with  $Q = L + M + 1$ . Equating these two equations, the coefficients ( $a_i$  and  $b_j$ ) can be found by solving:

$$\begin{bmatrix} E_L & E_{L-1} & E_{L-2} & \dots & E_{L-M+1} \\ E_{L+1} & E_L & E_{L-1} & \dots & E_{L-M+2} \\ E_{L+2} & E_{L+1} & E_L & \dots & E_{L-M+3} \\ \vdots & \vdots & \vdots & \ddots & \vdots \\ E_{L+M-1} & E_{L+M-2} & E_{L+M-3} & \dots & E_L \end{bmatrix} \begin{bmatrix} b_1 \\ b_2 \\ b_3 \\ \vdots \\ b_M \end{bmatrix} = - \begin{bmatrix} E_{L+1} \\ E_{L+2} \\ E_{L+3} \\ \vdots \\ E_{L+M} \end{bmatrix} \quad (3.10)$$

$$a_i = \sum_{j=0}^i b_j E_{i-j} \quad 0 \leq i \leq L$$

The system degrees of freedom can then be determined at other frequencies by substituting these coefficients into equation 3.9.

The choice of  $L$  and  $M$  needs to be made. Reddy et al. suggest in [15] that for a fixed value of  $L + M$ , the error is the smallest when  $L = M$  or  $L = M + 1$ . The AWE technique is implemented in section 3.2 for a seventh order expansion. The same implementation can be used to calculate the Padé approximation with  $L = M = 3$ .



### 3.3.2 MB-AWE implementation issues

This implementation of this technique is elementary, provided that the AWE technique has been successfully implemented. The only issue that needs addressing is the solution of equation 3.10. The equation as written has a matrix of vectors multiplied by a vector of vectors equal to a vector of vectors (each degree of freedom has its own expansion). The correct way to implement this code is to solve the equation for each degree of freedom. This means that equation 3.10 needs to be solved for each degree of freedom that is required to calculate an observable. This equation requires (in this case) the solution of three simultaneous linear equations which is a computationally trivial task.

### 3.3.3 MB-AWE results

The same models used in section 3.2.3 are used in this section. The geometric and model information is not duplicated here. Only the results are given. The results show that the radius of convergence for the MB-AWE technique is actually smaller than that of the AWE technique. This is discussed in section 3.3.4.

#### 3.3.3.1 Single Inductive septum

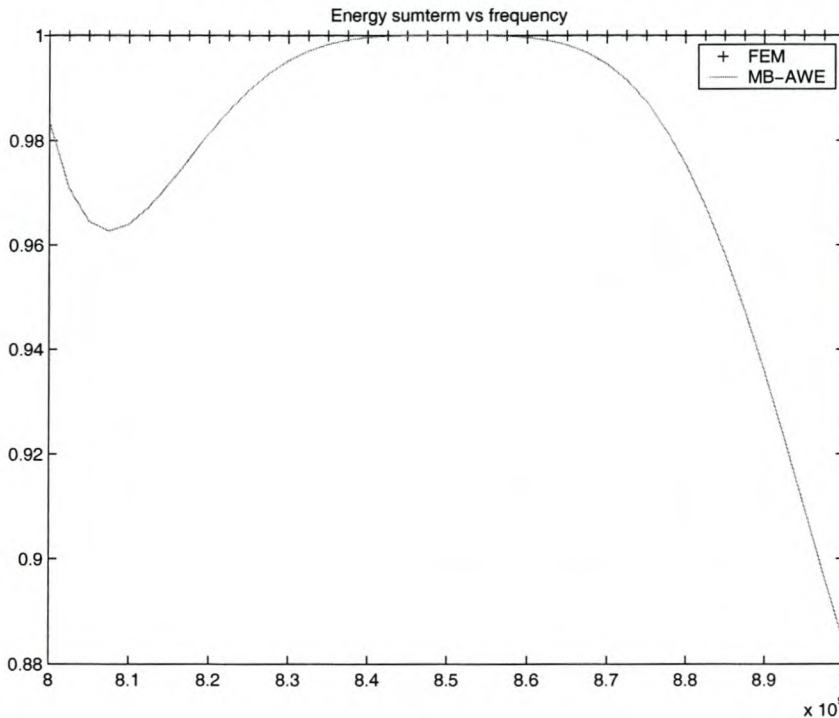


Figure 3.13: The sum of the squares of the magnitudes of the reflection and transmission coefficients for a single inductive septum: comparison of FEM and MB-AWE results.

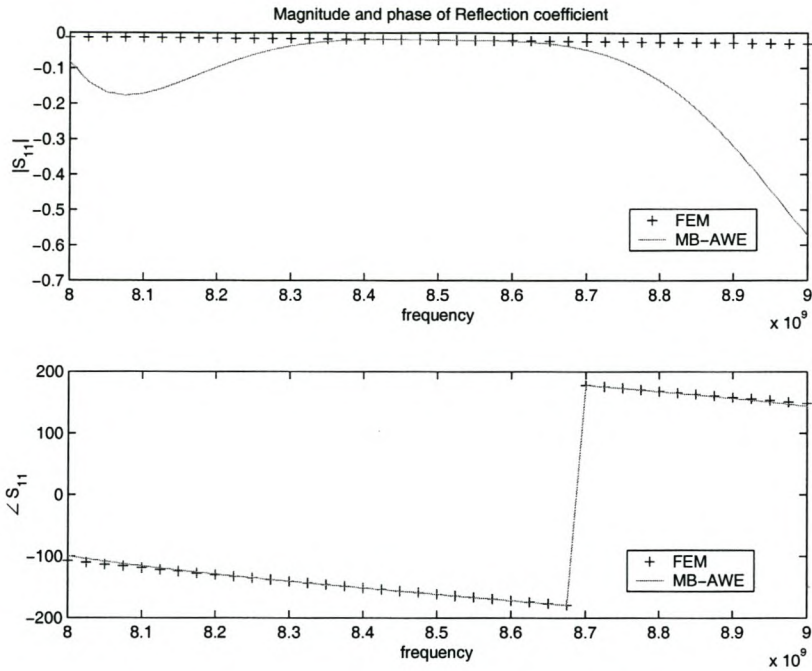


Figure 3.14: Reflection coefficient of the single inductive septum: comparison of FEM and MB-AWE results.

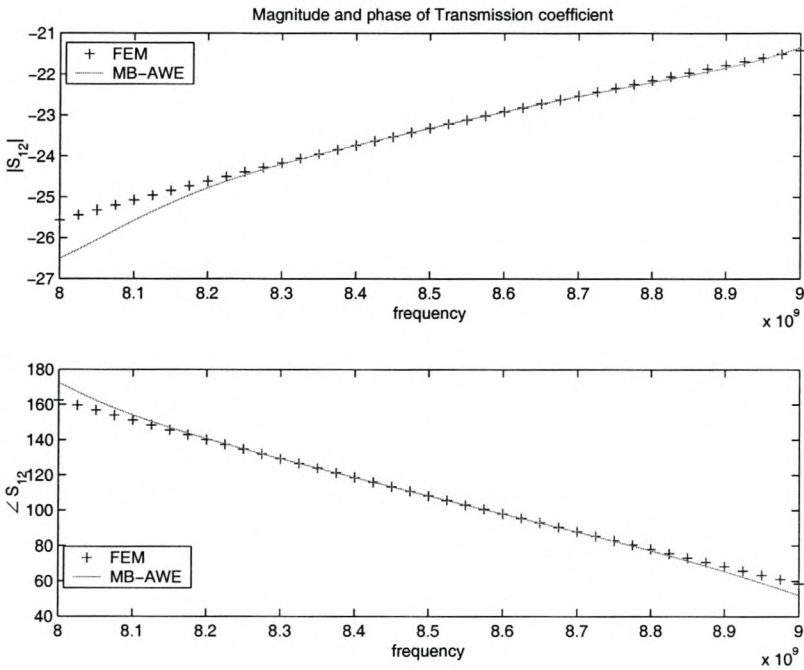


Figure 3.15: Transmission coefficient of the single inductive septum: comparison of FEM and MB-AWE results.



3.3.3.2 Single pole filter

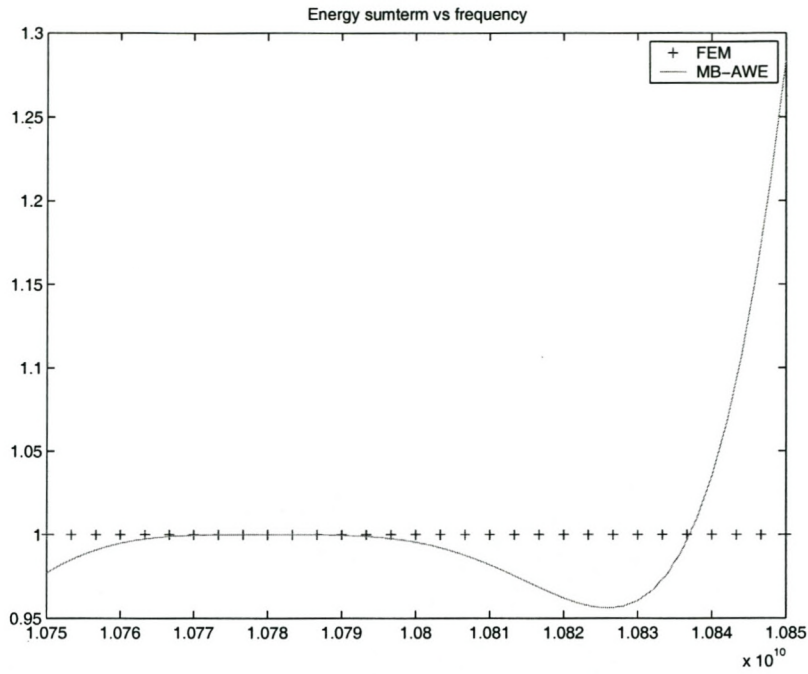


Figure 3.16: The sum of the squares of the magnitudes of the reflection and transmission coefficients for the single pole filter: comparison of FEM and MB-AWE results.

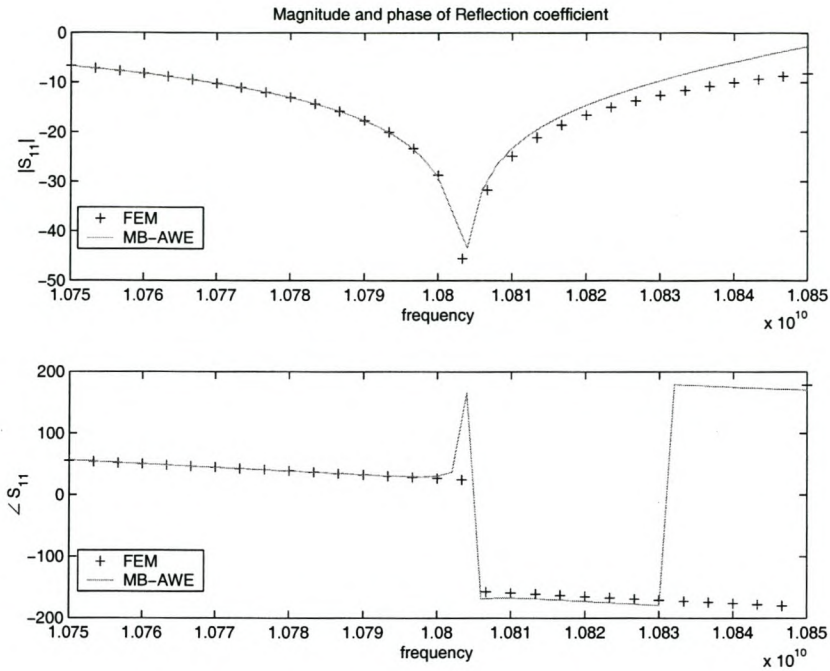


Figure 3.17: Reflection coefficient of the single pole filter: comparison of FEM and MB-AWE results.

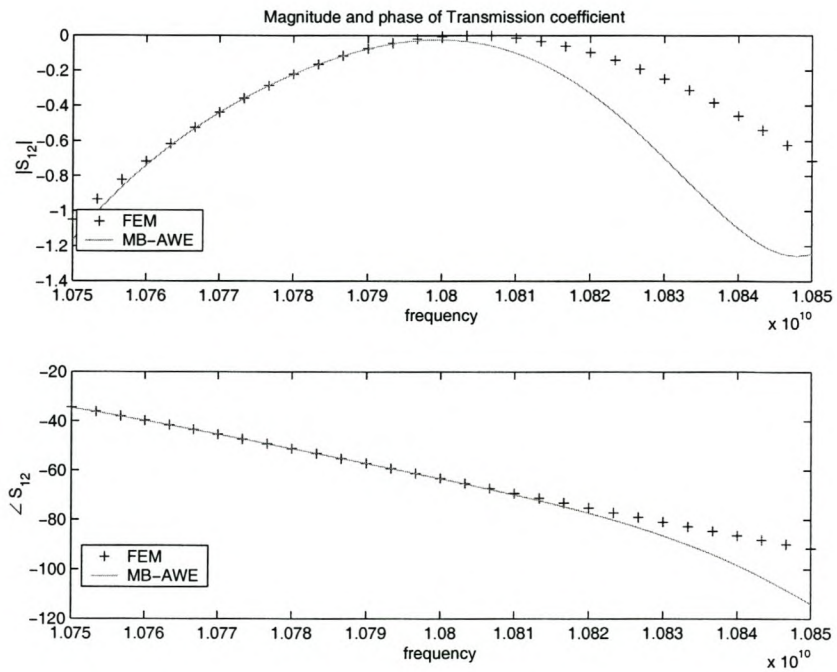


Figure 3.18: Transmission coefficient of the single pole filter: comparison of FEM and MB-AWE results.



### 3.3.3.3 Two pole filter

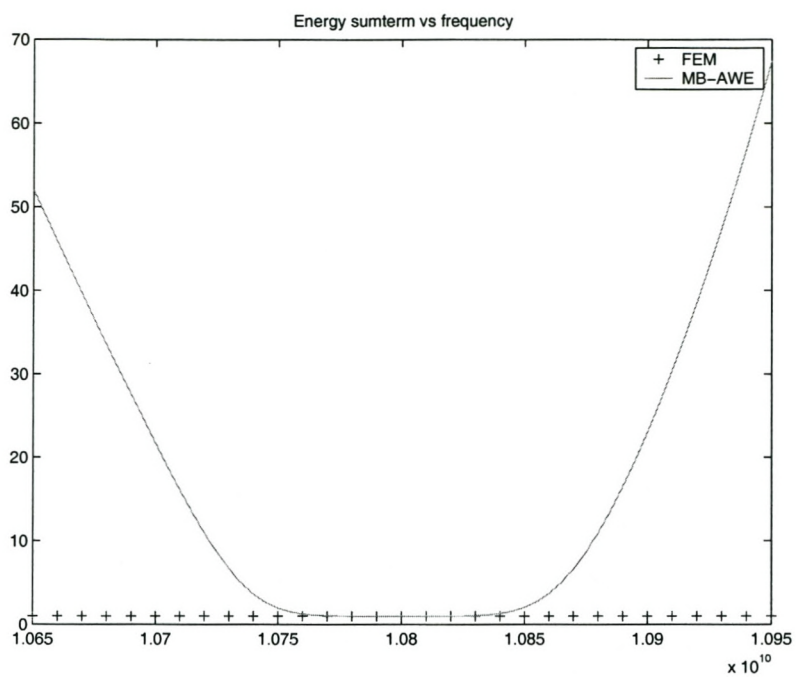


Figure 3.19: The sum of the squares of the magnitudes of the reflection and transmission coefficients for the two pole filter: comparison of FEM and MB-AWE results.

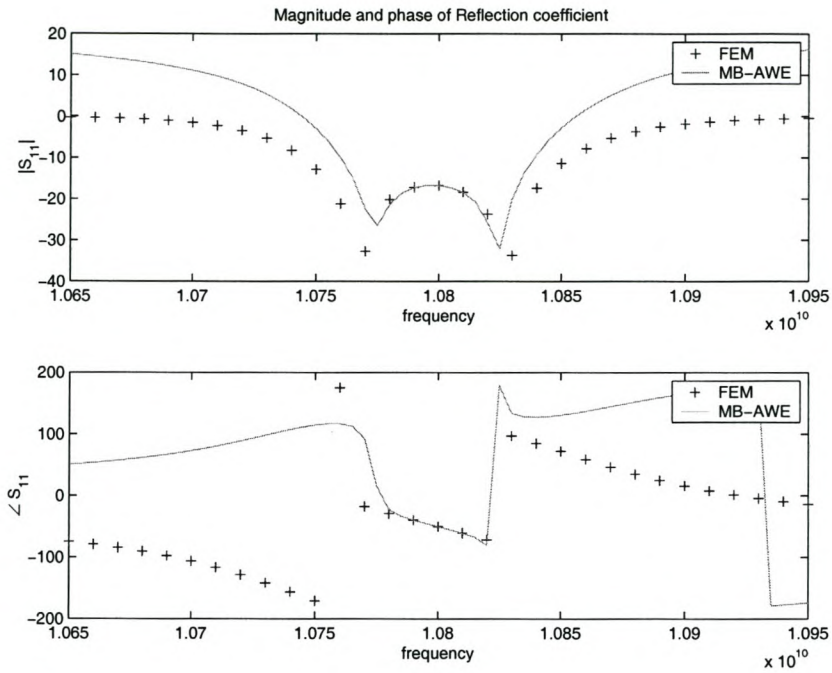


Figure 3.20: Reflection coefficient of the two pole filter: comparison of FEM and MB-AWE results.

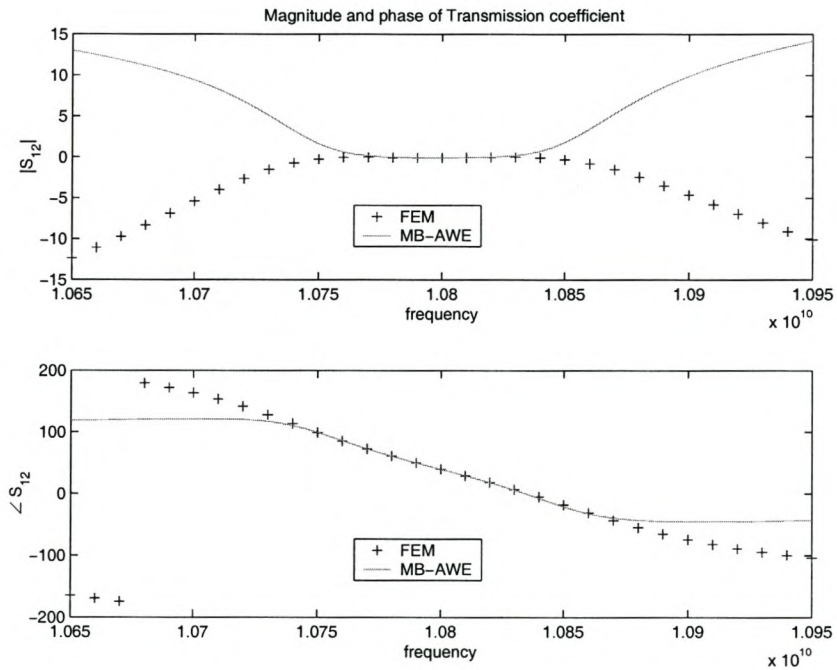


Figure 3.21: Transmission coefficient of the two pole filter: comparison of FEM and MB-AWE results.



### 3.3.4 Investigation into undesired performance of MB-AWE

MB-AWE is reported to increase the accuracy bandwidth of AWE. The results presented in this section show that MB-AWE has a smaller bandwidth. This observation needs to be investigated in order to ascertain whether this error is a failure of the technique or an implementation error. When using MB-AWE, information about the expected characteristics of the system unknowns are included into the model. If this information is not accurate, the accuracy of the model is affected. In this case, it is assumed that the degrees of freedom can be written as the solution of a rational Padé function, that has equal numbers of zeros and poles. The degrees of freedom in this case are related to the electric field in a waveguide.

Pozar [25] gives the electric field in the transverse plane of a hollow rectangular waveguide, with a  $TE_{10}$  mode wave propagating as shown in equation 3.11.

$$\begin{aligned} E_x &= 0 \\ E_y &= 0 \\ E_z &= \frac{-j\omega\mu a}{\pi} A_{10} \sin\left(\frac{\pi y}{a}\right) e^{-j\beta x} \end{aligned} \quad (3.11)$$

Equation 3.11 shows that the amplitude of the electric field varies linearly with frequency (assuming that  $A_{10}$  is constant) and the phase rotates with frequency.

This argument has been presented for a hollow waveguide. The behavior of the electric field in the presence of an obstruction needs to be investigated for specific geometries. If the electric field at the port of a waveguide is considered, the presence of an obstruction could cause a sharp amplitude and phase change over a narrow frequency band. This behavior is modelled well by Padé functions. The use of a Padé model is therefore validated by physical arguments.

The only remaining question is the order of the Padé model. This is investigated, using the single pole filter geometry, and the results of the different order models are shown for the sum of the squares of the S-parameters only. This result shows that, for the problem under consideration, and the number of derivatives calculated, the best Padé model is the one that has a zero'th order pole term, which is equivalent to the AWE model. In other words, the zeros dominate the poles in the expression for the fields. The results of the sum of the squares of the magnitudes of the reflection and transmission coefficients for the different models is shown in figure 3.22.

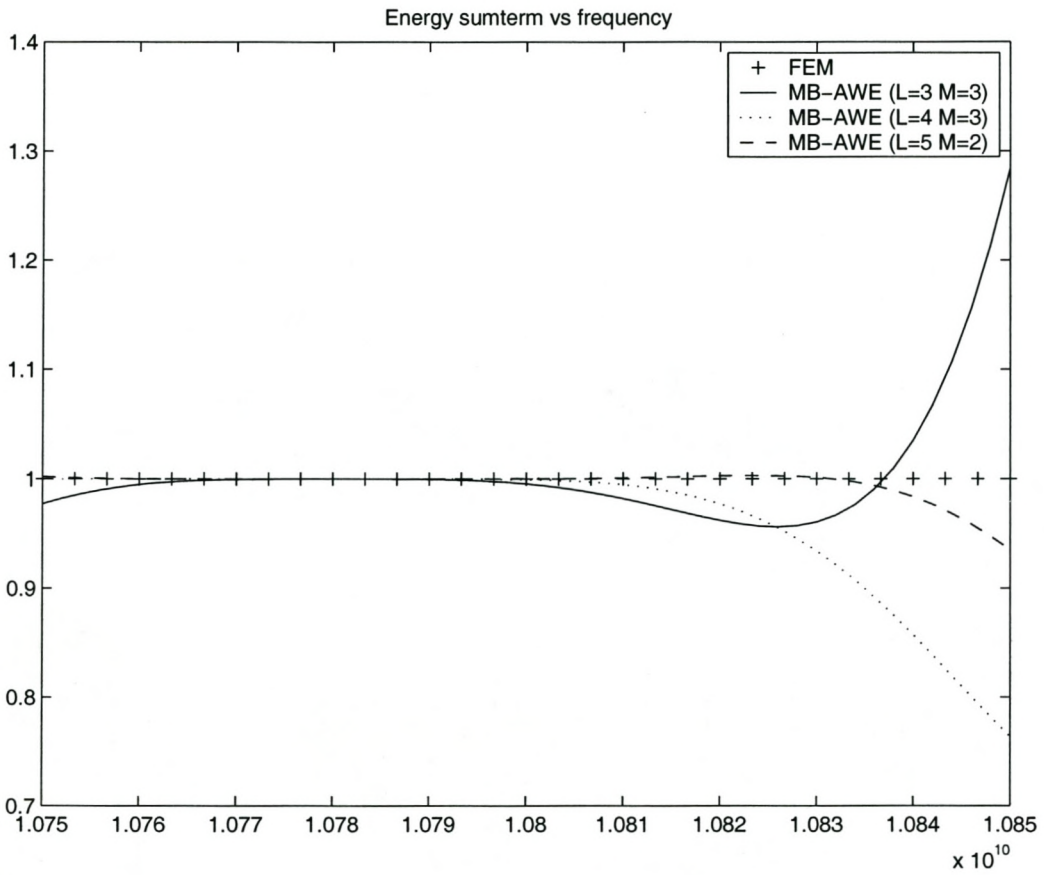


Figure 3.22: The sum of the squares of the magnitudes of the reflection and transmission coefficients for the single pole filter, comparison between different order MB-AWE models.



## 3.4 Model Based Parameter Estimation

Model based parameter estimation falls under the category of MOR techniques that model the observables and not the FE system. The observables of interest in this case are S-parameters. The model suggested in [11] is a rational Padé function. This technique uses parameter sampling (either parameter value or parameter derivative) to calculate the coefficients of the Padé function. This technique is described in [27, 11, 28, 29, 30, 31, 32, 33]. The model coefficients are determined from the parameter samples using either a matrix equation or recurrence formulas. The formulation used for the MBPE is described below, with implementation issues. The results obtained using MBPE are then presented.

### 3.4.1 MBPE formulation

This section describes how function samples can be used to obtain model coefficients for system observables. Assume that the observable under consideration is denoted by  $S(X_i)$  at frequency  $X_i$ . The physical meaning of  $S(X_i)$  is not defined, and can be any system observable, for example, input impedance or electric field at a point. Miller [11] suggests using a spectral domain fitting model for the observable, given by:

$$S(X_i) = \frac{N(X_i)}{D(X_i)} = \frac{\sum_{L=0}^n N_L X_i^L}{\sum_{M=0}^d D_M X_i^M} \quad (3.12)$$

which can be re-written in shorthand notation as:

$$S_i = \frac{N_i}{D_i}$$

where,

$$\begin{aligned} S_i &= S(X_i) \\ \underline{N}_i &= N(X_i) = N_0 + N_1 X_i + N_2 (X_i)^2 + \dots + N_n (X_i)^n \\ \underline{D}_i &= D(X_i) = D_0 + D_1 X_i + D_2 (X_i)^2 + \dots + D_d (X_i)^d \end{aligned} \quad (3.13)$$

The model coefficients,  $N_L$  and  $D_M$ , can be obtained by function sampling or by function derivative sampling. Once these coefficients are known, the response of the reduced order model can be calculated.

#### 3.4.1.1 Recurrence formulas or Matrix solution?

As indicated in the introduction to this chapter, the model coefficients can be obtained by using either recurrence formulas or a matrix inversion. The generation of the matrix is dependant on the nature of the parameter samples used. For parameter value sampling, the matrix is shown in section 3.4.1.2. For parameter derivative sampling, the matrix is shown in section 3.4.1.3. The recurrence equations are shown by Peik et al. [30] and Lehmsiek and Meyer [33]. The reason that recurrence equations are introduced is to prevent potential numerical problems arising from the inversion of (near)singular matrices.



The first issue that needs attention is the understanding and cause of a singular matrices. This gives insight into the cause of the problem and determines whether or not recurrence equations are the best solution to the problem. Consider  $[A]\{x\} = \{b\}$ . If the matrix  $[A]$  is singular, there is no unique solution for  $\{x\}$ . This is precisely what happens if the parameter is over-sampled. In such a case, the model has a higher order than the system - the location of the additional poles/zeros is undetermined. To avoid over-sampling, the order of the system must be known and the samples must be well chosen. The order of the system is information that is unlikely to be available. The choice of sample points will usually not be at absolutely optimal locations, even if adaptive sampling is used. This means that over sampling, and thus ill-conditioned matrices are unavoidable, as an under-sampled system will not give results with the specified accuracy. Recurrence equations are proposed to avoid matrix inversion.

An alternative to using recurrence equations is to use the pseudo-inverse matrix solution method [34, 11, 35, 36]. This technique is based on singular value decomposition (SVD). The article by Long [36] gives an excellent description of what it means to use SVD to obtain the solution to a matrix equation. Long goes on to show how SVD can be thought of as providing a least square best fit approximation of the solution.

SVD can be explained quite simply. The basic idea is that any matrix  $[A]$  can be written as a series of the form in equation 3.14.

$$[A] = \sigma_1[R_1] + \sigma_2[R_2] + \dots + \sigma_k[R_k] \quad (3.14)$$

The algorithm that is used to obtain the series shown in equation 3.14, is shown in [36]. The values  $\sigma$  are the singular values of the system. A new matrix can be constructed from the series, using only the significant singular values. The inverse of the new matrix is easily obtained from the new matrix.

Van Wyk [31] proposed an alternative method of eliminating the conditioning problem. The technique uses a fixed order Padé approximation. Instead of increasing the order of the approximation to add sample points, Van Wyk uses a sliding window. If  $n$  and  $d$  are fixed, the number of data samples used to generate the model,  $D$ , is fixed. If  $D + 2$  samples are available, a model is generated using the first  $D$  samples. A second model is generated using  $D$  samples, starting at sample 2. Then a third model is generated, using  $D$  samples, starting at sample 3. An adaptive technique is used to place samples. One foreseeable problem with this technique is that the system could have a different number of poles and zero's to the model. If, for instance, the system has one dominant zero and three dominant poles for a specific frequency window, and the model specifies that the order of the numerator is one less than the denominator, six samples will be needed to model the system. This means that the model has two zero's and three poles. The matrix used to solve for the pole/zero locations is thus necessarily near-singular. The technique proposed by Van Wyk will thus only avoid ill-conditioned matrices if the order of the system is equal to that of the model.

It should be noted that the system poles are not only located in the frequency band of interest - in both the model and the FE system. A specified frequency band can be dominated by the same poles/zeros as another band, which means that subdividing the frequency band of interest will not necessarily help to prevent over-sampling. This means that there is no obvious advantage to using frequency windows, as the models in both windows could be attempting to locate the same system poles/zeros, while if one frequency band is used, remote poles will not affect the entire band anyway. Computational resources can thus be wasted in locating the



same system poles a number of times.

The initial question posed for this section is whether to use recurrence equations or matrix inversion. The matrix is (near)singular as a result of over sampling. It is not clear how the use of recurrence equations eliminates redundant information. Pseudo inversion offers the advantage that only accurate coefficients are obtained from the matrix. This means that the redundant information generated by over sampling is eliminated. This method seems the most attractive and is what was used.

### 3.4.1.2 Calculating Model coefficients using parameter sampling

The Padé model presented in equation 3.12 has  $n + d + 2$  unknown coefficients. To make the equations homogenous, a constraint is needed [11]. This choice is not unique. If the constraint  $D_d = 1$  is chosen, the set of linear equations can be written down as in equation 3.15. The equation is constructed by equating coefficients at each sample point. Note that  $D = n + d + 1$  sample points are needed to solve for the coefficients.

$$\begin{aligned}
 S_0 D_0 + X_0 S_0 D_1 + \cdots + S_0 (X_0)^{d-1} D d - 1 \\
 \qquad \qquad \qquad - N_0 - X_0 N_1 - \cdots - (X_0)^n N_n &= -(X_0)^d S_0 \\
 S_1 D_0 + X_1 S_1 D_1 + \cdots + S_1 (X_1)^{d-1} D d - 1 \\
 \qquad \qquad \qquad - N_0 - X_1 N_1 - \cdots - (X_1)^n N_n &= -(X_1)^d S_1 \\
 \qquad \qquad \qquad \vdots \qquad \qquad \qquad \vdots \qquad \qquad \qquad \vdots \qquad \qquad \qquad \vdots \\
 S_{D-1} D_0 + X_{D-1} S_{D-1} D_1 + \cdots + S_{D-1} (X_{D-1})^{d-1} \\
 \qquad \qquad \qquad - N_0 - X_{D-1} N_1 - \cdots - (X_{D-1})^n N_n &= -(X_{D-1})^d S_{D-1}
 \end{aligned} \tag{3.15}$$

The independent variable  $X$  is not limited to be the independent variable of the FE method, namely frequency. Since no assumptions are made about this variable in the derivation of equation 3.15, this variable can be written as a function of frequency. The reason that it is desirable to do this is to increase the numeric stability of the procedure [11]. A function can be chosen that normalizes the frequency window to extend from -1 to 1. Such a function is shown in equation 3.16.  $f_{cent}$  is the frequency at the center of the frequency window and  $f_{high}$  and  $f_{low}$  are the upper and lower frequency boundaries respectively.  $f_i$  is the frequency corresponding to the normalized frequency  $X_i$ .

$$X_i = \left[ \frac{f_i - f_{cent}}{f_{cent} - f_{low}} \right] \tag{3.16}$$

### 3.4.1.3 Calculating Model coefficients using parameter derivative sampling

The model coefficients can also be obtained using parameter derivative sampling. This is achieved by differentiating both the model and the FE solution, with respect to frequency, and equating derivatives of the same order. The derivatives of the model are linear combinations

of the coefficients of the model. These linear combinations can be equated to the system derivatives of the FE system. This process can be used to assemble a set of linear equations to obtain the model coefficients. Miller [11] shows a general set of linear equations that can be used to obtain the coefficients from derivative samples for any  $n$  and  $d$ . The derivation was done independently, by the author of this dissertation, for  $n = 3$  and  $d = 4$  with  $D_0 = 1$ , with the result shown in equation 3.17. The derivation does not increase insight into the technique and is thus not reproduced here.

$$\begin{bmatrix} 1 & 0 & 0 & 0 & 0 & 0 & 0 & 0 \\ 0 & 1 & 0 & 0 & -F_0 & 0 & 0 & 0 \\ 0 & 0 & 1 & 0 & -2F_1 & -F_0 & 0 & 0 \\ 0 & 0 & 0 & 1 & -3F_2 & -3F_1 & -F_0 & 0 \\ 0 & 0 & 0 & 0 & -4F_3 & -6F_2 & -4F_1 & -F_0 \\ 0 & 0 & 0 & 0 & -5F_4 & -10F_3 & -10F_2 & -5F_1 \\ 0 & 0 & 0 & 0 & -6F_5 & -15F_4 & -20F_3 & -15F_2 \\ 0 & 0 & 0 & 0 & -7F_6 & -21F_5 & -35F_4 & -35F_3 \end{bmatrix} \begin{bmatrix} N_0 \\ N_1 \\ 2N_2 \\ 6N_3 \\ D_1 \\ 2D_2 \\ 6D_3 \\ 24D_4 \end{bmatrix} = \begin{bmatrix} F_0 \\ F_1 \\ F_2 \\ F_3 \\ F_4 \\ F_5 \\ F_6 \\ F_7 \end{bmatrix}$$

where,

$$F_i = \left. \frac{\partial^i}{\partial X^i} S(X) \right|_{X=X_s} \quad (3.17)$$

Equation 3.17 shows that the derivatives of the system observables are required to calculate the model coefficients. Only the derivatives of  $S_{11}$  are shown here.  $S_{11}$  is given by equation 2.14. Notice that  $S_{11}$  is a function of the degrees of freedom of the system, which are in turn dependant on the wavenumber,  $k$ . Equation 2.14 in discretized form can be written as equation 3.18, where all the variables have the same meanings as in section 2.2.10 and  $N_s$  and  $E_s$  relate to the unknowns in the surface of the port.

$$S_{11} = \sum \{p\} \{E_s\} - 1$$

where,

$$\{p\} = \frac{2}{y_l z_l E_0} \int \int_{S_1} \{N_s\} \cdot \mathbf{e}_{10}(y, z) dS \quad (3.18)$$

In equation 3.18, it can be seen that only the vector  $\{E_s\}$  has a dependance on frequency. The first derivative of  $S_{11}$  with respect to  $X$  as defined in equation 3.16 can be calculated using the chain rule for differentiation.

$$\begin{aligned} F_1 &= \left. \frac{\partial S_{11}(X)}{\partial X} \right|_{X=X_s} \\ &= \left. \frac{\partial S_{11}(X)}{\partial k} \frac{\partial k}{\partial X} \right|_{X=X_s} \end{aligned} \quad (3.19)$$

It is possible to write

$$\begin{aligned} k &= \frac{2\pi}{c} (X(f_{high} - f_{low}) + f_{cent}) \\ \implies \frac{\partial k}{\partial X} &= \frac{2\pi(f_{high} - f_{low})}{c} \end{aligned} \quad (3.20)$$



Equation 3.18, equation 3.19 and equation 3.20 can be combined to give the first derivative.

$$F_1 = \frac{2\pi(f_{high} - f_{low})}{c} \sum \{p\} \{E_s^{(1)}\} \quad (3.21)$$

In equation 3.21,  $\{E^{(1)}\}$  has been calculated in Appendix A. The  $n$ -th derivative of  $S_{11}$  is written down in equation 3.22, with  $\{E^{(n)}\}$  as in Appendix A

$$F_n = \left[ \frac{2\pi(f_{high} - f_{low})}{c} \right]^n \sum \{p\} \{E_s^{(n)}\} \quad (3.22)$$

### 3.4.2 MBPE implementation issues

MBPE is particularly easy to implement. Once the appropriate model has been chosen and a set of linear equations to calculate the model coefficients is known, the majority of the work is done. The other significant effort is in calculating parameter derivatives. If the model coefficients are to be obtained from derivative information, the derivatives of all system observables needs to be known.

#### 3.4.2.1 Implementation of MBPE, with parameter sampling

The first issue that needs to be addressed for this implementation is the choice of the location of sample points and the number of sample points. As an initial set of test samples, seven equally spaced samples in the frequency window of interest were used. More complicated schemes are available, using adaptive sample selection to ensure that points that contribute most significantly to the model are sampled. Such a scheme is the topic of Chapter 4.

The second issue is the choice of  $n$  and  $d$ . Miller [28] plots a graph of accuracy versus the order of  $n$  and  $d$ . It is further suggested that the choice is problem dependant. The problem shown has 15 poles. The highest accuracy is obtained with  $n = 7$  and  $d = 7$ . The number of poles being solved for is a maximum of two for this section. In keeping with the  $n = d$  approach,  $n = d = 3$  is chosen.

#### 3.4.2.2 Implementation of MBPE, with parameter derivative sampling

The issues are very similar to those required for the parameter sampling algorithm. Prior knowledge of the form of the parameter is used to choose the sample locations to test this technique. Adaptive algorithms could be designed and implemented, should this method be pursued. For the reasons outlined in the discussion on implementation issues for parameter sampling,  $n = 3$  and  $d = 4$  was used.

### 3.4.3 MBPE results

The same models used in section 3.2.3 are used in this section. The geometric and model information is not duplicated here. Only the results are given. The results show that accurate

parameter estimation is obtained using both techniques. The derivative sampling algorithm has similar convergence radius problems to the AWE and MB-AWE techniques. The parameter sampling algorithm works exceptionally well, with a zero error at the location of every sample. The parameter is potentially over sampled in all the results, but the model is accurate, as a result of the pseudo-inversion.

### 3.4.3.1 Single Inductive septum

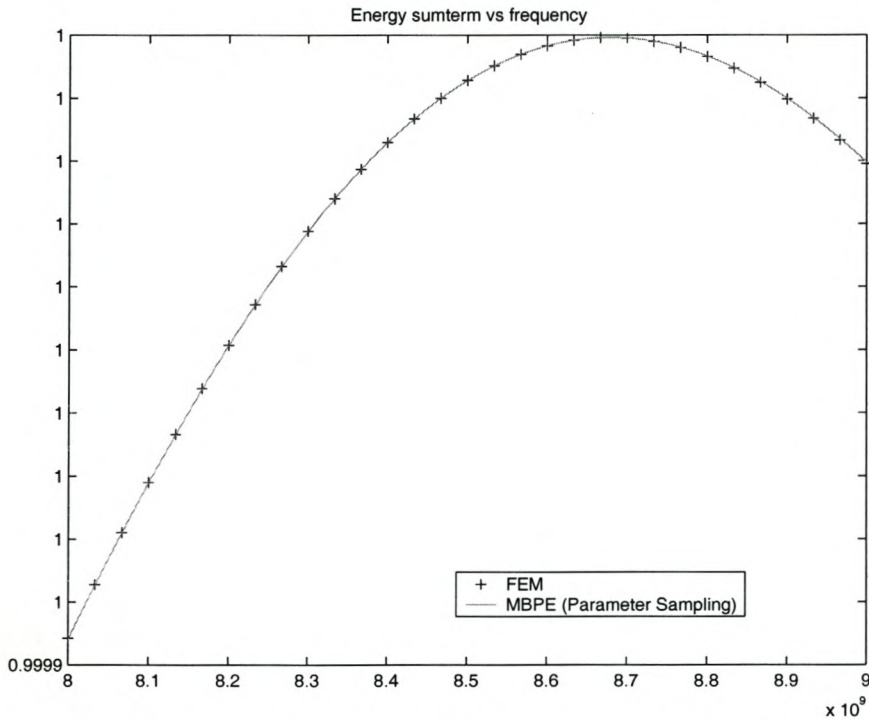


Figure 3.23: The sum of the squares of the magnitudes of the reflection and transmission coefficients of the single inductive septum: comparison of FEM and MBPE (Parameter Sampling) results.



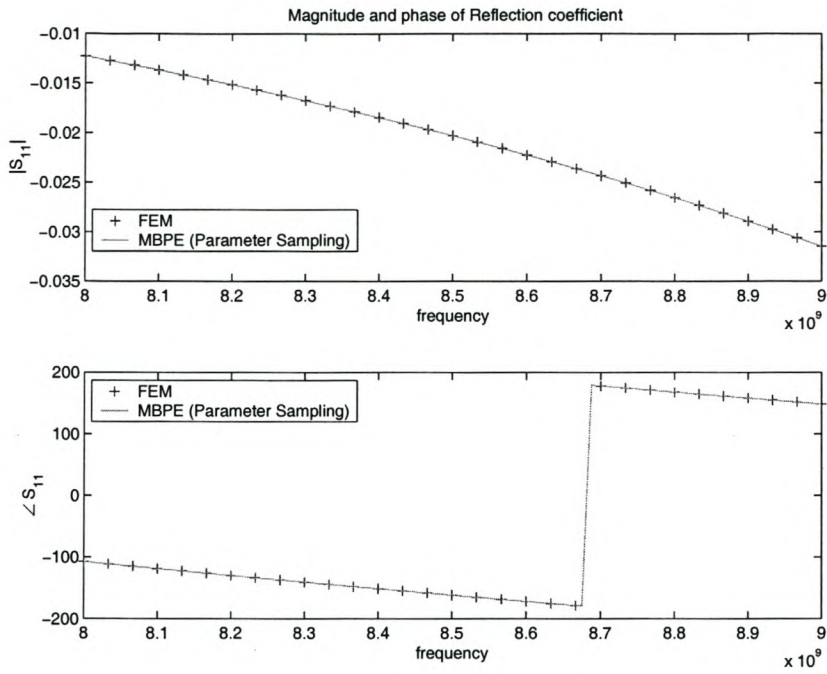


Figure 3.24: Reflection coefficient of the single inductive septum: comparison of FEM and MBPE (Parameter Sampling) results.

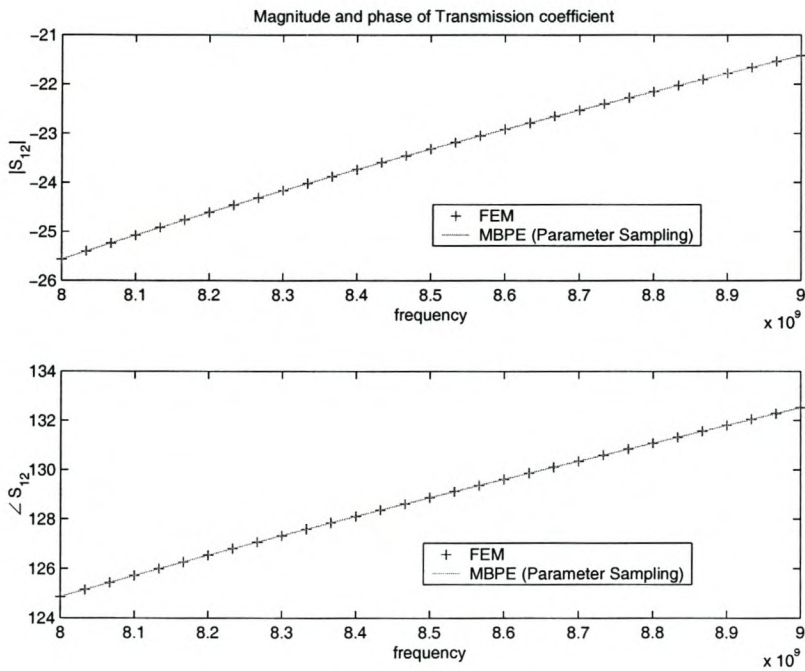


Figure 3.25: Transmission coefficient of the single inductive septum: comparison of FEM and MBPE (Parameter Sampling) results.

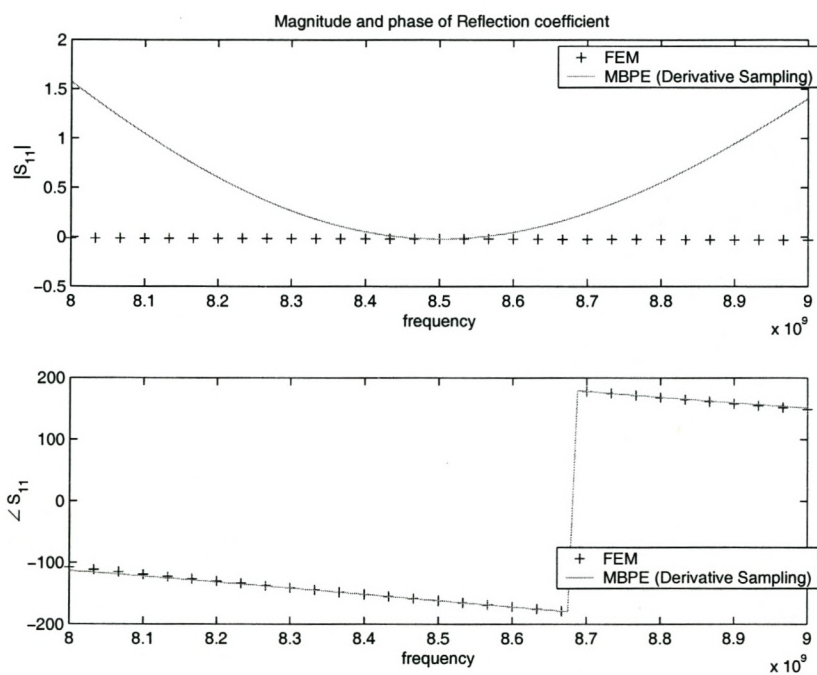


Figure 3.26: Reflection coefficient of the single inductive septum: comparison of FEM and MBPE (Derivative Sampling) results.



### 3.4.3.2 Single pole filter

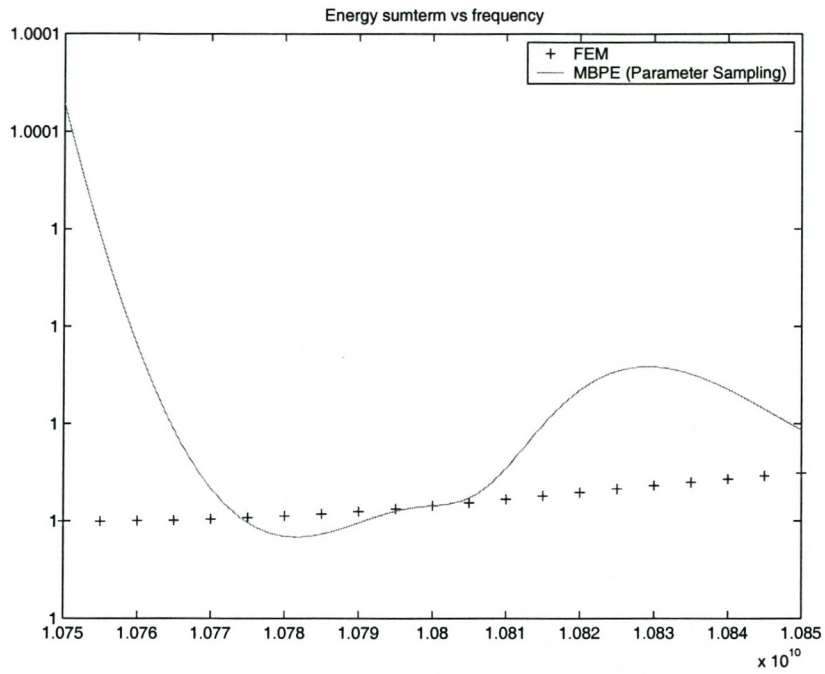


Figure 3.27: The sum of the squares of the magnitudes of the reflection and transmission coefficients for the single pole filters: comparison of FEM and MBPE (Parameter Sampling) results.

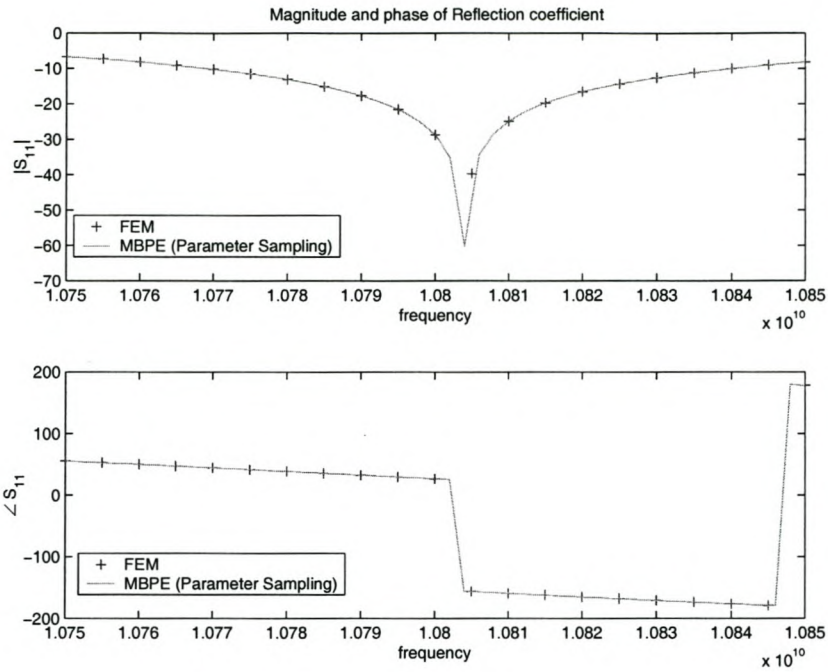


Figure 3.28: Reflection coefficient of the single pole filter: comparison of FEM and MBPE (Parameter Sampling) results.

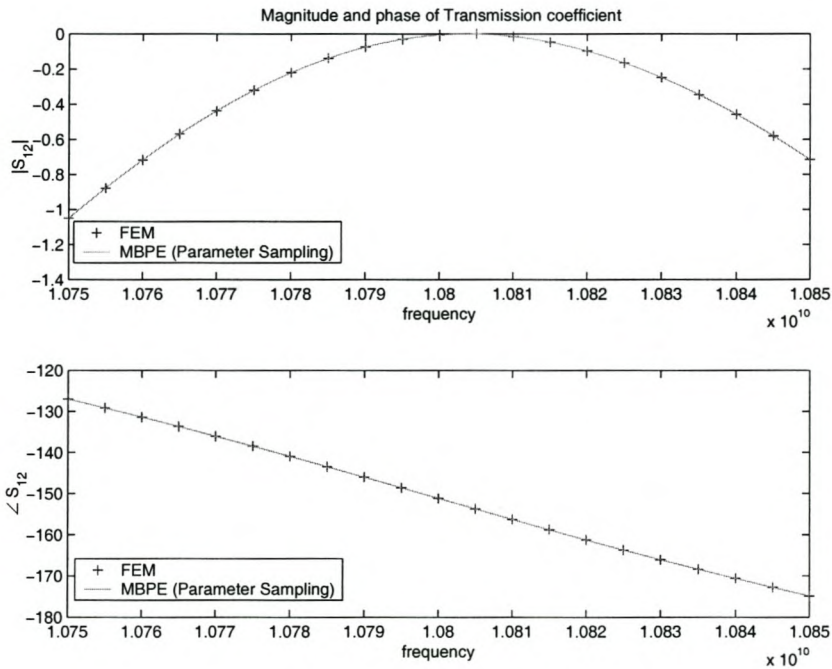


Figure 3.29: Transmission coefficient of the single pole filter: comparison of FEM and MBPE (Parameter Sampling) results.



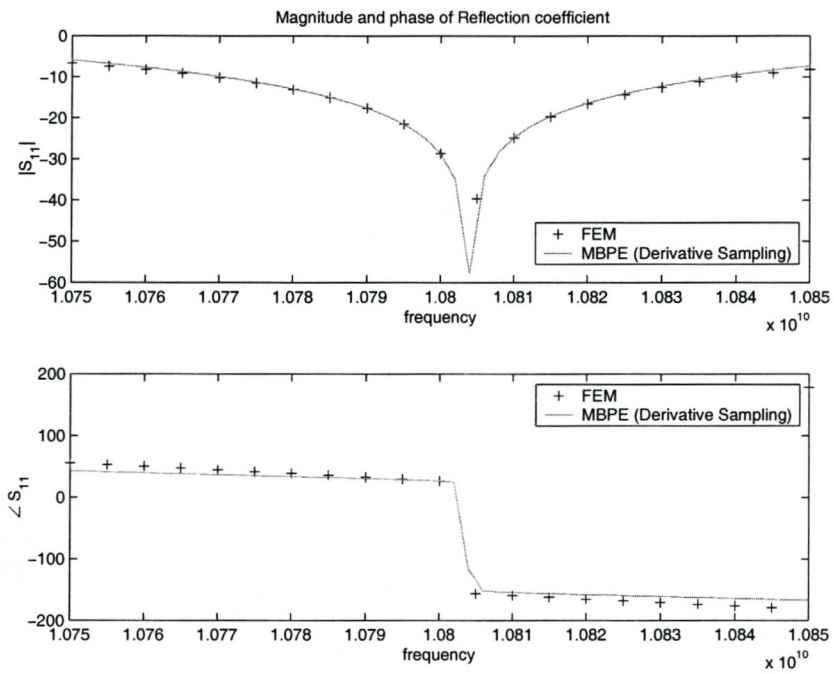


Figure 3.30: Reflection coefficient of the single pole filter: comparison of FEM and MBPE (Derivative Sampling) results.

### 3.4.3.3 Two pole filter

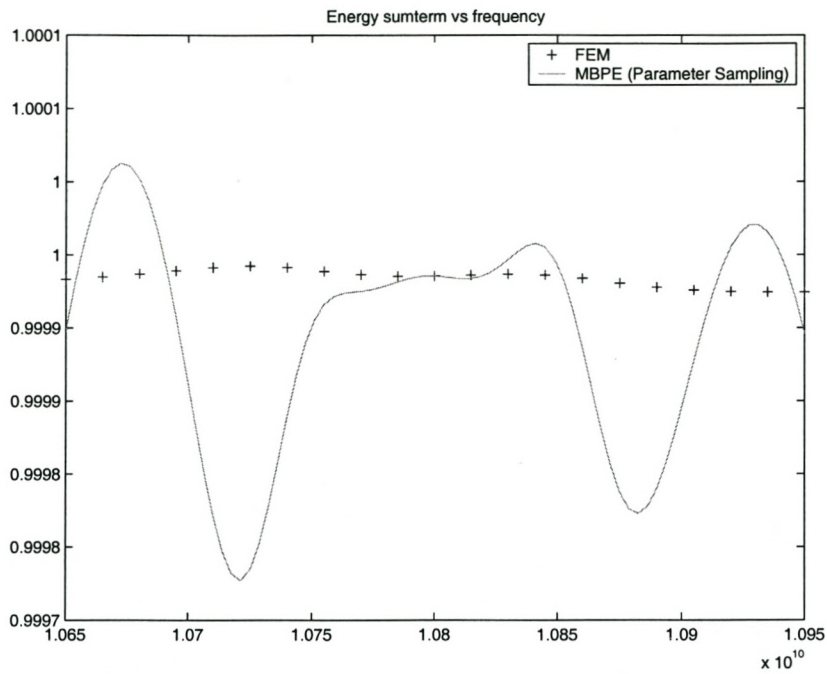


Figure 3.31: The sum of the squares of the magnitudes of the reflection and transmission coefficients for the two pole filter: comparison of FEM and MBPE (Parameter Sampling) results.

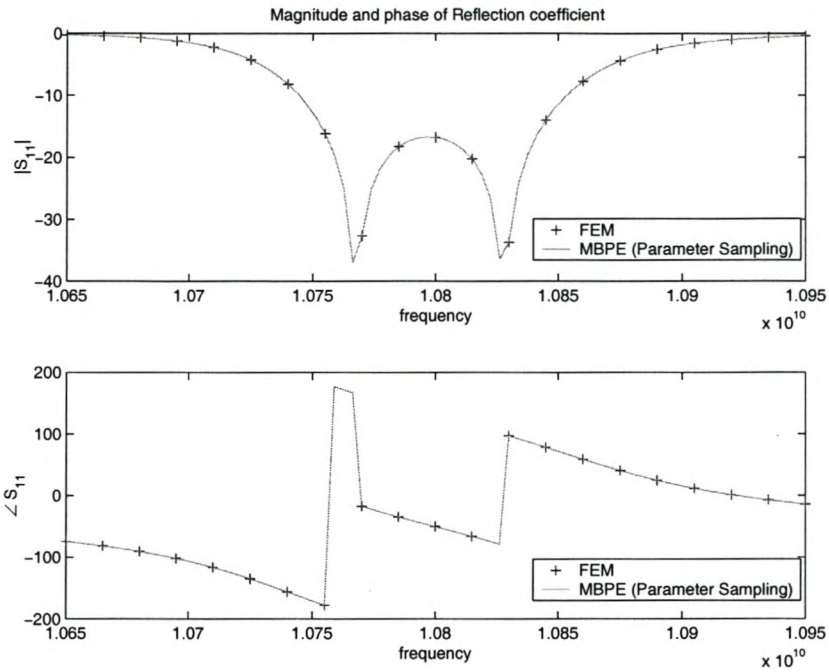


Figure 3.32: Reflection coefficient of the two pole filter: comparison of FEM and MBPE (Parameter Sampling) results.

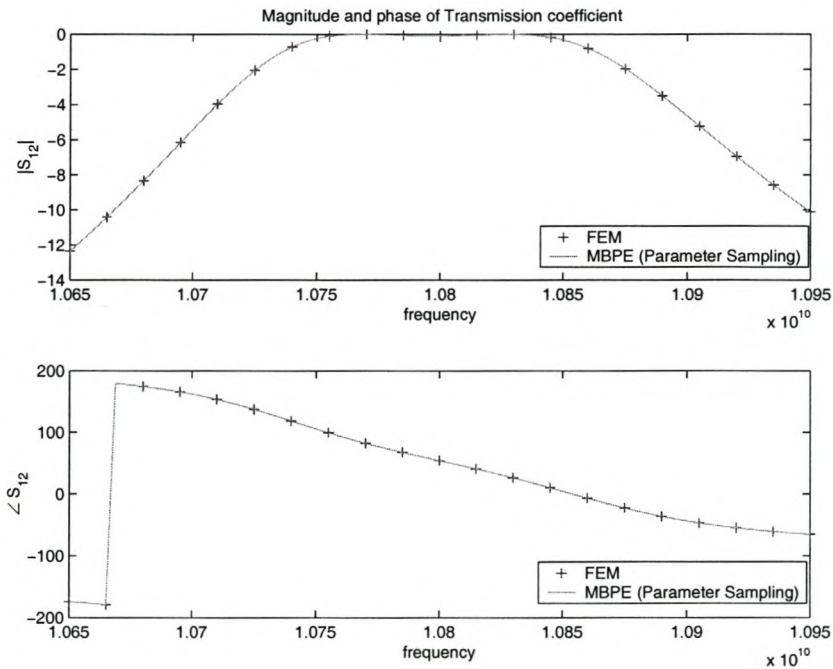


Figure 3.33: Transmission coefficient of the two pole filter: comparison of FEM and MBPE (Parameter Sampling) results.



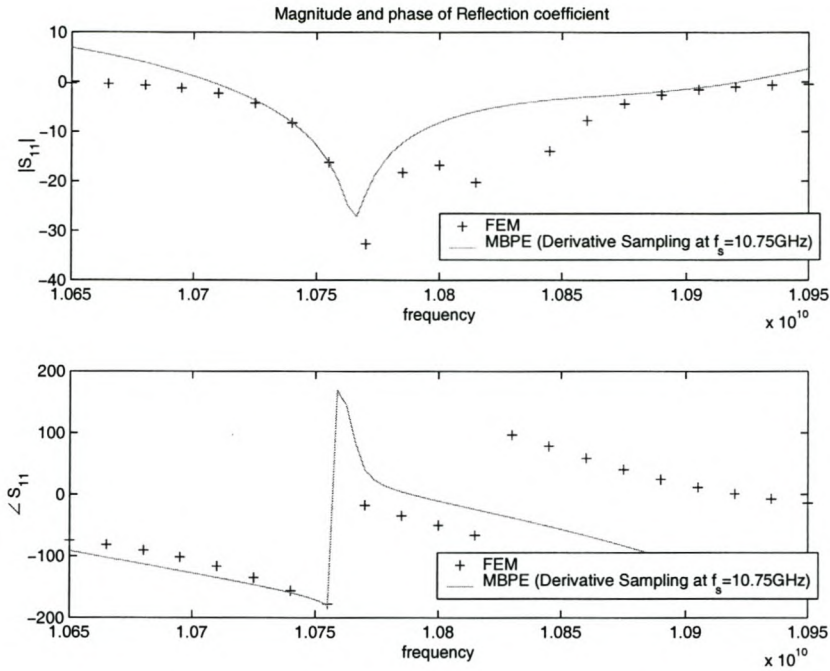


Figure 3.34: Reflection coefficient of the two pole filter: comparison of FEM and MBPE (Derivative Sampling) results.

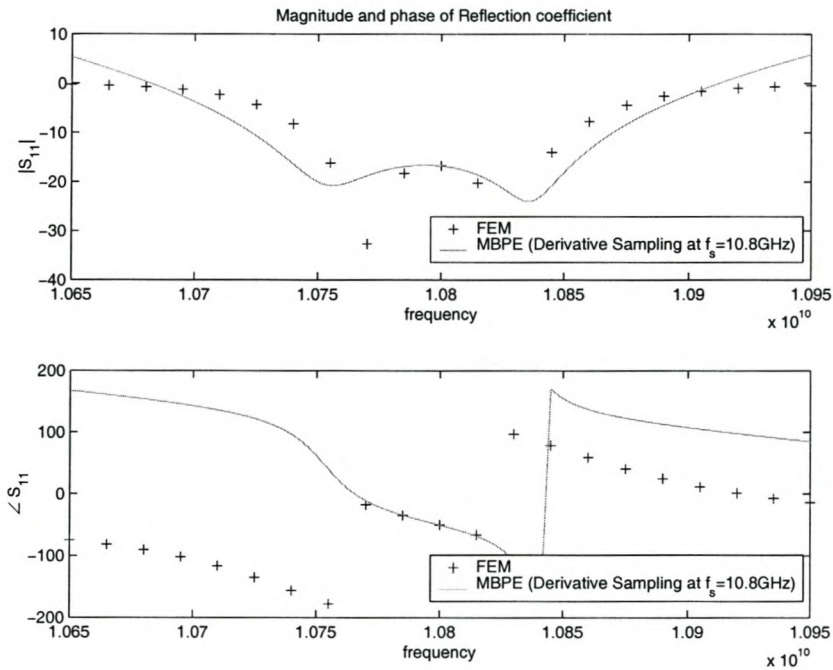


Figure 3.35: Reflection coefficient of the two pole filter: comparison of FEM and MBPE (Derivative Sampling) results.

## 3.5 Discussion and Comparison of Fast Frequency Techniques

All of the techniques presented thus far have merits and drawbacks. This section will compare the techniques both quantitatively and qualitatively. These techniques attempt to reduce the computational cost of obtaining a frequency resolution. The computational cost of each technique needs to be investigated. It is related to the number of floating point operations required to obtain a solution. This cost is calculated for each technique and then a direct comparison between the different techniques can be made.

The use of a FF techniques implies a trade off between accuracy and speed. A finite element solution can be very accurate ( $< -100\text{dB}$ ). Measurements and specifications are typically not this accurate. The FF technique must make an acceptable compromise between accuracy and speed. The acceptable error is a specified tolerance.

Comparisons that are more qualitative than computational costs are also made. Since the frequency resolution is the parameter of interest, the computational cost of establishing a model must be compared to the bandwidth in which it can be used. The difference between the techniques is not expected to be orders of magnitude.

To assist with the evaluation of the computational cost, a few variables are defined. These variables are related to the various techniques. The definitions are summarized in Table 3.1.

### 3.5.1 A note on computational costs

In order to compare algorithms, an objective method of comparison must be found. Davidson [37] suggests the use of asymptotic approximations of the number of floating point operations (FLOPS) required to execute the algorithm. This is an effective method only if the problem satisfies the asymptotic constraints. The constraints are discussed in section 3.5.1.1. The implication of the asymptotic nature of these approximations becomes apparent in this section.

Another computational factor is memory. If the computer being used for a simulation runs out of RAM, virtual memory is used. The hard disk access times for computations is excessive and will dominate solution times. If virtual memory is used, the computation time increases dramatically. Thus an  $\mathcal{O}(N^2)$  operation that is performed on data in virtual memory could take longer than an  $\mathcal{O}(N^3)$  operation that is performed on data stored in RAM. This is a particularly important consideration when programming in MATLAB, as MATLAB uses double precision to store all numbers. The storage of a 4 096 by 4 096 matrix of complex numbers requires 256 MB RAM! This means that only very small dense matrices can be stored in RAM. The computational cost of any operation that requires a dense matrix that is large can not be compared to the same operation on a smaller matrix. The limit on matrix size is not fixed. It is dependant on the available RAM for a given computer. Any technique that uses dense matrices is evaluated as if there is enough RAM to store the matrix. Any reference to a small matrix refers to a matrix that can be stored in core and any reference to a large matrix refers to a matrix that needs to be stored out of core.



Table 3.1: Definition of the variables to assist computational cost discussion.

Variable	Definition
$N$	The number of unknowns in the system.
$n_{it}$	Number of iterations required by an iterative solver to solve a set of linear equations.
$n_{fp}$	Number of frequency points evaluated during a FEM solution.
$n_m$	Number of moments calculated for the AWE technique.
$n_{sp}$	Number of support points calculated for the MBPE technique.
$n_{ds}$	Number of derivative samples calculated for the MBPE technique.
$\mathcal{N}_{FEM}$	Cost of a FEM solution to the problem.
$\mathcal{N}_{AWEsm}$	Cost of a AWE solution to a problem of which the inverse matrix can be stored in core.
$\mathcal{N}_{AWEbm}$	Cost of a AWE solution to a problem of which the inverse matrix needs to be stored out of core.
$\mathcal{N}_{MB-AWE}$	Cost of a MB-AWE solution to the problem
$\mathcal{N}_{MBPE}$	Cost of a MBPE solution to the problem

### 3.5.1.1 Formal meaning of $\mathcal{O}(N^m)$

This section shows the mathematical meaning of  $\mathcal{O}(N^m)$ . It is important to understand this meaning to appreciate at what point the objective measure between algorithms fails.

Firstly we define  $N$  to be the number of rows in a matrix.  $m$  is defined as the polynomial order of the computation.  $a$  is a constant scale factor and  $\mathcal{N}$  is the number of FLOPS. For all the operations under consideration it is assumed that the FLOP count is given by the relationship in equation 3.23.

$$\mathcal{N} = aN^m \quad (3.23)$$

$$\Rightarrow \log \mathcal{N} = \log a + m \log N \quad (3.24)$$

in the limit,

$$\lim_{N \rightarrow \infty} \log \mathcal{N} = \lim_{N \rightarrow \infty} [\log a + m \log N] \quad (3.25)$$

$$\Rightarrow \lim_{N \rightarrow \infty} \log \mathcal{N} \approx \lim_{N \rightarrow \infty} m \log N \quad (3.26)$$



From equation 3.26 it can be seen that the FLOP count asymptotically approaches  $N^m$ . Therefore  $\mathcal{O}(N^m)$  means that the number of FLOP's required to compute the algorithm under consideration approaches  $N^m$ , when  $N \gg a$ .

### 3.5.1.2 A selection of common operators and their computational costs

The cost of any technique is the sum of the costs of all the arithmetic operations performed in its execution. For this reason, some common operations and their costs are tabulated here. Note that the computational costs for sparse and dense matrices are not the same. This means that careful consideration needs to be made when looking at a technique that has mixed matrices.

Table 3.2: The computational cost of a selection of Mathematical operators

Operation	Full Matrix Cost	Sparse Matrix Cost
Scalar * Vector	$\mathcal{O}(N)$	N/A
Scalar * Matrix	$\mathcal{O}(N^2)$	$\mathcal{O}(N)$
Vector * Matrix	$\mathcal{O}(N^2)$	$\mathcal{O}(N)$
Matrix addition	$\mathcal{O}(N^2)$	$\mathcal{O}(N)$
Matrix Inversion	$\mathcal{O}(N^3)$	$\leq \mathcal{O}(N^3)$
Iterative linear equation solvers	see section 3.5.3	see section 3.5.3

### 3.5.2 A note: pre- and post- processing costs

The computational cost of the pre- and post- processing operations needs to be assessed in order to establish whether or not they contribute to the computational cost of each fast frequency technique.

The computational cost of generating the mesh, evaluating the elemental integrals and assembling the system matrices ( $[S]$  and  $[T]$ ) is fixed for all the techniques under consideration. None of the techniques investigated attempt to reduce this time. This cost is therefore not included into the cost of each technique.

The generation of the frequency dependant  $[B]$  matrix and the excitation vector ( $\{b\}$ ) involves only multiplication on the degrees of freedom that lie in a port. An integral is required for the first frequency evaluation, and a multiplication can be used thereafter. Since the number of degrees of freedom that lie in a port are significantly less than the total number of degrees of freedom, this cost is trivial. This is not generally true. When FE/BI formulations are considered, the  $[B]$  matrix is a partially dense matrix as a result of the contribution from the degrees of freedom that lie on the boundary. In this case, the computational cost of generating this matrix needs to be taken into account.

The assembly of the system matrix from the  $[S]$  and  $[T]$  matrices is an  $\mathcal{O}(N)$  operation. This



cost needs to be added for each technique, as different techniques require this operation a different number of times.

Once the solution of the FE system is known, the system observables need to be calculated. In this case the only observables of interest are the S-parameters. This calculation involves an integration for the first frequency and a multiplication for every sample thereafter. This operation only needs to be performed on degrees of freedom that lie in a port. Since this is a small portion of the total number of degrees of freedom, the computational cost of this operation is insignificant.

### 3.5.3 Pre-conditioners and iterative solvers

Iterative solvers are used in many of the techniques presented. Each iteration of an iterative solver is an  $\mathcal{O}(N^2)$  operation. The number of iterations required can be  $N$ , rendering the cost of the operation  $\mathcal{O}(N^3)$ . The cost of an iterative solution is dependant on the convergence rate of the system. The rate of convergence is system dependant and can be improved by using pre-conditioners. There are additional computational costs associated with the calculation of a pre-conditioner. This is a topic on its own and is beyond the scope of this investigation. In this document, the cost of an iterative solution is given, without loss of generality, by equation 3.27.

$$\mathcal{N} \propto \mathcal{O}(n_{it}N^2) \quad (3.27)$$

### 3.5.4 The computational cost of a FEM frequency solution

The computational cost of a FEM frequency solution needs to be evaluated as a basis of comparison for the fast frequency techniques. This evaluation is presented here.

For each frequency evaluation, the only pre- and post- processing cost that needs to be considered is the system matrix assembly. This means that the total cost of the FEM frequency solution is given by equation 3.28, if an iterative solver is used.

$$\begin{aligned} \mathcal{N}_{FEM} &\propto \mathcal{O}(n_{fp}N) + \mathcal{O}(n_{fp}n_{it}N^2) \\ &\approx \mathcal{O}(n_{fp}n_{it}N^2) \end{aligned} \quad (3.28)$$

### 3.5.5 The computational cost of an AWE solution

The first fast frequency technique investigated is the AWE technique. This technique requires Taylor moments to be calculated. These moments can be obtained either by using full matrix inversion or a number of iterative solutions. The choice between these two techniques needs to be made on the basis of the number of unknowns of the system and the amount of RAM available. The computational cost is dependant on this number. Once the moments are known, the solution can be calculated at any number of frequency points at a trivial cost, as only the degrees of freedom required to generate observables need to be calculated.

To generate the AWE moments, for small matrices, one matrix inversion is needed. Thereafter



each moment requires five  $\mathcal{O}(N)$ - and one  $\mathcal{O}(N^2)$ - operations. The costs for this technique are therefore given by equation 3.29.

A similar argument can show that equation 3.30 is relevant for large matrices, where an iterative solver is used.

$$\begin{aligned}\mathcal{N}_{AWEsm} &\propto \mathcal{O}(N^3) + \mathcal{O}(n_m N^2) + \mathcal{O}(n_m N) \\ &\approx \mathcal{O}(N^3)\end{aligned}\tag{3.29}$$

$$\begin{aligned}\mathcal{N}_{AWEbm} &\propto \mathcal{O}(n_m n_{it} N^2) + \mathcal{O}(n_m N) \\ &\approx \mathcal{O}(n_m n_{it} N^2)\end{aligned}\tag{3.30}$$

### 3.5.6 The computational cost of a MB-AWE solution

The MB-AWE technique is used to increase the radius of convergence of the AWE technique. The AWE moments first need to be calculated. This cost is already evaluated in section 3.5.5. The only additional computation that needs to be performed is the calculation of the model coefficients. This operation only needs to be done for the degrees of freedom that are required to calculate the system observables. If all the system degrees of freedom are required, the computation would be an  $\mathcal{O}(N)$  operation. This is not usually the case, and thus the computational cost of this technique is also given by equation 3.29 and equation 3.30 for small and large systems respectively.

### 3.5.7 The computational cost of a MBPE solution

The cost of using MBPE lies in calculating the fitting data. Once this data is known, only low order linear equations need to be solved. This means that the entire cost is given by the cost to calculate the data points. For parameter value sampling, equation 3.28 is applicable, where  $n_{fp}$  corresponds to the required number of support points. For parameter derivative sampling, equation 3.29 and equation 3.30 are relevant, where  $n_m$  is now the number of derivatives required.

### 3.5.8 Comparison between the Fast Frequency Techniques

In the preceding sections, the computational cost of each technique is quantified. This quantitative data, coupled with qualitative measures of data developed throughout this chapter, gives an objective basis for comparison between the techniques.

The asymptotic computational cost between techniques does not differ considerably. The main factors that the techniques need to be evaluated on is the frequency resolution, accuracy bandwidth and implementation issues.

AWE has the advantage that it is possible to determine the number of derivatives required by testing linear dependance of the moments. If the small matrix technique is used, the maximum



amount of useful information obtainable from a single inversion is obtained. The technique becomes less desirable if the large matrix technique is used, as the product  $n_m n_{it}$  can easily be of the order of  $N$ , even with a pre-conditioner. In the work done for this thesis, the regular mesh results in a very well constructed system matrix. (A well constructed sparse matrix is one that only has entries in a band around the diagonal). This matrix could typically be solved with  $n_{it} < 0.1N$ . This means that if only 10 moments are required, the large matrix technique results in an  $\mathcal{O}(N^3)$  operation. For badly constructed system matrices requiring large numbers of moments, this technique could easily become costly. The most significant drawback of the technique is its failure to converge beyond a system pole. Waveguide sections of interest are typically structures that create a pole or zero. It is therefore unlikely that an AWE solution at one point will result in a solution over the entire band of interest. More information is also required to establish the exact point of divergence, resulting in additional computation.

To overcome the very finite radius of convergence associated with AWE, MB-AWE is presented. This technique does have the desired effect in waveguide structures for the reasons given in section 3.3.4. The disadvantage of this technique is that the computational cost is comparable with AWE and the convergence radius is smaller. The advantage of the technique is that multiple models with different numbers of poles and zeros can be compared to establish an idea of the region of convergence. Several techniques (such as Padé via Lanczos (PVL)) are available in the literature to improve the basic formulation.

MBPE has similar costs to the other methods, but has the advantage that additional information is supplied by the given model. MBPE using derivative sampling has the very substantial disadvantage that analytical derivatives of the observables in terms of the system unknowns need to be available. Using derivative sampling has no obvious advantage over parameter sampling and is thus undesirable in this case. Derivative sampling would be desirable in cases where the observable derivatives are continuous through system poles or where the natural output of the EM solver is parameter derivative information.

MBPE using parameter sampling has the advantage that the 'natural' observables from a FE system are used to support the model. Another advantage is that multiple models can be used to determine where errors can occur. Furthermore, sample spacing is not prescribed, allowing samples to be used where necessary. This technique should provide better resolution between FEM sample points, thus giving a lower computational cost for the obtained resolution. The disadvantage of the technique is that if the chosen model is not valid for a given observable, the determination of the model poles and zeros could become numerically unstable. This should not happen if models are carefully chosen.

## 3.6 Conclusion

Three different FF techniques were investigated and implemented. All the FF techniques investigated showed an improvement in computational cost for a specified frequency resolution. AWE and MB-AWE have the disadvantage that they break down at the system poles, which usually lie in the frequency range of interest. MBPE expects poles and zeros and models them well. The main disadvantage of MBPE with derivative sampling is that analytical derivatives of the observables need to be available.

MBPE with parameter sampling was ultimately chosen as the most suitable FF technique. The main reasons for this were the accurate modelling of system poles and zeros, and the fact that the technique only requires the natural output of the FE system.



## Chapter 4

# Adaptive Sampling for Fast Frequency Techniques

The FF techniques presented in Chapter 3 rely on reduced order models generated using system information. This information is obtained at one or more frequencies. The models generated from this/these point/points provides a desired frequency resolution in a specified bandwidth. If a larger bandwidth is desired, the reduced order model needs to be updated using additional information from another frequency point.

The method used to choose the new frequency point is the topic of this chapter. The new point should be chosen at the frequency that will reduce the error in the model the most. This will reduce the number of samples required to obtain an accurate solution in the entire bandwidth. A technique called Complex Frequency Hopping (CFH) is proposed in the literature for the AWE methods. Adaptive Frequency Sampling (AFS) is proposed for MBPE based models. Short descriptions of these techniques, as provided by the relevant literature, are given. Thereafter, an AFS algorithm is implemented and the results shown.

### 4.1 Adaptive method formulations

Both methods presented here rely on the same basic ideas. The only difference between the methods is the information available to them and the way in which the information is utilized. The first step in adaptively choosing frequency points to add to models, is to determine where the models fail. To establish regions of accuracy of the FF technique, additional information is required to generate an error function. Proposed error measures include:

1. Non-physical behavior.
2. Comparison of the model with additional FE solutions away from any model support points or expansion points.
3. Differences between two models.



To successfully implement the first error measure requires physical constraints, that are necessary and sufficient, to be known for the system. For a two port waveguide, the sum of the square of the S-parameters does seem applicable, but attention is drawn to the fact that this is a necessary but not sufficient condition for an accurate solution. The same is true of most physical constraints. Most *a posteriori* error estimators that are available for FE solutions attempt to obtain an estimate of the error between a FE solution and the exact solution and not the error between an unknown solution and the FE solution [38]. For a MOR reduction technique that models the entire FE system (as opposed to the observables), the residual of  $[K]\{E\} - \{b\}$ , where  $[K]\{E\} = \{b\}$  is the FE linear equation, can be used. The undesirable feature of this error indicator is that the system matrix needs to be evaluated at many frequencies.

Comparing the model to FEM solutions away from the model support points as an error estimate is undesirable because this is a computationally expensive process - just the sort that is being avoided by using a FF technique!

The only feasible way to obtain the error estimate is to calculate the difference between two models in the same frequency range. Exactly how this is done, and the method used to update the models, is discussed separately for each technique.

## 4.2 Complex Frequency Hopping

An adaptive strategy for AWE and MB-AWE called Complex Frequency Hopping (CFH) is described in [14, 22, 26, 39, 40]. AWE and MB-AWE have the property that they provide accurate low order models of the FE system for a finite radius of convergence. The radius of convergence for AWE is from the expansion point to the first complex system pole. The location of the system poles is assumed to be unknown.

Two models are required in order to calculate an error as described in the preceding section. CFH, as described in literature, uses two models generated using expansion points at the extremities of the frequency window of interest. The normalized difference between these models is then inexpensively evaluated throughout the frequency window. If the maximum error is larger than a specified tolerance, a new sample is generated at the location of the maximum error.

The frequency window is then split at the location of the new expansion point. Each window is then evaluated separately following the same procedure as above. The models at the extremities of each frequency window are available from the previous iteration and do not need to be recalculated. This process is repeated until no error is greater than the tolerance.

This technique will work with any FF technique that produces a model about an expansion point. This includes AWE, MB-AWE and MBPE (with derivative sampling at a point). CFH is not directly applicable to FF techniques that use multiple support points. For these techniques, AFS should be used. These techniques include MBPE (parameter sampling) and MBPE (multiple expansion point derivative sampling). Only slight modifications to the CFH strategy need to be made in order for it to work with these techniques, but AFS is a strategy specifically suited to them.



### 4.3 Adaptive Frequency Sampling

An adaptive strategy named adaptive frequency sampling (AFS) is described for MBPE in [41, 28, 27, 42, 43, 33]. The AFS methods proposed in these references have differences. Each technique is briefly described here.

Miller [27, 28] and Van Tonder [41] propose the use of an AFS technique that uses an initial distribution of sample points. No adaptation is used to choose the location of the initial set of data points. Several overlapping models are generated in the frequency range of interest. The difference between overlapping models is used as the error measure. If overlapping models are used over the entire frequency range of interest, an error estimate is also available over the entire frequency range. A new sample point is chosen at the maximum of this error estimate, unless the estimated error is within a specified tolerance across the frequency band.

For example, assume that 12 linearly spaced parameter samples have been obtained by simulation. Four models are generated using this data. The first model spans samples 1 to 6 and the second spans samples 7 to 12. The third model spans samples 1 to 8 and the fourth spans samples 5 to 12. This means that at any given frequency at least 2 models overlap. (This example is used from [28]). A new sample is added at the maximum difference between models. The models that span the new point are re-generated using the previous samples and the new one. The new point either increases the order of the denominator or the numerator of the model by maintaining the relationship  $d \leq n \leq d + 1$ . The process then iterates until the error is below a specified tolerance.

Lehmensiek and Meyer [33] describe a AFS technique that compares the models generated using different numbers of samples. The algorithm is only described for the  $k$ -th iteration. The first iteration operates in a slightly different manner as indicated in [33].

This algorithm uses subintervals of the frequency range of interest. The entire frequency range is given by  $[f_0, f_1]$ . Assume that a sample  $S_k$  is generated at frequency  $f_k$  in frequency range  $[f_i, f_j]$ . The models are updated, but the old models are kept. The difference-related error function between the new models and the old models is then evaluated in the frequency range  $[f_0, f_i]$  and  $[f_j, f_1]$ . A new parameter sample is then obtained at a frequency corresponding to the maximum error, until the error is less than a specified tolerance. Note that the frequency range  $[f_i, f_j]$  is excluded from the error function. The frequency range that is excluded reduces in size with each iteration and no two iterations will exclude the same frequency range.

A simpler algorithm is proposed by Dhaene et al. [43] and Timmons and Wu [42]. This algorithm uses two models that span the entire frequency range of interest. These two models differ only in the number of poles and zeros - exactly the same information is used to generate the models, but the two models have different parameters. The error is given by the difference between the two models. A new point is added at the frequency location that corresponds to the maximum error. Both models are re-generated using all points. The first model's order is always chosen to satisfy  $d_1 \leq n_1 \leq d_1 + 1$  and  $D = n_1 + d_1 + 1$ . The second model's order is obtained by  $n_2 = n_1 - 1$  and  $d_2 = D - n_2 - 1$ . The reason for this choice is that real S-parameters usually have more poles than zeros. If this is not true, it is not a problem, as



SVD is used (see section 3.4.1.1). The system will have to be over-sampled in order to increase the numerator order of the model to the higher order of the system.

The final adaptive strategy, proposed by Timmons and Wu [42], is implemented. This strategy offers adaptation from the fourth sample point. This is the only advantage over the multiple span strategy, proposed by Miller [27, 28] and Van Tonder [41]. The technique proposed by Lehmensiek and Meyer [33] has the disadvantage that the mismatch error is not evaluated over the entire band of interest.

## 4.4 Results on a test function

The adaptive technique of Dhaene et al. and Timmons and Wu, described in the preceding section, is implemented and tested on a test function. The purpose of this is to test the adaptive scheme more rigorously than can be done using FE systems.

The test function is in the form of a rational Padé polynomial. The complex poles and zeros are chosen randomly. The function is evaluated on the real axis. The order of the numerator is  $l$  and the order of the denominator is  $m$ .

The results are not shown graphically, as so many are produced. Observations on the performance of the technique on different order test functions is given.

Firstly it is noted that if  $l + 2 = m$ , the method converges with the number of samples equal to  $l + m + 1$ . This is the expected best case scenario, as the models always maintain this relationship. If  $l$  and  $m$  are large, the method converges with far fewer samples than  $l + m + 1$ . This model does have a larger error with respect to the exact solution. The error is less than -200dB when  $l$  and  $m$  are small. When they are large, the error is within the specified tolerance (-80 dB).

If  $l \ll m$  similar results are noticed with respect to convergence. If  $l > m$ , the performance degrades dramatically. Convergence is still reached, but significantly slower. The number of samples required before convergence can be as high as 3 times  $l + m + 1$ !

The observations on test functions show that the method converges quickly for the types of systems that it is designed to solve, and much slower for systems that do not have the required constraints.

## 4.5 Adaptive Results of FE Systems

Following the success of this adaptive scheme on the test system, all that remains is for it to be implemented for a FE system and tested.

The same models used in section 3.2.3 are used in this section. The geometric and model information is not duplicated here. Only the results are given.



### 4.5.1 Single inductive septum

The adaptive procedure converged on a model using only 6 samples. The samples locations are at 8 GHz, 8.075 GHz, 8.2125 GHz, 8.5 GHz 8.825 GHz and 9 GHz. The results are not plotted, as the error is within tolerance, and is therefore not visible on a graph.

### 4.5.2 Single pole filter

The adaptive procedure converged on a model using only 5 samples. The samples locations are at 10.75 GHz, 10.8 GHz, 10.836 GHz, 10.848 GHz and 10.850 GHz. The results are not plotted, as the error is within tolerance, and is therefore not visible on a graph.

### 4.5.3 Two pole filter

The adaptive procedure converged on a model using only 8 samples. It is decided that a tougher test would be to test the adaptive scheme on the entire 8 to 12 GHz frequency range. This was done and the adaptive process converged after 14 samples! The results are shown here, with the support points plotted as points on the same graph. Note that the energy sumterm only varies in the fifth decimal, and hence the vertical scale does not reflect a numerical change between points. The graph is shown to illustrate that the model passes through the FEM solution points exactly.

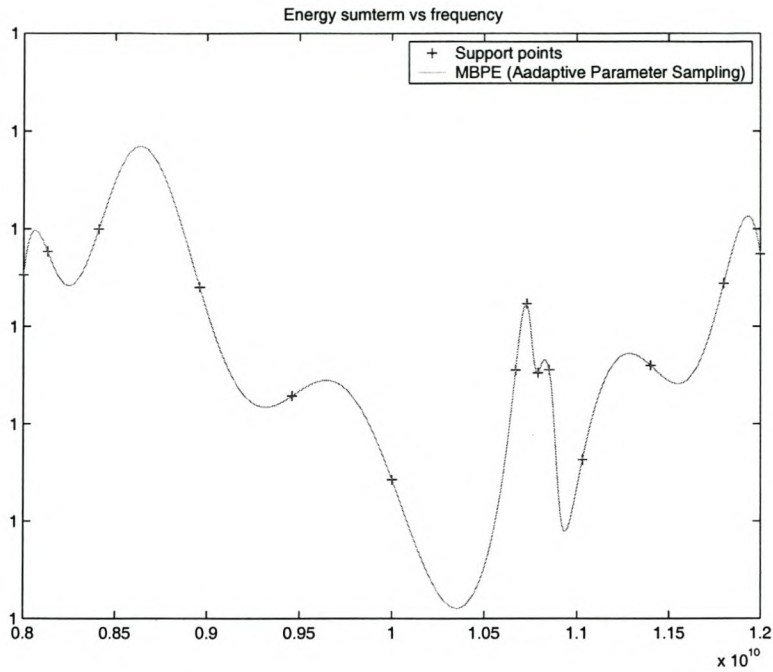


Figure 4.1: The sum of the squares of the magnitudes of the reflection and transmission coefficients for the two pole filter: MBPE (Adaptive Sampling) results and support points.

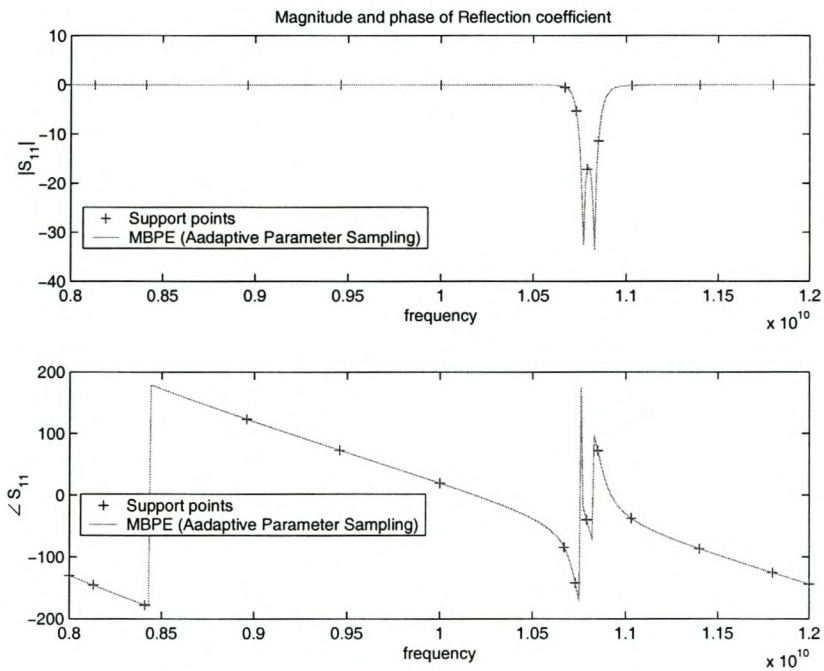


Figure 4.2: Reflection coefficient of the two pole filter: MBPE (Adaptive Sampling) results and support points.



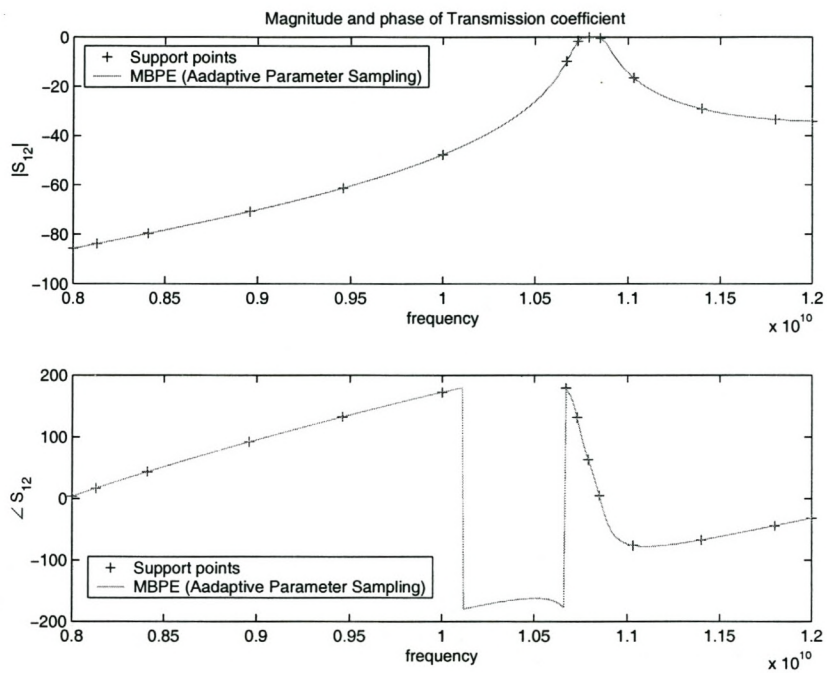


Figure 4.3: Transmission coefficient of the two pole filter: MBPE (Adaptive Sampling) results and support points.

A rigorous test of the error across the frequency band is to evaluate both the FE system and the model at the same points across the frequency and plot the difference. This is done at 401 points. The results for both the reflection and transmission coefficients are shown. It is seen that the error is less than -100 dB throughout, on both coefficients!

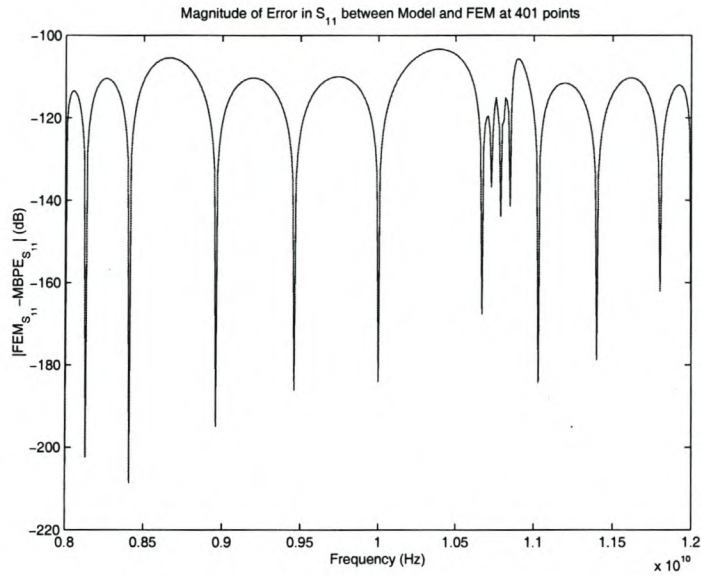


Figure 4.4: Error in reflection coefficient of the two pole filter between MBPE (Adaptive Sampling) and FE solution.

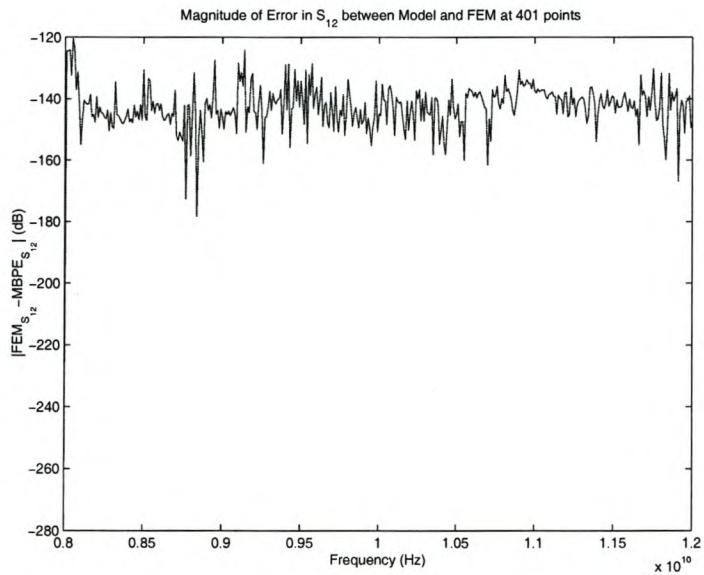


Figure 4.5: Error in transmission coefficient of the two pole filter between MBPE (Adaptive Sampling) and FE solution.



Another interesting result is to generate a model that uses the same support points as the MBPE, but interpolates linearly (in the complex plane) between them. The error obtained in both the transmission and reflection coefficients is shown below. These results clearly indicate that even if linear interpolation was capable of adaptive sampling, the error between this interpolation and MBPE differ by orders of magnitude.

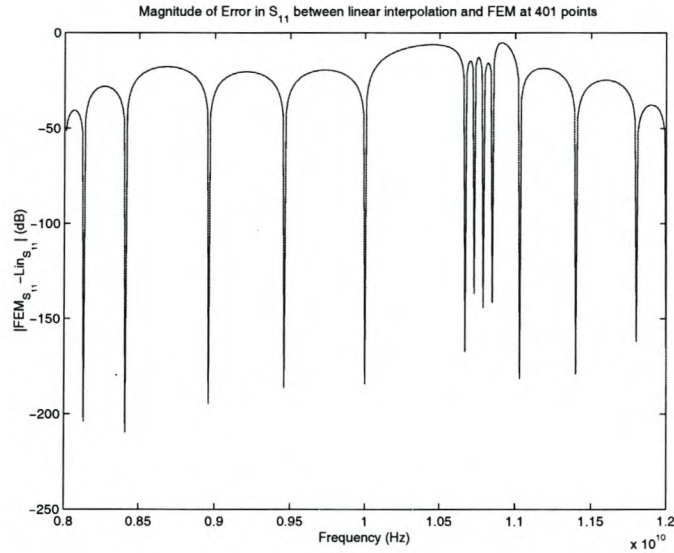


Figure 4.6: Error in reflection coefficient of the two pole filter between Linear interpolation (Adaptive Samples) and FE solution.

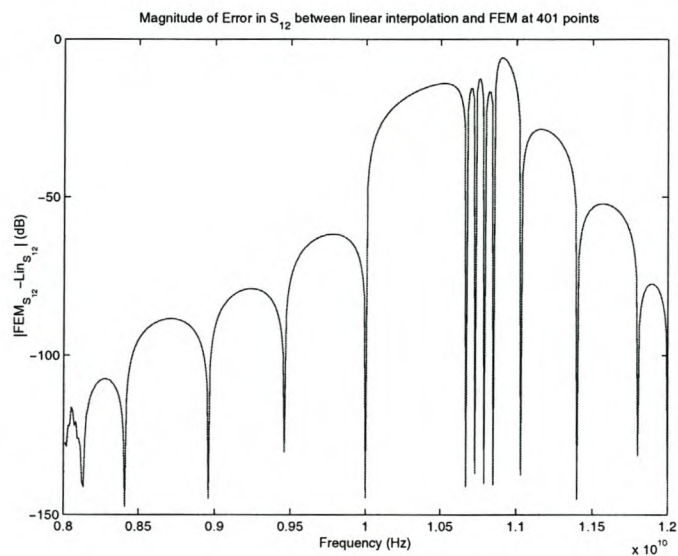


Figure 4.7: Error in transmission coefficient of the two pole filter between Linear interpolation (Adaptive Samples) and FE solution.

## 4.6 Conclusion

This Chapter has shown the development and results of an adaptive sampling scheme for MBPE with parameter sampling. The adaptive sampling technique works very well with only 14 FEM solution points required to accurately model a 0.5% bandpass filter in the entire X-band. From the results presented for this filter, it can be seen that the adaptive scheme chooses more points in the 'active' frequency band of the filter, as expected.



## Chapter 5

# A Sample Optimization Routine

The goal of this study is to create a tool that can be used to investigate synthesis of waveguide structures, by using numerical optimization. To illustrate the use of this tool, a sample synthesis via optimization is done.

There are many numerical optimization techniques that can be used for synthesis. Since the synthesis of components is not the main thrust of this study, a complete investigation into the most suitable algorithm is not required. Algorithm parameter selection is also of a first order nature.

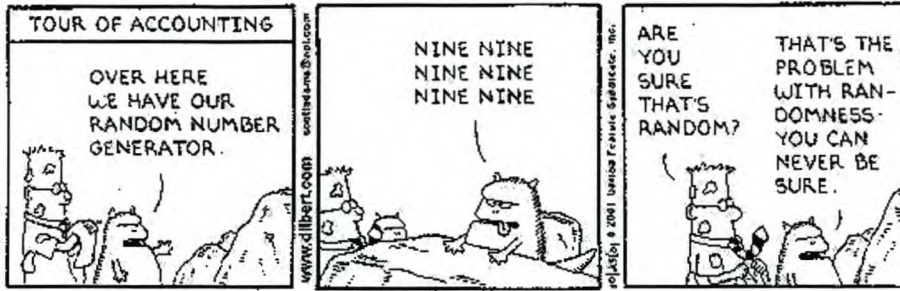
The algorithm that has been chosen is Generalized Simulated Annealing [44]. This is a guided random search. The use of random numbers by this optimization routine requires the implementation of a random number generator. The implementation of the random number generator is discussed before the simulated annealing algorithm. Thereafter the objective function is chosen. The results of the synthesis are then shown.

The work presented in this chapter makes use of an unpublished report written by the author of this dissertation [45] for a post-graduate subject at the University of Stellenbosch, under the guidance of Dr. C. van Niekerk.

### 5.1 The proposed synthesis specifications

In order to test synthesis by optimization, an example specification is required. The specifications for microwave components are usually in terms of impedance bandwidths and insertion losses. As only a first order illustration is required for the purposes of this chapter, the device specifications are significantly simplified.

The only specification for the device to be synthesized is that it must be a single pole filter with a center frequency of 9 GHz. No limitation is placed on the physical dimensions of the component.



Copyright © 2001 United Feature Syndicate, Inc.

Figure 5.1: Dilbert on Random numbers. Reprinted with permission

## 5.2 Random Number Generator

Guided random searches use random numbers during their execution. It is therefore desirable to have a random number generator that is as 'random' as possible. A separate study [45] notes that if the random number generator supplied with MATLAB 5.3 is used, the optimization technique starts to use the same sequence of random numbers, and therefore oscillating around a solution. Park [46] shows many examples of bad random number generators that are used in practice. Park further proposes a random number generator, that is implemented and used in this simulated annealing algorithm.

The random number generator supplied by Park is implemented and showed much better results [45]. The source code for the generator is provided in the article [46]. Figure 5.2 shows the normalized distribution of random numbers generated by the algorithm after 100 000 calls.

### 5.2.1 Generalized Simulated Annealing

The generalized simulated annealing algorithm is described by Bohachevsky et al [44]. This algorithm is shown to be effective on search spaces that have many local minima. The algorithm for a  $n$ -parameter search can be summarized as follows:

1. Choose a starting point.
2. Evaluate the error at starting point.
3. Calculate a random direction in  $n$ -dimensional space
4. Evaluate the error at a new point, located at specified distance,  $dr$ , from the previous point in the calculated random direction.
5. If the error at the new point is lower than the previous error, accept the new point and go back to step 3, with the new point is used as the base point.



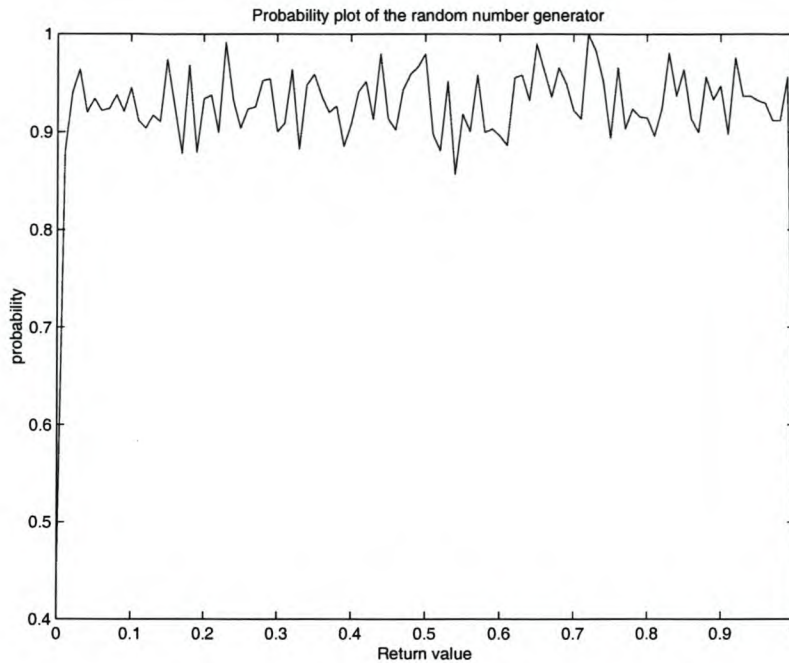


Figure 5.2: Random number distribution for the random number generator proposed by Park

6. Otherwise, calculate the probability of accepting the detrimental step using:

$$p = e^{-\beta * (error_{this}^g) * |error_{this} - error_{previous}|} \quad (5.1)$$

Accept the step if a random number (obtained using the random number generator) is less than this probability  $p$ . If the step is accepted, go back to step 3 using the new point as the base point, otherwise go back to step 3 using the previous point as the base point.

7. Stop after a certain number of iterations or after a convergence criteria is reached.

The parameters  $dr$ ,  $\beta$  and  $g$  need to be selected. It is desirable that the step size  $dr$  is large enough to allow a speedy optimization, but small enough to make the fine steps required near the optimum. If  $g$  is chosen as zero, the probability of accepting a worse solution is to depend only on the scaled magnitude of the error difference. If  $g$  is chosen as a negative number, the probability of accepting a detrimental step decreases as the global optimum is approached.  $\beta$  is used to scale the error difference term of the probability. If  $\beta$  is large, few detrimental steps are accepted.

The choice of these parameters for this example is discussed in section 5.5, after the objective function and the physical parameters have been defined.

### 5.3 The objective function

The specifications for this synthesis problem are very loosely described. A single pole filter at 9GHz is all that is required. The objective function is simply calculated as the square of



the frequency separation between the simulated filter center frequency and 9GHz. The center frequency of the simulated filter needs to be defined. For this example, the center frequency is defined as the frequency with the smallest reflection, provided that the reflection is less than -25dB.

## 5.4 The physical structure limitations for the synthesis algorithm

The physical geometry that the filter can use must be specified. It is desirable to minimize the number of parameters to be optimized. It is therefore undesirable to simply allow the algorithm to use any number of structures with any parameters. The single pole filter previously presented in this dissertation is constructed from 2 E-plane septa in X-band waveguide. The dimensions of the septa and their spacing are responsible for the selective frequency behavior of the device. It is therefore decided that the synthesized filter should be constructed of 2 E-plane septa only. The septa are also constrained to have the same dimensions and be along the centreline of the waveguide. With reference to figure 3.6, only dimensions  $A$  and  $B$  are allowed to vary. The dimension  $A$  cannot be passed to the parametric mesher (there is no building block that is described in this manner). Thus the distance from the end of the waveguide section that has the septum to the septum center is varied. This has the same effect as varying  $A$  directly. Physical limitations also need to be imposed on the problem. For instance, the width of a septum is not allowed to increase beyond the length of the section of waveguide that it is in. All physical limitations are implemented in the form of hard boundaries. This means that if the optimizer requests a non-physical result, the parameters are modified to be on the boundary. For instance, if the result of a filter is requested such that the septa are wider than section of waveguide in which they are located, the septum is truncated to the length of the section, without penalty in the objective function. Minimum lengths of septa and hollow sections of waveguide are also forced. This prevents the optimizer from removing one of the septa, or joining the two septa.

## 5.5 Choice of the optimizer parameters

The three generalized simulated annealing parameters need to be chosen. This choice is only done for a first order approximation. It is suspected that the search space will not have many local maxima and minima. This means that few detrimental steps should be taken, especially when the optimum is approached. The parameter  $g$  is chosen as -1 to achieve this. The step size  $dr$  is chosen as 0.5. This means that the sum of the change in septum width and the change in septum separation is 0.5mm. This choice should not prevent the optimum from being obtained, while allowing a sufficiently speedy descent. The final parameter,  $\beta$  is chosen to reduce the chances of a detrimental step being taken. If  $\beta$  is chosen as unity, a 50% error differential has a 61% chance of being accepted.  $\beta$  was chosen as 4.5, thus a 50% error differential has a 10% chance of being accepted.



## 5.6 Results

The optimizer obtains FE solutions using MBPE with adaptive sampling. The model of the reflection coefficient is solved at 401 frequency points between 8GHz and 11GHz.

The optimizer is implemented as described using the specifications as above. The optimizer was run for 150 iterations with no other convergence specification. The objective function scores versus iteration number are shown in figure 5.3. The reflection coefficient for the resultant filter is shown in figure 5.4. The dimensions of the best filter are  $A = 18.1146mm$  and  $B = 0.5mm$  as in figure 3.6. Note that  $B = 0.5mm$  was given as a the physical boundary for the minimum septum width.

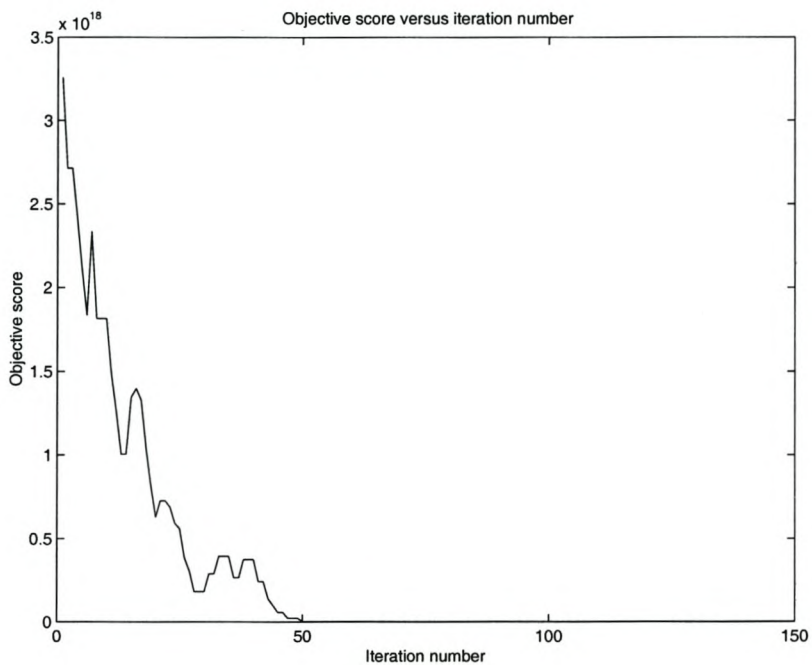


Figure 5.3: Objective function score versus iteration number for the simulated annealing synthesis.

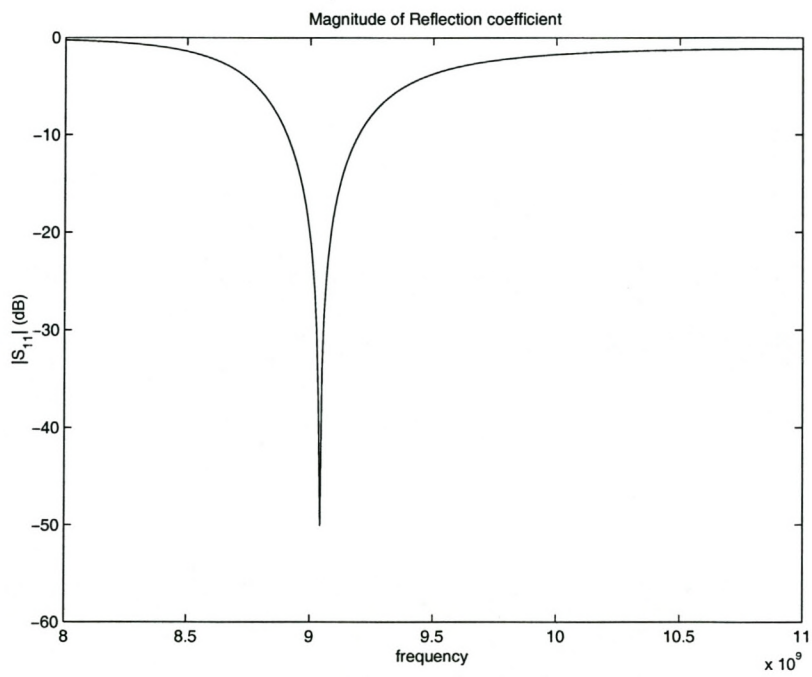


Figure 5.4: Magnitude of the reflection coefficient of the synthesized filter.



## 5.7 Conclusion

The synthesis results for the generalized simulated annealing procedure shown in this chapter appear promising.

A single pole filter at 9GHz was synthesized using the single pole filter, as described in figure 3.6, as a starting point. The center frequency of this filter was moved almost 1.7GHz. The results of the objective score versus iteration number show that the procedure would benefit from additional convergence criteria. One of the specified physical boundaries of the configuration was reached during the optimization process, and it is possible that the target center frequency cannot be realized with the specified physical limitations. This chapter has shown that the code developed during the work presented in this dissertation, can be used for synthesis via optimization.

The FEM was used in conjunction with MBPE and the adaptive scheme presented earlier in this dissertation. This means that each iteration of the optimizer required approximately 10 (varies between 9 and 11) support points to generate a 401 point model of the reflection coefficient. If no FF technique were used, each iteration of the optimizer would have taken 40 times as long. The algorithm took approximately 28 hours to execute on a SGI Origin 200 workstation. If the same algorithm was used without any FF Techniques and the same frequency sampling density, it would require approximately 47 days. The frequency sampling density could be reduced, but this is not recommended when solving narrow band devices. If the frequency sampling density were halved, the algorithm would only require 23 days. This discussion clearly shows that this synthesis would be too costly to solve without the use of FF techniques.

# Chapter 6

## General Conclusions

The aim of this study has been to produce a tool that can be used to study the synthesis of passive waveguide components using numerical optimization. All the stages of development of such a tool were documented in this dissertation, in the form of formulation, implementation issues and results. More than one solution has been shown for any stage of the development in cases where there was no obvious solution choice. The different solution choices were then compared and one was chosen.

A parametric, 'Brick' element mesher was implemented for two-port structures. The mesher is defined in terms of fundamental 'building blocks'. The mesher that was developed provides mesh information in a form that is directly usable by the FEM algorithm.

The FEM algorithm was implemented using curl-conforming brick elements. The unknowns that are solved for are related to the tangential electric fields on the surface of the elements. A Galerkin variational functional was used. The stationary point of this functional is the solution of the system. This implementation of the FEM was validated against results in the literature and independent FEM algorithms.

FF techniques were investigated to reduce the number of times that the FE system equation needs to be solved to generate a specified sampling density. Three different techniques were investigated and implemented. These techniques were AWE, MB-AWE and MBPE. The advantages and disadvantages of each technique was discussed.

An adaptive sampling scheme was investigated and implemented for MBPE. The results show that considerable savings in execution times can be obtained using this technique. In the results presented, a saving of 28.7 times was obtained.

In order to illustrate the use of the algorithm that was developed, a sample synthesis via optimization routine was implemented. The optimization routine showed excellent results without human intervention.

If this tool had not been developed, the same algorithm would have taken 40 times as long to execute - if no human intervention is required to generate the mesh. If human intervention is required to generate the mesh, the time saving would be difficult to estimate, but definitely far above the 40 times already calculated. The total computational cost saving that this algorithm obtains is difficult to estimate accurately, but it is clear that the saving is significant.

An effective tool for further research into synthesis via optimization has been obtained.

The next stage in this study is to use the tool for numerical synthesis. If the results from this research are promising, the FEM portion of the algorithm can be extended to handle more



devices e.g.  $n$ -port devices, radiating structures, etc. The mesher would also need to be extended if this is to be done. Higher order elements could be implemented, and used with a adaptive error estimation to improve the accuracy of the FEM at the locations of errors. The port boundary conditions could also be extended to handle higher order modes.

Further research possibilities into FF techniques include a study on the models used to model EM observables and possibly a model with an adaptive order for MBPE. This will prevent the 'wasting' of parameter samples that is caused by having terms in the model that are not present in the system.

## Appendix A

# Derivation of Taylor series for linear equation

This appendix shows the calculation of the derivatives of the solution to the set of equations that describe the FE system. The derivation starts with the equation in the form shown in equation 3.5. These are the Taylor series moments [12]. It is expected that only the first moment will differ from those presented by Gong and Volakis. The reason for this is that the excitation vector has an added constant term that is absent in their paper.

The first moment  $\{E_0\}$  is given by:

$$\{E_0\} = [\bar{A}_{cent}]^{-1}(mk_{cent} + c)f_1 \quad (\text{A.1})$$

The first derivative is given by:

$$\begin{aligned} \frac{\partial\{E\}}{\partial k_0} = \{E_1\} &= [\bar{A}_{cent}]^{-1} (mf_1 - [A^*][\bar{A}_{cent}]^{-1}(mk_{cent} + c)f_1) \\ \Rightarrow \{E_1\} &= [\bar{A}_{cent}]^{-1} (mf_1 - [A^*]\{E_0\}) \end{aligned} \quad (\text{A.2})$$

where,

$$[A^*] = \frac{\partial[\bar{A}_{cent}]}{\partial k_0} = [A_1] + 2k_0[A_2] \quad (\text{A.3})$$

From equation A.2 it is clear that only  $\{E_0\}$  differs from the result given by Gong and Volakis [12]. This is as a result of the constant in the frequency term. If a higher order polynomial is used to approximate  $k_w g$  to  $k_0$ , more moments will differ.



# Bibliography

- [1] J. Johnson and Y. R. Samii, "Genetic algorithms and method of moments (GA/MOM) for the design of integrated antennas," *IEEE trans. Antennas and Propagation*, vol. 47, pp. 1606–1614, October 1999.
- [2] J. Jin, *The Finite Element Method in Electromagnetics*. John Wiley & Sons, Inc, 1993.
- [3] P. P. Silvester and R. L. Ferrari, *Finite elements for electrical engineers*. Cambridge University Press, third ed., 1996.
- [4] J. Webb, "Edge elements and what they can do for you," *IEEE Trans. Magn.*, vol. 29, pp. 1460–1465, March 1993.
- [5] D. B. Davidson, "Higher-order (LT/QN) vector finite elements for waveguide analysis," *Applied Computational Electromagnetics Society Journal*, vol. 17, pp. 1–10, March 2002. Special Issue on Approaches to Better Accuracy/Resolution in Computational Electromagnetics.
- [6] D. B. Davidson, "LT/QN Vector finite elements for 3D waveguide analysis," *17th Annual review of progress in Applied Computational Electromagnetics, Monterey, CA*, pp. 323–329, March 2001.
- [7] D. B. Davidson, "Implementation issues for three dimensional vector FEM programs," *IEEE Antennas and Propagation Magazine*, vol. 42, pp. 100–107, December 2000.
- [8] E. Topsakal, R. Kindt, K. Sertel, and J. Volakis, "Evaluation of the BICGSTAB(1) algorithm for the finite-element/boundary-integral method," *IEEE Antennas and Propagation Magazine*, vol. 43, pp. 124–131, December 2001.
- [9] P. Meyer, "The design of a narrow band E-plane waveguide filter - original in afrikaans," Master's thesis, University of Stellenbosch, Stellenbosch, South Africa, 1988.
- [10] K. Ise, K. Inoue, and M. Koshihara, "Three-dimensional finite element method with edge elements for waveguide discontinuities," *IEEE Trans. Microwave Theory and Tech.*, vol. 39, pp. 1289–1295, August 1991.
- [11] E. K. Miller, "Model-based parameter estimation in electromagnetics: Part i. background and theoretical development," *IEEE trans. Antennas and Propagation*, vol. 40, pp. 42–52, February 1998.



## BIBLIOGRAPHY

- [12] J. Gong and J. Volakis, "AWE implementation for electromagnetic FEM analysis," *Electronics Letters*, vol. 32, pp. 2216–2217, November 1996.
- [13] X.-M. Zhang and J.-F. Lee, "Application of the AWE method with the 3-D TVFEM to model spectral responses of passive microwave components," *IEEE Trans. Microwave Theory and Tech.*, vol. 46, pp. 1735–1741, November 1998.
- [14] W. C. Chew, J.-M. Jin, E. Michielssen, and J. Song, *Fast and efficient algorithms in computational electromagnetics*. Artech House, 2000.
- [15] C. Reddy, M. Deshpande, C. Cockrell, and F. Beck, "Fast RCS computation over a frequency band, using method of moments in conjunction with asymptotic waveform evaluation technique," *IEEE trans. Antennas and Propagation*, vol. 46, pp. 1229–1233, August 1998.
- [16] R. D. Slone, R. Lee, and J.-F. Lee, "Multipoint galerkin asymptotic waveform evaluation for model order reduction of frequency domain fem electromagnetic radiation problems," *IEEE trans. Antennas and Propagation*, vol. 49, pp. 1504–1513, October 2001.
- [17] R. D. Slone, R. Lee, and J.-F. Lee, "Automating multipoint galerkin AWE for a FEM fast frequency sweep," *IEEE trans. Antennas and Propagation*, vol. 38, pp. 637–640, March 2002.
- [18] Y. Ermeldi, J. Gong, C. Reddy, and J. Volakis, "Fast RCS pattern fill using AWE technique," *IEEE trans. Antennas and Propagation*, vol. 46, pp. 1752–1753, November 1998.
- [19] J. E. Bracken and Z. J. Cendes, "Asymptotic waveform evaluation for s-domain solution of electromagnetic devices," *IEEE Trans. on Magnetics*, vol. 34, pp. 3232–3235, September 1998.
- [20] Y. Ermeldi, C. Reddy, and J. Volakis, "AWE technique in frequency domain electromagnetics," *Journal of Electromagnetic Waves and Applications*, vol. 13, pp. 359–378, 1999.
- [21] S. V. Polstyanko, R. Dyczij-Edlinger, and J. Lee, "Fast frequency sweep technique for efficient analysis of dielectric waveguides," *IEEE Trans. Microwave Theory and Tech.*, vol. 45, pp. 1118–1126, July 1997.
- [22] J. E. Bracken, D. K. Sun, and Z. J. Cendes, "S-domain methods for simultaneous time and frequency characterization of electromagnetic devices," *IEEE Trans. Microwave Theory and Tech.*, vol. 46, pp. 1277–1290, September 1998.
- [23] Y. E. Erdemli, A. Brown, and J. Volakis, "Frequency and angular extrapolations in hybrid finite element-boundary integral systems," *ACES Conference Proceedings*, 1999.
- [24] J. E. Bracken, D. K. Sun, and Z. J. Cendes, "Characterization of electromagnetic devices via reduced-order models," *Comput. Methods Appl. Mech. Engrg.*, vol. 169, pp. 311–330, 1999.
- [25] D. M. Pozar, *Microwave Engineering*. John Wiley and Sons, Inc., 1998.



- [26] M. Kolbehdari, M. Srinivasan, M. Nakhla, and Q.-J. Zhang, "Simultaneous time and frequency domain solutions of EM problems using finite element and CFH techniques," *IEEE Trans. Microwave Theory and Tech.*, vol. 44, pp. 1526–1534, September 1996.
- [27] E. Miller, "PC's for AP and other EM reflections," *IEEE Antennas and Propagation Magazine*, vol. 36, pp. 60–63, April 1994.
- [28] E. K. Miller, "Model-based parameter estimation in electromagnetics: Part ii. applications to EM observables," *IEEE trans. Antennas and Propagation*, vol. 40, pp. 51–65, April 1998.
- [29] E. K. Miller, "Model-based parameter estimation in electromagnetics: Part iii. applications to EM integral equations," *IEEE trans. Antennas and Propagation*, vol. 40, pp. 49–66, June 1998.
- [30] S. Peik, R. Mansour, and Y. Chow, "Multidimensional Cauchy method and adaptive sampling for an accurate microwave circuit modeling," *IEEE Trans. Microwave Theory and Tech.*, vol. 46, pp. 2364–2371, December 1998.
- [31] M. van Wyk, "Development of a three-octave bandwidth printed log-periodic dipole array," Master's thesis, University of Stellenbosch, December 1998.
- [32] J. van Tonder, "Model-based parameter estimation," tech. rep., EM Software and Systems, [www.emss.co.za](http://www.emss.co.za), March 2000.
- [33] R. Lehmensiek and P. Meyer, "Using efficient model-based estimation for pole-free solutions of modal propagation constants, as applied to shielded planar structures," *ACES Journal*, vol. 16, pp. 1–10, March 2001.
- [34] Mathworks, "Matlab help file."
- [35] D. Lay, *Linear Algebra and its Applications*. Addison Wesley, second ed., 1997.
- [36] C. Long, "Visualization of matrix singular value decomposition," *Mathematics Magazine*, vol. 56, pp. 161–167, May 1983.
- [37] D. B. Davidson, *Parallel Algorithms for Electromagnetic Moment Method Formulations*. PhD thesis, University of Stellenbosch, November 1991.
- [38] M. M. Botha, *Efficient finite element electromagnetic analysis of antennas and microwave devices: the FE-BI-FMM formulation and a posteriori error estimation for p adaptive analysis*. PhD thesis, University of Stellenbosch, Stellenbosch, South Africa, 2002.
- [39] M. Li, Q.-J. Zhang, and M. Nakhla, "Finite difference solution of EM fields by asymptotic waveform techniques," *IEE Proc. Microwave Antennas and Propagation*, vol. 143, pp. 512–520, December 1996.
- [40] F. Ling, D. Jiao, and J.-M. Jin, "Efficient electromagnetic modeling of microstrip structures in multilayer media," *IEEE Trans. Microwave Theory and Tech.*, vol. 47, pp. 1810–1818, September 1999.

- [41] J. van Tonder, "ADAPTFEKO: Adaptive frequency sampling," tech. rep., EM Software and Systems, [www.emss.co.za](http://www.emss.co.za), May 2001.
- [42] I. Timmins and K.-L. Wu, "An efficient systematic approach to model extraction for passive microwave circuits," *IEEE Trans. Microwave Theory and Tech.*, vol. 48, pp. 1565–1573, September 2000.
- [43] T. Dhaene, J. Ureel, N. Faché, and D. De Zutter, "Adaptive frequency sampling algorithm for fast and accurate s-parameter modeling of general planar structures," *IEEE MTT-S Digest*, vol. 3, pp. 1427–1430, 1995.
- [44] I. O. Bohachevsky, M. Johnson, and M. Stein, "Generalized simulated annealing for function optimization," *Technometrics*, vol. 28, pp. 209–216, August 1986.
- [45] S. Clarke, "Task 5: Bounded optimization, ill-conditioned problems, random searches." Task for the course Optimization 813 at the University of Stellenbosch, November 2001.
- [46] S. Park and K. Miller, "Random number generators: Good ones are hard to find," *Communications of the ACM*, vol. 31, pp. 1192–1201, October 1988.